NTNU – Trondheim
Norwegian University of
Science and Technology

Impurities in Ilmenite: Magnesium

Pyung-Hwa Kim

Light Metals, Silicon and Ferroalloy Production
Submission date: June 2015
Supervisor: Leiv Kolbeinsen, IMTE

Norwegian University of Science and Technology
Department of Materials Science and Engineering

Preface

This thesis is submitted for the fulfillment of a Master's Degree at the Norwegian University of Science and Technology (NTNU). The project work has been carried out at the Department of Material Science and Engineering (DMSE) during the spring semester of 2015.

This Master's project is part of the GASFERROSIL (Use of Natural Gas in Ferroalloy, Silicon Production and Ilmenite Processing) project, which have been funded by the Norwegian Research Council in collaboration with TiZir Titanium & Iron AS as industrial partners.

Trondheim, June 2015

Pyunghwa (Peace) Kim

Acknowledgements

First, I would like to give all thanks and glory to God. Although it has been a difficult journey far away from home, God has been my milestone in every moment. I cannot think that every choice I had made was on my own account, but I believe it was His guidance, which lead me through my studies. I thank God for blessing my studies and giving me confidence, as I'm ready to go further beyond.

Second, I am extremely grateful to all the academic staffs. My supervisor, Professor Leiv Kolbeinsen, has been a great teacher and mentor to me. His age-long academic guidance was priceless, and I greatly appreciate the weekly discussion in spite of his busy schedule. I give many thanks to Stephen Lobo. His advice regarding my thesis was a tremendous help, and I especially thank him for his writing techniques and tips. I also like to thank Professor Merete Tangstad and her SiManTi (Silicon, Manganese, Titanium) group. It was great to learn about different project areas and presentation techniques. I can only guess that it was her various feedbacks and trainings, which gave me more confidence in my presentation. Special thanks to Delphine Leroy, Dmitry Slizovskiy, Edith Thomassen (SINTEF) and Irene Bragstad (SINTEF). They have been very kind and helpful when I was learning and using the equipment for my work. I appreciate them for the proper trainings and guidance.

Third, I would like to extend my gratitude to the staffs of TiZir Titanium & Iron AS. My trip to Tyssedal had gave me more confidence in my work by seeing each part of the operation, along with awe from the majestic scenery of the fjord. Many thanks to Stian Seim who guide us through the operation. His guide was crystal clear and easy to understand.

Next, I would like to mention all my friends who have helped me during my study. Thanks to Andrea Broggi, Feng Ni and Bilal khan. As we are all in the same study program, we have shared many ideas regarding each project and friendly banters through various activities. I would like to thank Sondre Norhaug who was my co-student during my project work. We surely had shared a lot of surprising yet meaningful experiences when tackling through the challenges of synthesizing ilmenite. I would also like to thank Bjarte Nygård. He was the jolliest Norwegian I've ever met. I give credit to him for helping me getting more accustomed to the Norwegian

culture. A very special thanks to Reinaldo Penso and his wife Brigitte. Although they were far away from Trondheim, their constant greetings were encouraging through my studies. I consider them as my brother and sister beyond friends.

Lastly but not least, I would like to give thanks to my family for their constant love and support. I miss my late grandparents very much. Although they have lost everything and lived a tough life after the Korean War, I'm sure that they are smiling in heaven as they see their offspring doing well. I will never forget the love and devotion they have given to me. Also, many thanks to my loving parents for their invariable love and support.

But he knows the way that I take;
when he has tested me, I will come forth as gold.
- Job 23:10 -

Men han kjenner den veien jeg fulgte.
Prøver han meg, kommer jeg ut som gull.
- Job 23:10 -

나의 가는 길은 오직 그가 아시나니

그가 나를 단련하신 후에는 내가 정금같이 나오리라.

- 욥기 23:10 -

Abstract

The influence of Mg as main impurity in ilmenite during gaseous reduction with CO and H_2 gas was studied in this work. This is of interest for the ilmenite pre-reduction step in the Tyssedal Process as where the impurities in ilmenite tend to give impact to the reduction rate. The work comprises an experimental investigation of synthetic Mg-rich ilmenite pellets with their conversion (reduction) degree, which have been used to isolate the influence of Mg in ilmenite pre-reduction.

Producing synthetic Mg-rich ilmenite, where the target compound is $FeTiO_3$-$MgTiO_3$ (M_2O_3) solid solution, was the initial task. Synthetic Mg-rich ilmenite ores with different amount of Mg were made by using a CCIF (Cold Crucible Induction furnace) in an inert atmosphere. The slow cooling method used for the synthesis proved the possible production of the $FeTiO_3$-$MgTiO_3$ solid solution without other phases. The XRD analysis showed confirmation of only $FeTiO_3$-$MgTiO_3$ peaks.

Then, the oxidation of synthetic Mg-rich ilmenite was done after pelletizing. Synthetic Mg-rich ilmenite pellets were oxidized in a muffle furnace at the temperature of 1000℃ for 2 hours. The resulted phases after oxidation were ferric pseudobrookite ($Fe_2^{3+}TiO_5$), rutile (TiO_2) and magnesium dititanate ($MgTi_2O_5$) as expected but also an addition of hematite (Fe_2O_3). The Mg in ilmenite was thought to hinder the pseudobrookite formation of ilmenite by forming magnesium dititanate ahead in reaction.

The reduction of synthetic Mg-rich ilmenite pellets was done with different ratio of CO and H_2 gas for 4 hours. The TGA (Thermo-Gravimetric Analyzer) vertical retort furnace was used, and the mass loss of each sample was recorded and further calculated into conversion degree. Synthetic Mg-rich ilmenite pellet samples with different amount of Mg were reduced with 50% CO + 50% H_2 gas, and they showed lower conversion degree with increasing amount of Mg in ilmenite. Synthetic Mg-rich ilmenite pellets with same amount of Mg were reduced with different amount of H_2 gas in the gas mixture, and they showed higher conversion degree with increasing amount of H_2 gas. The comparison of conversion degrees of each sample showed two clear indications: Mg in ilmenite hinders the reduction rate, whereas H_2 gas enhances the

reduction rate.

In addition, the conversion degree for the sample reduced with only H_2 gas was approximately "1.18" after 4 hours, which indicated addition mass from the supposedly inert rutile (TiO_2). Instead of finding phases of reduced rutile however, only phases of Mg, Ti oxide species were detected. It was thought that Mg in ilmenite diffuses ahead and immediately stabilizes the reduced rutile species by forming Mg, Ti oxide species.

From the experiment of synthetic Mg-rich ilmenite pellets, a clear indication for the influence of Mg in ilmenite reduction was given. The data observed from the relatively pure synthetic ilmenite pellets are believed to give accurate results compared to natural ilmenite pellets.

Key words: synthetic, ilmenite, Mg-rich, oxidation, reduction, CO, H_2

Contents

List of figures

List of tables

Chapter 1 Introduction

TITANIUM (Ti) is recognized for its outstanding chemical and physical properties, and its application has a wide range. As a metallic element, titanium is a corrosion resistive metal with a high strength-to-weight ratio [1]. When titanium is oxidized in air, it will immediately form a thin passive oxide layer which protects the bulk metal from further oxidation [2]. Also, titanium is 60% more dense than aluminum (Al), but twice as strong as the most commonly used aluminum alloys [3]. These properties make aerospace and electrode related applications favorable [4, 5].

Titanium dioxide (TiO_2) is a naturally occurring oxide of titanium, and it also has a wide range of applications. Due to its brightness and very high refractive index, most of titanium dioxide is used as white pigment [6]. Approximately 95% of titanium usage is accounted for in the titanium dioxide pigment industry [7]. Titanium dioxide can also be used in the air and water purification industry since it behaves as a photo-catalyst under ultraviolet (UV) light [8, 9].

The raw materials for titanium and titanium dioxide production are mainly ilmenite ($FeTiO_3$) and rutile (TiO_2). Ilmenite is considered as the major source for titanium, and rutile is utilized on a commercial scale [7]. There are currently four main producers worldwide of titanium dioxide. These are QIT-Fer & Titane Inc. (QIT, Canada), Richards Bay Minerals (RBM, S. Africa), Exxaro (S. Africa) and TiZir Titanium & Iron AS (TTI), formerly Eramet Titanium & Iron (ETI, Norway) [10]. RioTinto owns the first two.

The smelting of ilmenite among those producers is a carbothermal reduction process in an electric arc furnace. Detailed description of producers is not widely known due to keeping their technologies a secret. However, their smelting principles are similar: The iron in the molten ilmenite is reduced by carbon to yield liquid metallic iron and titanium oxide rich slag phase, where the slag produced serve as a raw material for pigment or titanium metal production [11].

In this chapter, the raw materials, ilmenite and rutile, are introduced along with their different smelting technologies. Moreover, the pre-reduction step in the Tyssedal Process, which is the ilmenite smelting technology done by TTI, Norway is emphasized. The Tyssedal Process carries a unique pre-reduction step of ilmenite prior to smelting, and the impact of impurity (Magnesium, Mg) during this step is of interest in this work.

1.1 Raw Materials

1.1.1 Ilmenite

Ilmenite as an iron-titanium oxide mineral with the idealized formula, $FeTiO_3$, is one of the major titanium dioxide containing minerals from which titanium metal and titanium dioxide is produced [12]. Ilmenite deposits can be found worldwide, and there are two types of ilmenite deposits that are utilized today: hard rock deposits and beach sand deposits. The two main hard rock deposits that are being mined today are the Lac Allard mine in Quebec, Canada and the Tellnes mine in Rogaland, Norway, and the beach sand deposits are mined mostly in Australia, South Africa and India among others [10]. Both deposits contain various impurity elements such as Mg, Mn, V, Cr, Al, Si, etc., with different amounts according to its local weathering. Beach sand deposits usually have a lower iron and impurity content due to the weathering of ilmenite, which will wash out impurities and lighter metals [13]. Due to the impurities found in ilmenite, the chemical formula of ilmenite may be more fully expressed as $(Fe, M)TiO_3$ where, M is the impurity element. Usually, the impurities are Mg, Mn and Cr because they may substitute for Fe or Ti in the original ilmenite lattice [14]. For example, the Norwegian ilmenite contains a significant amount of Mg [15], and can be simply expressed as $(Fe, Mg)TiO_3$. More details considering Mg in ilmenite is discussed later in this thesis.

1.1.2 Rutile

Rutile is a mineral composed mostly titanium dioxide with few impurities and is a far richer source of titanium dioxide than ilmenite [10]. This makes rutile favorable for raw material choice for production of titanium products. In 2008, most of the mining was done in Republic of Sierra Leone (W. Africa) and had a production capacity of 30% of the world's annual rutile supply [16]. However, the world reserves are limited and the worldwide production of rutile is approximately only a tenth of the ilmenite production [7]. Rutile is not found in large quantities and has less importance in the titanium industry than ilmenite.

1.2 Ilmenite Smelting

1.2.1 Direct feed of ilmenite into EAF (Electric Arc Furnace) – Canada & S. Africa

In QIT (Canada), RBM and Exxaro (S. Africa), a charge of ilmenite ore and coal is directly put into an electric arc furnace. The smelting is done by supplying an electric power source through the carbon electrodes. The furnaces at QIT and RBM are operated on an AC power source, and the process is operated with 6 graphite electrodes placed in line in a rectangular shell. At Exxaro, a single graphite electrode is placed in the center of a cylindrical furnace shell and a DC power source is used [10].

The carbothermal reduction of the ilmenite for these producers can be simply illustrated by **Reaction (1)**.

$$FeTiO_3 + C = Fe_{(l)} + TiO_{2\,(slag)} + CO_{(g)} \qquad \textbf{(1)}$$

The reduction of ilmenite gives a melt consisting a liquid iron phase and a titanium dioxide rich slag phase [17].

The tapping is done by using the difference of the specific gravity of both phases. The approximate specific gravity of liquid iron and titanium dioxide rich slag is about 7.0 g/cm^3 and 4.5 g/cm^3, respectively. Since the specific gravity of liquid iron is higher than the titanium dioxide rich slag, liquid iron will settle down at the bottom and titanium dioxide rich slag will be floating on the top. This separation of liquid iron and titanium oxide rich slag enables tapping at different levels.

After tapping, the liquid iron is desulphurized and alloyed with carbon and silicon to the desired quality before casted into billets (or pigs), and the liquid titanium dioxide rich slag is further cooled and crushed to a desired size [18].

1.2.2 The Becher Process – Australia

The Becher Process was patented in 1963 in Australia by Becher (Aust. pat. 247110) as cited by Becher et al [19]. This process is an extraction method for upgrading ilmenite from 55% TiO_2 to about 94% TiO_2 by reducing with coal. First, an ilmenite feed is put into a rotary kiln and heated in air at about 1000℃ to be oxidized into ferric pseudobrookite ($Fe_2^{3+}TiO_5$). Then pseudobrookite is reduced with coal in another rotary kiln at the temperature of approximately 1100℃. This carbothermic reaction reduces the iron in the pseudobrookite to the metallic iron. The oxidation and reduction of ilmenite at each temperature is shown in **Reactions (2)**, **(3)** and **(4)**. More details concerning oxidation and reduction of ilmenite are documented in the theory part of this thesis.

$$4FeTiO_3 + O_{2\,(g)} = 2Fe_2TiO_5 + 2TiO_2 \qquad (T > 800℃) \qquad \textbf{(2)}$$

$$Fe_2TiO_5 + TiO_2 + CO_{(g)} = 2FeTiO_3 + CO_{2\,(g)} \qquad (T \sim 1100℃) \qquad \textbf{(3)}$$

$$FeTiO_3 + CO_{(g)} = Fe + TiO_2 + CO_{2\,(g)} \qquad (T \sim 1100℃) \qquad \textbf{(4)}$$

Next, the reduced ilmenite is leached in water and air heated in a stainless steel vessel. The heating causes oxidation of metallic iron into a form of $Fe(OH)_2$, which is a form of iron rust, and the separation of this rust is easily done by simple decantation. The remaining result is a product of about 94% TiO_2 and referred as synthetic rutile.

However, the iron content of the ilmenite is not recovered as it is in the smelting operation. Also, the process requires a relatively pure ilmenite (especially low Mg and Mn content), as the impurities will lower the degree of iron reduction [20].

1.2.3 The Tyssedal Process – Norway

The Tyssedal Process is a unique ilmenite smelting process, which is only operated in Tyssedal, Norway. This process consists of two main steps: Pre-reduction step and Smelting step. The simplified flow sheet for the Tyssedal Process is shown in **Figure 1.1**.

In the pre-reduction step, ilmenite ores are initially fed in a wet ball mill and ground to a suitable size for pelletization. Then the ground ilmenite slurry is filtrated and leaves a filtered cake with about 10% moisture. The filter cake is mixed with a binder (0.8% bentonite), and pelletization is done by a pelletizing drum. Since the green pellets are very fragile and they require sufficient strength to remain intact through a rotary kiln, a heat treatment is necessary and the green pellets are fired. Next, the fired pellets are further fed to a rotary kiln along with coal to be pre-reduced. In the rotary kiln, the temperature is approximately 1100℃. From the gasification of coal, CO gas will reduce the iron oxides in the ilmenite to metallic iron. However, there has been indication that impurities in ilmenite affect the reduction kinetics and mechanisms during pre-reduction [21]. More details about the pre-reduction step and the influence of Mg as the main impurity are documented in the theory part. After the pre-reduction, the ilmenite pellets have pre-reduced to metallic iron and rutile. Then the pre-reduced pellets are cooled down in a rotary cooler in a reducing atmosphere for preventing re-oxidation and are ready for smelting.

In the smelting step, a charge of pre-reduced pellets and reductants (coke, char, coal, etc.) is fed into an electric arc furnace. The pellets are melted by the high heat from the electric arc, and the reduction of the remaining unreduced ilmenite from the pre-reduction will occur in the furnace [18]. Then the liquid iron and titanium dioxide rich slag will separate into two layers due to the difference in specific gravity. The tapping of liquid iron and titanium dioxide rich slag is similar which was briefly explained in **Section 1.2.1**.

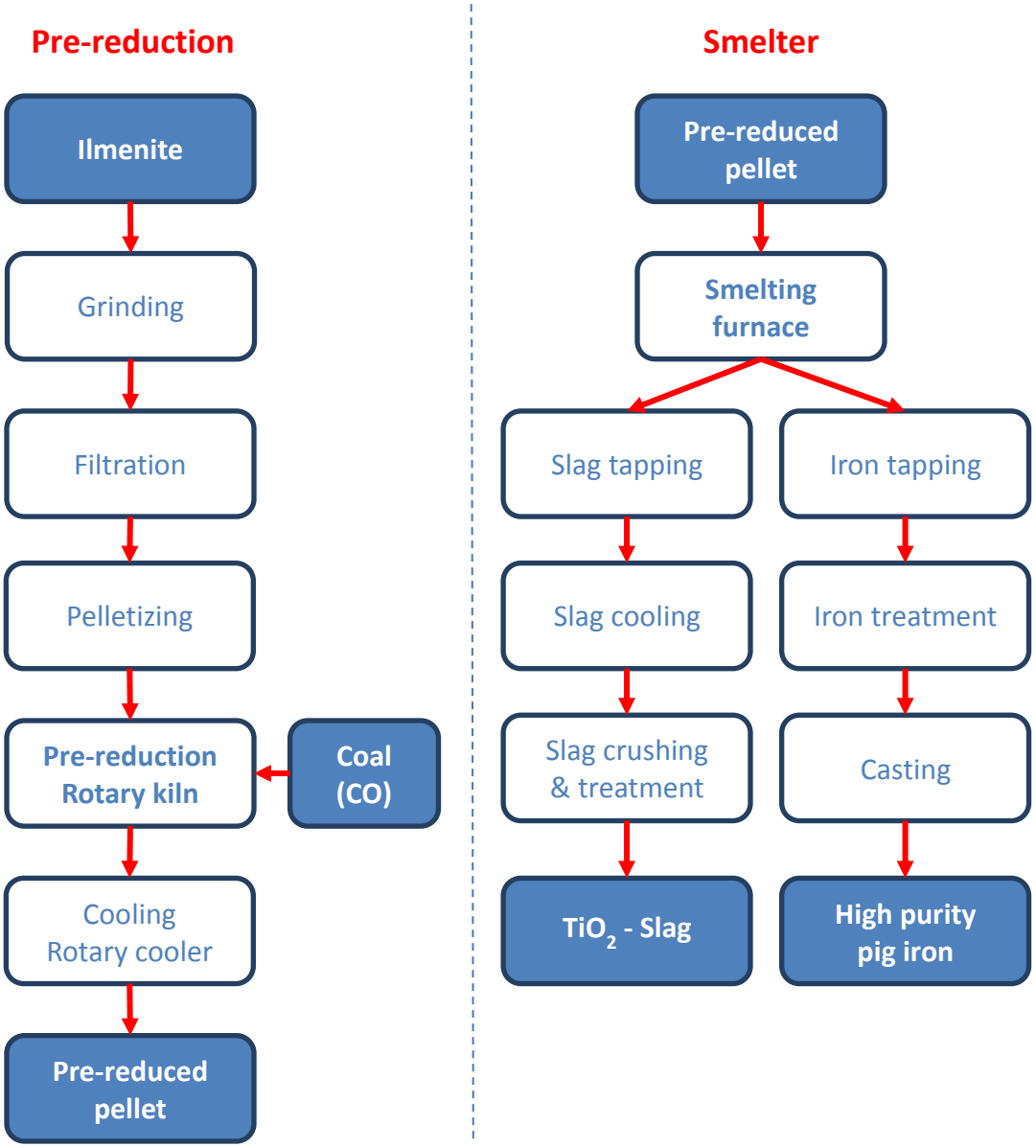

Figure 1.1 Simplified flow sheet for the Tyssedal Process [18]

1.3 Objectives & Outline of the thesis

1.3.1 Objectives

The main objective of this work is to isolate the impact of impurity while solid-state reduction of ilmenite during the pre-reduction step (Tyssedal Process). Since natural ilmenite contains several kinds of impurities with different amounts, the focus will be on the synthesis, oxidation and reduction of synthetic impurity-rich ilmenite to isolate the impact of impurity in ilmenite. Mg will be the impurity in question because the Norwegian ilmenite used in the Tyssedal Process contains a significant amount of Mg [15]. In addition, the use of H_2 gas in reduction will also be handled in this thesis to find the impact of hydrogen as additional reductant gas.

This work was done in cooperation with co-student Sondre Norhaug who shares the similar research area. Magnesium as impurity in ilmenite was studied by the author, whereas excess-iron as impurity in ilmenite was studied by Norhaug. As a mutual reference point for further comparison, the author and Norhaug have collaborated in making pure synthetic ilmenite.

- Main Objective: Isolating the impact of magnesium in ilmenite during solid-state reduction with CO and H_2 gas.

- Sub Objectives: Synthetic Mg-rich ilmenite ore production.
  Finding the impact of H_2 gas as an additional reductant.

1.3.2 Outline of the thesis

Chapter 1 was the introduction part where raw materials and production of TiO_2 in general were explained. The pre-reduction step in the Tyssedal Process was focused to give an overall introduction of the project work.

Chapter 2 explains the related theories for synthetic ilmenite ore along with Mg as impurity. The synthesis, oxidation and reduction of synthetic ilmenite are described with thermodynamic data such as phase diagrams. The following chapters will also depict its part according to each synthesis, oxidation and reduction.

Chapter 3 describes the experimental set-up of this thesis work. Laboratory equipment used for each synthesis, oxidation and reduction are depicted in details with figures, and experimental parameters are shown with calculation. Detailed procedures of each equipment and parameter calculations are further explained in appendices.

Chapter 4 presents the results obtained from the experimental work from each synthesis, oxidation and reduction. Analyses from chapter 3, such as XRD and EPMA results, are shown for each part, and reduction results are described as conversion degree curves.

Chapter 5 discusses the experimental results from each synthesis, oxidation and reduction. Interpretation and discussion of each part are based on the theory in chapter 2. In addition, future work is also briefly introduced for achieving further objectives.

Chapter 6 summaries the thesis work by listing conclusion of each synthesis, oxidation and reduction in bulleted list.

Chapter 2 Theory

In order to isolate the impact of Mg in ilmenite during pre-reduction, the first step is to understand the ilmenite crystal structure and how different kinds of impurities associate in the host. Although the type and amount of impurity differs from location and is dependent to its local weathering, the Norwegian ilmenite, which contains a significant amount of Mg, is explained [15].

Next, theoretical background concerning synthesis, oxidation and reduction of synthetic ilmenite is documented in this chapter. For synthesis, the Fe-Ti-O ternary system and the FeO-TiO_2-MgO ternary system are described by phase diagrams. The main focus will be the synthesis of the $FeTiO_3$-$MgTiO_3$ (M_2O_3) solid solution. The oxidation path of ilmenite is mainly described by the Fe-Ti-Mg-O quaternary system. The Fe-Ti-Mg-O quaternary system is conveniently illustrated by a three-dimensional sketch, and further details concerning the phase transition according to reaction temperature are explained. The reduction section contains a detailed description of the pre-reduction step in the Tyssedal Process prior to reduction and the theoretical reduction stages of oxidized ilmenite.

Lastly, the effect of hydrogen (H_2) gas as an additive to reduction is considered. There have been studies indicating that H_2 gas is a better reducing agent than CO gas alone [21-23]. The use of H_2 gas in the pre-reduction step is likely to enhance the reduction degree.

2.1 Ilmenite crystal structure & impurities

2.1.1 Ilmenite crystal structure

The ilmenite crystal structure crystallizes in the trigonal system [24]. The crystal structure of ilmenite is similar to hematite but with distortion in the oxygen layers. The crystal structure of hematite and ilmenite is shown in **Figure 2.1**.

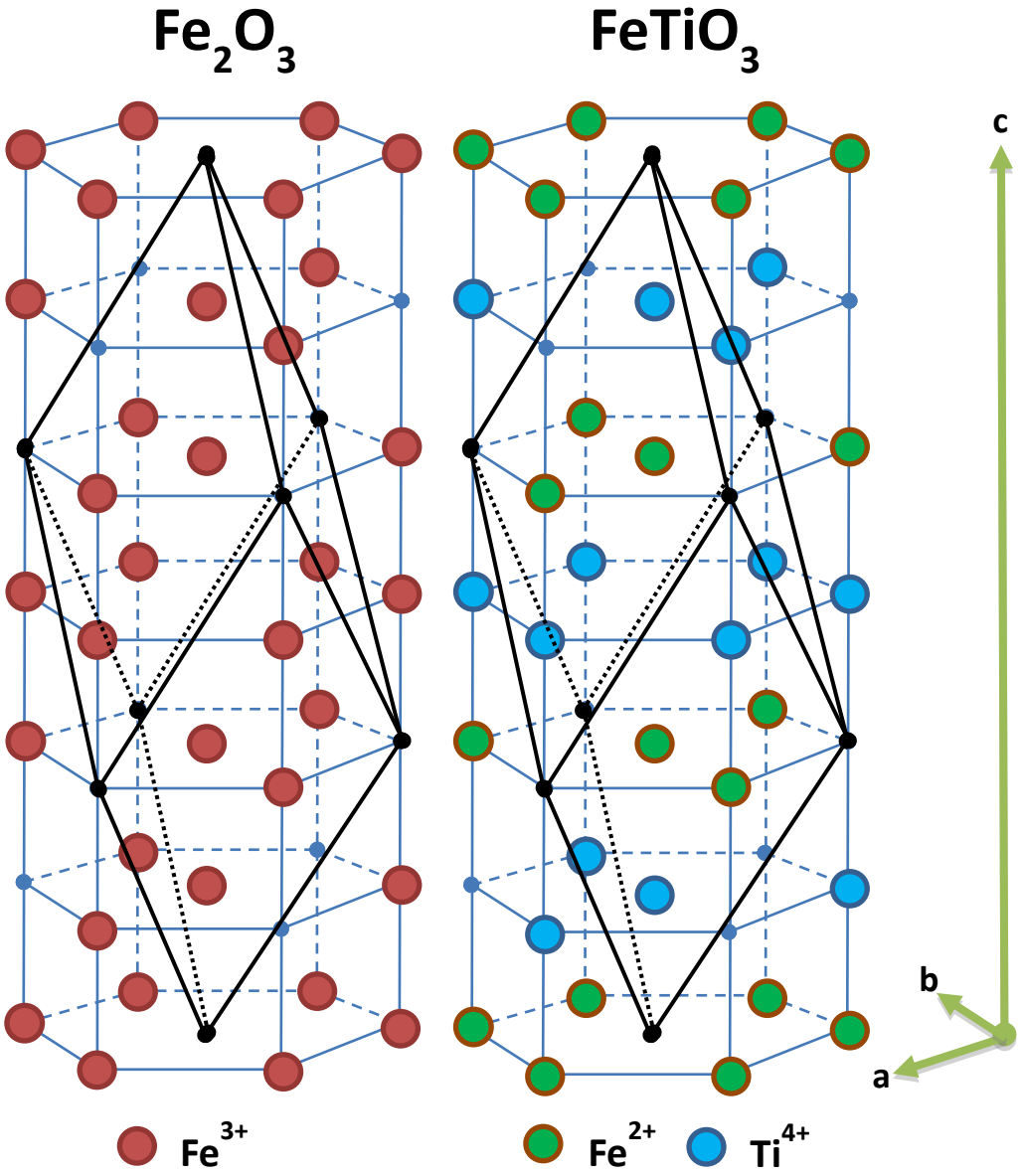

Figure 2.1 Crystal structure of hematite and ilmenite [25]

The cations in hematite layers are all identical but in ilmenite, the Ti^{4+} ions alternate with pairs of the Fe^{2+} ions along the direction of the triad axis: each cation layer in an ilmenite crystal is a mixture of Ti^{4+} ions and Fe^{2+} ions. Thus, the chemical formula of impurity free ilmenite may be fully expressed as $Fe^{2+}Ti^{4+}O_3$. The lattice parameters for hematite and ilmenite are a = 5.038 Å, c = 13.772 Å and a = 5.088 Å, c = 14.092 Å, respectively [25].

2.1.2 Impurities

Unlike stoichiometric ilmenite ($FeTiO_3$), natural ilmenite contains various elements, such as Mg, Mn, V, Cr, Al, Si, etc., with different amounts according to its local weathering. The chemical composition of natural ilmenite differs according to location. **Table 2.1** shows a list of natural ilmenite ore with different chemical composition. The ilmenite ores in **Table 2.1** are from Allard lake ilmenite deposits (Canada), southeast coast of Africa (S. Africa), Murray Basin (Australia) and Tellnes mine (Norway).

Table 2.1 Chemical composition of ilmenite ores among different location [wt%] [21, 26, 27]

Canada	**TiO_2**	**Fe**	**S**	**Mn**	**Cu**	**Ni**	**Co**	**V**	**P_2O_5**
	36.0	42.8	0.4	0.08	0.12	0.01	0.013	0.21	0.01

S. Africa	**TiO_2**	**Fe**	**C**	**MnO**	**CaO**	**SiO_2**	**Al_2O_3**	**Cr_2O_3**	**V_2O_5**	**Nb**	**P_2O_5**	**ZrO_2**
	47.0	35.0	0.03	1.10	0.06	1.11	0.42	0.13	0.17	0.03	0.02	0.08

Australia	**TiO_2**	**FeO**	**Fe_2O_3**	**MnO**	**CaO**	**SiO_2**	**Al_2O_3**	**Cr_2O_3**	**V_2O_5**	**Nb_2O_5**	**P_2O_5**	**ZrO_2**
	51.7	23.1	17.6	1.59	0.12	1.31	1.41	0.04	0.13	0.18	0.03	0.08

Norway	**TiO_2**	**Fe**	**MnO**	**MgO**	**CaO**	**SiC**	**Al_2O_3**	**Cr_2O_3**	**V_2O_5**	**Nb**	**P_2O_5**	**ZrO_2**
	43.7	35.6	0.31	3.70	0.27	2.25	0.56	0.096	0.19	0.005	0.016	0.05

Among the impurities in ilmenite, Mg^{2+}, Mn^{2+}, and V^{4+} can be considered as the most important ions due to their subtle differences in ionic radii. The radii of these ions are Mg^{2+} (0.720 Å) < Fe^{2+} (0.780 Å) < Mn^{2+} (0.830 Å) and V^{4+} (0.580 Å) < Ti^{4+} (0.605 Å). Substitution of Fe^{2+} with Mg^{2+} or Mn^{2+} and Ti^{4+} with V^{4+} is likely to occur during the weathering of ilmenite. Recent studies have confirmed that Mg^{2+} and Mn^{2+} are mainly substituted for Fe^{2+} and V^{4+} is substituted for Ti^{4+} [28, 29]. The other minor impurity elements such as Al, Si, Ca, P, Zr, etc. are commonly incorporated into the ilmenite grains during chemical weathering and they will not be further discussed in this thesis.

Considering the Norwegian ilmenite, which contains a significant amount of Mg [15] (about 4.6 wt% MgO), Mg plays an important role in the ilmenite crystal structure. Since the ionic radius of Mg^{2+} is lower than the ionic radius of Fe^{2+}, the substitution of Fe with Mg decreases the lattice parameters and cell volume of ilmenite. The partly Mg substituted ilmenite is ($FeTiO_3$)-$MgTiO_3$ which is also called geikielite [30]. The lattice parameters for ideal ilmenite are a = 5.088 Å, c = 14.092 Å and for geikielite are a = 5.086 Å, c = 14.093 Å. The cell volume for stoichiometric ilmenite and geikielite is 315.839 $Å^3$ and 315.573 $Å^3$, respectively. The substitution of Mg in the ilmenite structure also significantly decreases the specific gravity. This is in good agreement with the specific gravity of Mg and Fe, which are as follows: Mg (1.738 g/cm^3) < Fe (7.874 g/cm^3) [29].

2.2 Synthesis

2.2.1 Synthetic ilmenite

Synthetic ilmenite will be considered as a reference material regard to the synthetic Mg-rich ilmenite in this thesis. The preparation of synthetic ilmenite was studied earlier at the Norwegian University of Science and Technology (NTNU) by Canaguier during his master's thesis [31]. The synthesis of ilmenite was based on the previously studied Fe-Ti-O system [32-34], which is shown in **Figure 2.2**. At the temperature of 1200℃, four areas have been reported to be stable.

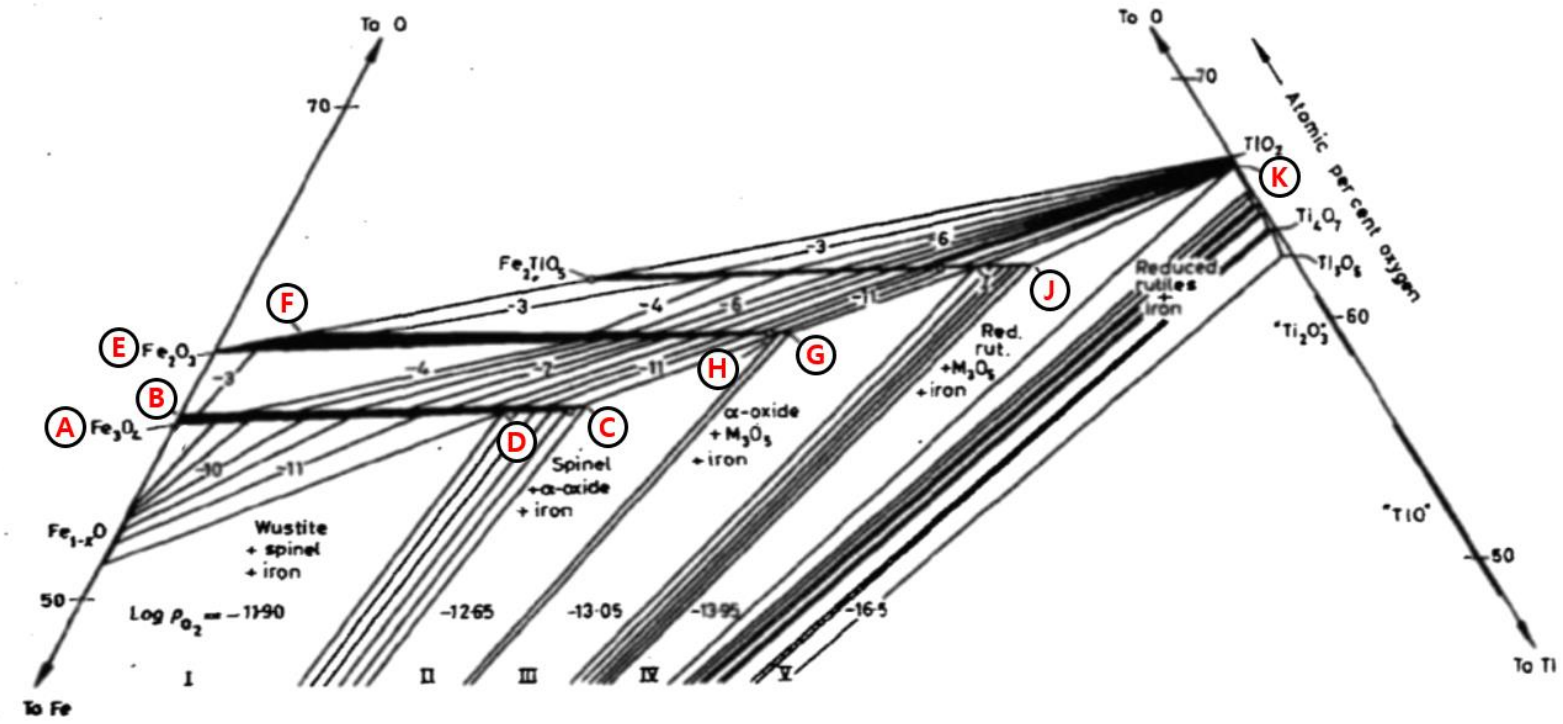

Figure 2.2 Partial phase diagram for Fe-Ti-O system at 1200℃ [33]

1. *The Spinel solid solution*

The spinel solid solution is limited between magnetite (Fe_3O_4), cation-deficient magnetite ($Fe_{2.95}O_4$) and ulvöspinel (Fe_2TiO_4) [35]. The first two phases are points A and B, respectively, where both points lie on the Fe-O binary line. Point C is assumed to be cation-deficient ulvöspinel ($Fe_{1.95}Ti_{1.02}O_4$) and this may be expressed as a solution of ilmenite in ulvöspinel $(Fe_2TiO_4)_{0.913}$-$(FeTiO_3)_{0.087}$. Point D between the point A and ulvöspinel represents the composition of the spinel that is simultaneously in equilibrium with wüstite and metallic iron. The boundary BC defines the limit of non-stoichiometry of the spinel, which can be slightly iron-deficient. The extent of non-stoichiometry is seen to decrease with increasing titanium content.

2. *The α-oxide solid solution*

The α-oxide solid solution is limited by the hematite (Fe_2O_3), which is point E on the Fe-O binary line. Point F is rutilic hematite $(Fe_2O_3)_{0.87}$-$(TiO_2)_{0.13}$ and is slightly moved towards TiO_2 because this solid solution shows solubility for rutile (TiO_2). This solubility for rutile decreases with increasing titanium content in the α-oxide solid solution. The α-oxide solid solution extends partly towards Ti_2O_3, which is the terminal composition, point G ($Fe_{0.97}Ti_{1.03}O_3$). Point H is found to be $Fe_{0.98}Ti_{1.02}O_3$, and at this point on the boundary of the single-phase α-oxide region metallic iron, α-oxide and spinel coexist at equilibrium.

3. *The M_3O_5 solid solution*

The M_3O_5 solid solution is continuous between Fe_2TiO_5 and reduced rutile (TiO_{2-x}). The corners of this area are Fe_2TiO_5, $FeTi_2O_5$, point I ($Fe_{0.90}Ti_{2.10}O_5$) and point J ($Fe_{0.02}Ti_{2.98}O_5$). This solid solution consists the Fe_2TiO_5 and $FeTi_2O_5$ compounds, and the area widens with decreasing temperature.

4. *The Magnéli phase* [36]

The Magnéli phase is displayed at point K and is obtained at oxygen partial pressures lower than 10^{-14} atm. In this condition, pure iron appears to be stable with reduced rutile phase. The iron is presented in a ferrous form, and the compositions can be considered as solid solutions between the Magnéli phases (Ti_nO_{2n-1}) and their ferrous iron counterparts ($FeTi_{n-1}O_{2n-1}$).

From these areas, an ideal of how ilmenite with other species related to each other is provided. By setting an experimental assumption, Canaguier was able to make synthetic ilmenite by using a cold crucible induction furnace with Ar atmosphere [31]. Assuming a melt containing chemical elements in proportions corresponding to the stoichiometric composition of ilmenite, the result after cooling was determined. The materials used were iron (Fe), hematite (Fe_2O_3) and rutile (TiO_2) and the synthesis reaction is shown in **Reaction (5)**.

$$Fe + Fe_2O_3 + 3TiO_2 = 3FeTiO_3 \quad \textbf{(5)}$$

2.2.2 Synthetic Mg-rich ilmenite: $FeTiO_3$-$MgTiO_3$ (M_2O_3) solid solution

In order to investigate the influence of Mg in ilmenite during pre-reduction, it is crucial to have Mg in the ilmenite crystal structure. In other words, synthesizing the $FeTiO_3$-$MgTiO_3$ (M_2O_3) solid solution, where Mg substitutes the Fe in the ilmenite crystal structure, is the initial task of the investigation.

The FeO-TiO_2-MgO system, which has been studied in detailed by Borowiec and Rosenqvist previously [15], can be useful for synthesizing the $FeTiO_3$-$MgTiO_3$ solid solution. The phase diagrams of this system for temperatures of 1100, 1000, and 900℃ are shown in **Figures 2.3-5**.

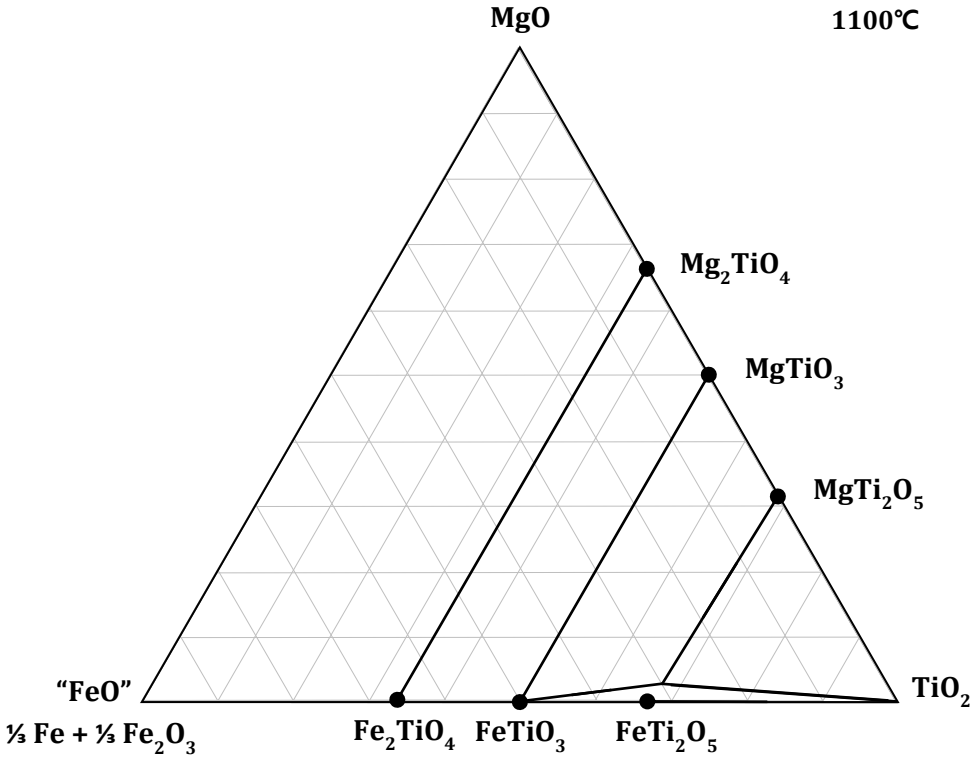
MgO
1100℃
Mg_2TiO_4
$MgTiO_3$
$MgTi_2O_5$
"FeO"
⅓ Fe + ⅓ Fe_2O_3
TiO_2
Fe_2TiO_4
$FeTiO_3$
$FeTi_2O_5$

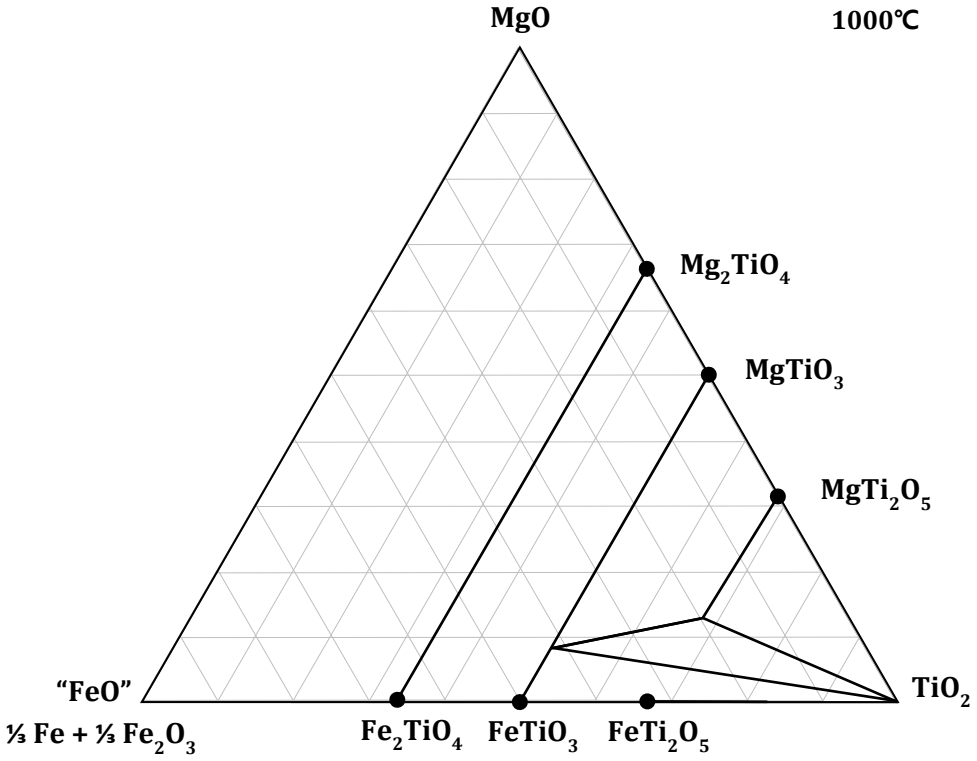
MgO
1000℃
Mg_2TiO_4
$MgTiO_3$
$MgTi_2O_5$
"FeO"
⅓ Fe + ⅓ Fe_2O_3
TiO_2
Fe_2TiO_4
$FeTiO_3$
$FeTi_2O_5$

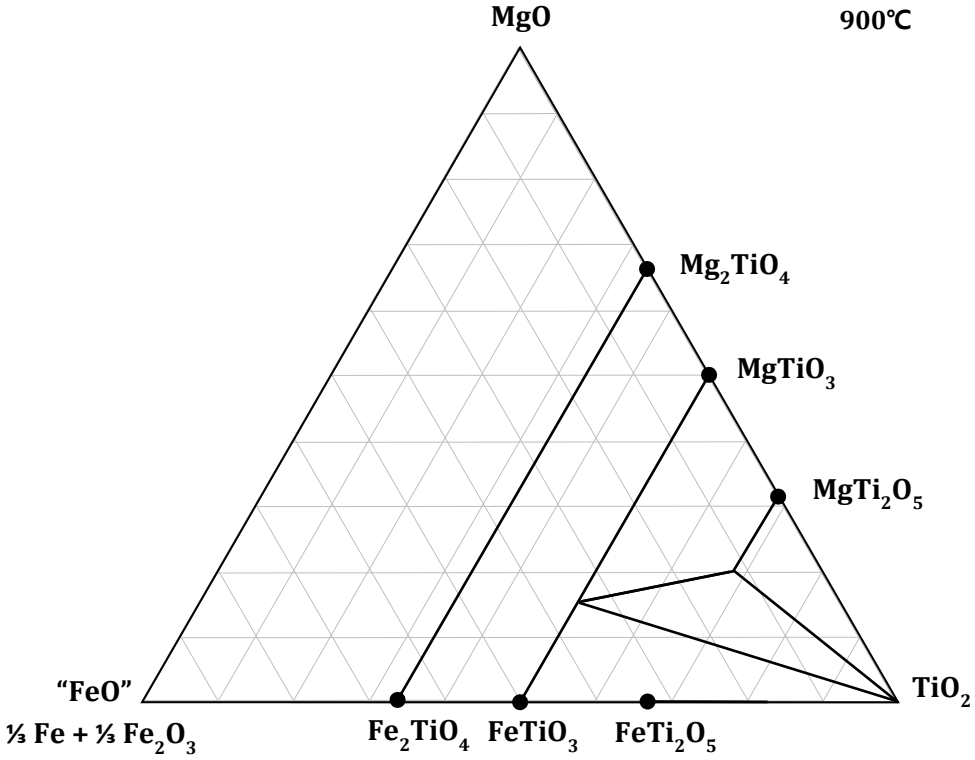

Figure 2.3-5 The FeO-TiO_2-MgO systems at 1100, 1000 and 900℃ [15]

Considering the Mg amount of the Norwegian ilmenite, the target synthesis should satisfy two conditions. First, the synthesis should be on the Alkemade line, which connects the $FeTiO_3$ phase and $MgTiO_3$ phase, in order to have the $FeTiO_3$-$MgTiO_3$ solid solution as the target compound. Second, the synthesis should be close to the $FeTiO_3$ phase, because the Norwegian ilmenite has a Mg/Ti ratio of about 0.2 [15]. The lower part on this Alkemade line, which is the part under the three-phase triangle, is an example.

Another aspect to consider for synthesis is the $FeTi_2O_5$-$MgTi_2O_5$ (M_3O_5) solid solution. In the figures above, a three-phase area exists on the lower right of each diagram. This area corresponds to a mixture of $FeTiO_3$-$MgTiO_3$ solid solution, $FeTi_2O_5$-$MgTi_2O_5$ solid solution and TiO_2. In the $FeTi_2O_5$-$MgTi_2O_5$ solid solution, the ferrous pseudobrookite ($Fe^{2+}Ti_2O_5$) phase should be avoided.

The ferrous pseudobrookite phase tends to decompose into a two-phase combination of M_2O_3+TiO_2 at temperature range of 900-1100℃. The concentration of $MgTiO_3$ in the $FeTiO_3$-

$MgTiO_3$ solid solution, which can coexist with TiO_2, increases with decreasing temperature [15]. However, previous studies show indications of the ferrous pseudobrookite phase being stabilized by Mn^{2+} or Mg^{2+} ions during gaseous reduction with CO gas [37, 38]. The stabilization of the M_3O_5 phase by Mn or Mg is likely to retain the iron in the oxide phase and thus results in a lower degree of iron conversion. More details considering the gaseous reduction of ilmenite and the conversion degree are documented in **Section 2.4** and **3.3**.

From the considerations for Mg-rich ilmenite synthesis, the three-phase area should be avoided to ensure the synthesis of the $FeTiO_3$-$MgTiO_3$ solid solution. To avoid this area, a slow cooling of the melt can be useful. The three-phase area at temperature of 1100℃, as in **Figure 2.3**, shifts upward towards the $MgTi_2O_5$ phase with decreasing temperature. **Figure 2.6** shows the three-phase area shifting towards the $MgTi_2O_5$ phase as the temperature decreases. The lower part of the $FeTiO_3$-$MgTiO_3$ solid solution's Alkemade line then exists below the three-phase area. The method of slow cooling of melt is further explained in **Section 3.1.3**.

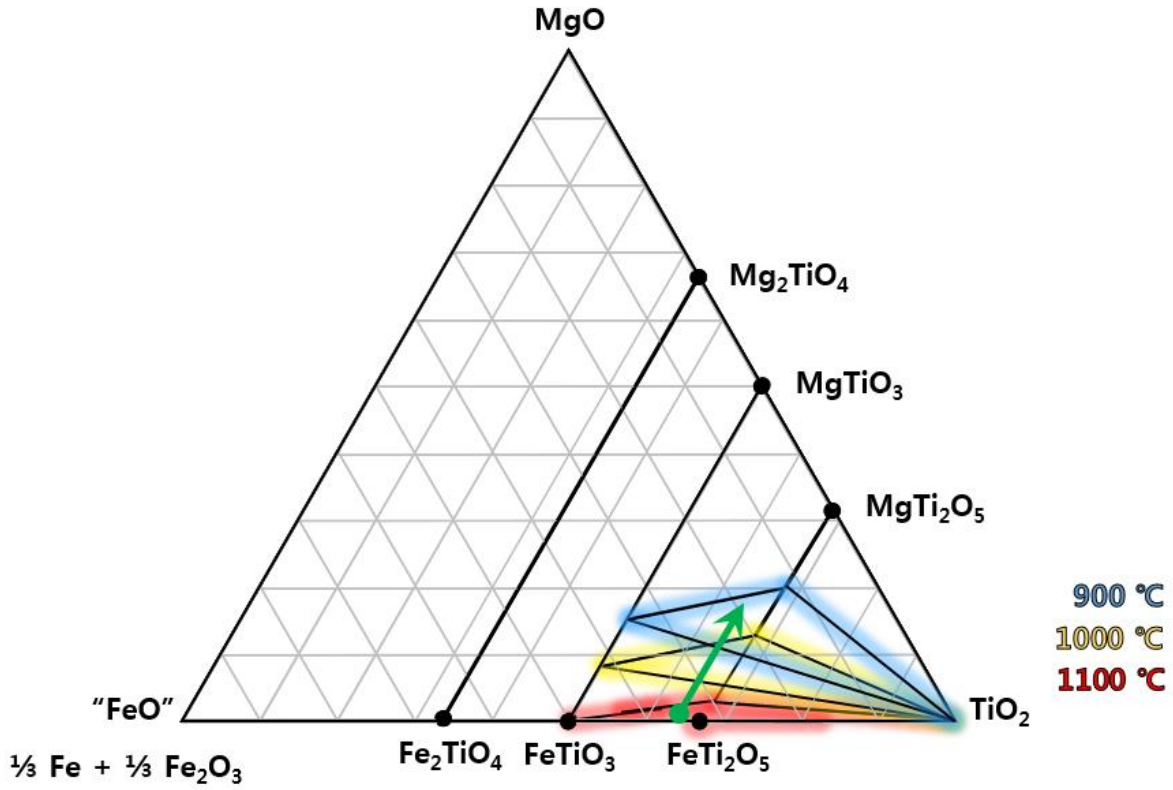

Figure 2.6 The three-phase area shifting towards the $MgTi_2O_5$ phase by decreasing temperature in the FeO-TiO_2-MgO system at 1100, 1000 and 900℃

2.3 Oxidation

2.3.1 The benefits of oxidation

The oxidation of ilmenite prior to reduction is considered to be beneficial for two main reasons. First, the oxidation of ilmenite is likely to give a better overall reduction. Previous studies show that oxidizing ilmenite leads to a better overall reduction degree [39-41]. It has been suggested by Jones that the iron in ilmenite becomes homogeneously distributed throughout the oxide grains such that when it is reduced there is less agglomeration of iron around the grain boundaries and reduction is not hindered by diffusion through iron shells [40]. Second, pelletized ilmenite is too fragile to be handled for reduction experiment. After synthesizing bulk ilmenite, it is ground into fine powder and pelletized into small pellets. Green pellets are very fragile and they require heat treatment prior to reduction. The ilmenite pellets should be intact through the remaining experiments. A more detailed description of pelletizing is presented in **Section 3.2.1**.

2.3.2 Oxidation of ilmenite

The phase transition of ilmenite during oxidation in different temperatures has been studied previously. Below the temperature of 800℃, ilmenite will oxidize to form hematite (Fe_2O_3), or pseudorutile ($Fe_2Ti_3O_9$), according to **Reactions (6)** and **(7)** [42].

$$4FeTiO_3 + O_{2\,(g)} = 2Fe_2O_3 + 4TiO_2 \quad \textbf{(6)}$$

$$12FeTiO_3 + 3O_{2\,(g)} = 2Fe_2O_3 + 4Fe_2Ti_3O_9 \quad \textbf{(7)}$$

The rate of **Reaction (6)** is faster than **Reaction (7)**, and rutile with hematite are the main products in the relatively low temperature oxidation. For **Reaction (7)**, the formation rate of pseudorutile increases slightly with increasing oxygen partial pressure, and it has been reported that pseudorutile may be an intermediate product, which only exists in the relatively low temperature oxidation process [43].

Above the temperature of 800℃, ilmenite will oxidized to form mainly ferric pseudobrookite ($Fe_2^{3+}TiO_5$) and rutile, according to **Reactions (8)** and **(9)** [44].

$$4FeTiO_3 + O_{2\,(g)} = 2Fe_2TiO_5 + 2TiO_2 \quad \textbf{(8)}$$

$$Fe_2Ti_3O_9 = Fe_2TiO_5 + 2TiO_2 \quad \textbf{(9)}$$

At the temperature higher than 800℃, pseudobrookite is known to be the stable phase: the crystal lattices of rutile, hematite and pseudorutile disintegrate and a new pseudobrookite crystal phase is formed [43]. Pseudorutile at this temperature is not stable as mentioned before and is considered as an intermediate phase, which will decompose into pseudobrookite and rutile.

From **Reactions (8)** and **(9)**, the complete oxidation of ilmenite at temperature higher than 800℃ implies that ferric pseudobrookite and rutile are the final products. Note that all the iron in ilmenite is now in the ferric (Fe^{3+}) state in pseudobrookite ($Fe_2^{3+}TiO_5$). The ferric state of iron is also the key mechanism for iron to become homogeneously distributed throughout the oxide grains as mentioned in **Section 2.3.1**. The tentative mechanism is illustrated in **Figure 2.7**, and it has been suggested that iron is mobile towards the interface layer where it is oxidized [45].

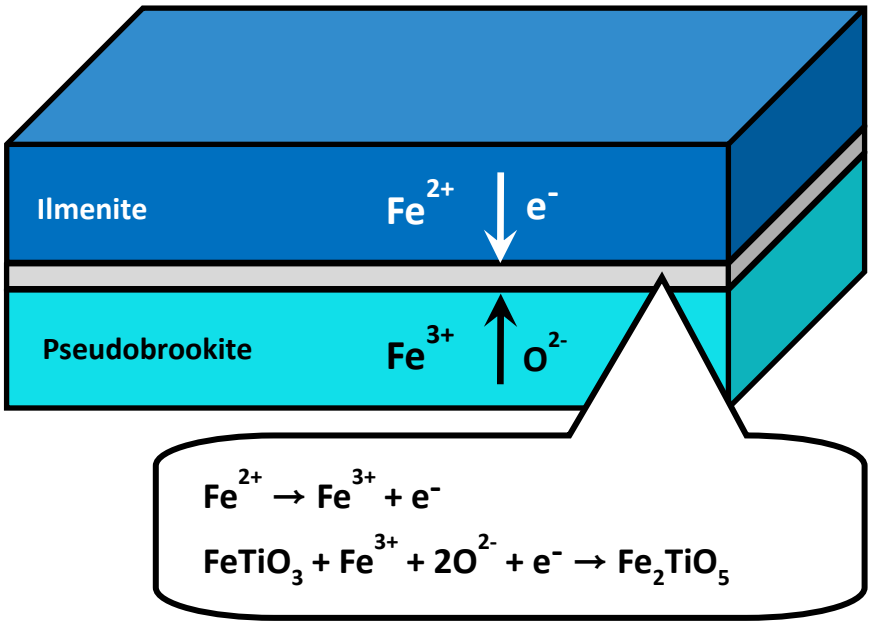

Figure 2.7 An illustration of proposed mechanism for oxidation of ilmenite: Pathway at high temperature (≥ 800℃) [43]

2.3.3 Oxidation of Mg-rich ilmenite

The Fe-Ti-Mg-O quaternary system, which is re-illustrated by a three dimensional sketch in **Figure 2.8**, can be useful to predict the phase transition during the oxidation of Mg-rich ilmenite. Borowiec and Rosenqvist have previously investigated the Fe-Ti-Mg-O system in detail [15].

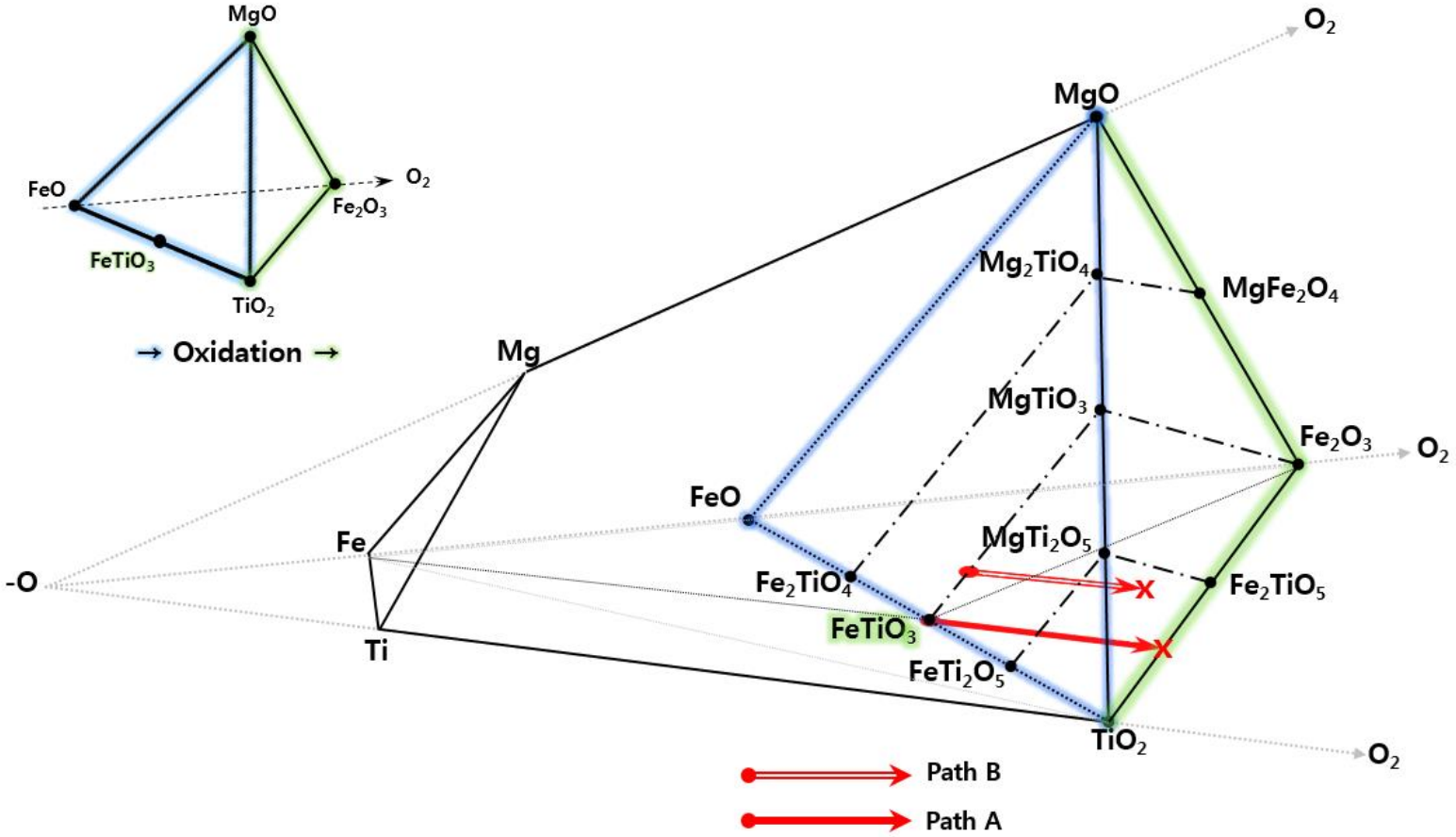

Figure 2.8 The re-illustrated Fe-Ti-Mg-O quaternary system [15]

The oxidation for a given composition of Fe-Ti-Mg is given by lines drawn through its composition and the point "-O". For instance, the oxidation of Fe will travel to the right side on its O_2 line to reach FeO and further Fe_2O_3. Mg and Ti will also travel to the right side of each O_2 line and reach MgO and TiO_2, respectively.

The likely oxidation path for both reference ilmenite (ilmenite without impurities) and Mg-rich ilmenite is also expressed in the Fe-Ti-Mg-O quaternary system. Assuming relatively high temperature oxidation (≥ 800 ℃), the reference ilmenite will follow "Path A" and reach the TiO_2-Fe_2O_3 binary system. The resulting product for a complete oxidation is a mixture of ferric pseudobrookite and rutile, which is the line between Fe_2TiO_5 and TiO_2. This is in a good agreement since ferric pseudobrookite is the new stable phase at temperatures higher than 800 ℃ as mentioned in **Section 2.3.2**. If the oxidation temperature was below 800 ℃, the new pseudobrookite phase will not be formed and the main product will be a mixture of hematite and rutile.

For the Mg-rich ilmenite, the oxidation path is thought to follow "Path B". The assumptions for "Path B" are temperature higher than 800 ℃ and Mg amount relating to the Norwegian ilmenite. The result of oxidation is considered to be on the Fe_2O_3-TiO_2-MgO system in the Fe-Ti-Mg-O quaternary system. The Fe_2O_3-TiO_2-MgO system at 1100 ℃ is shown in **Figure 2.9**.

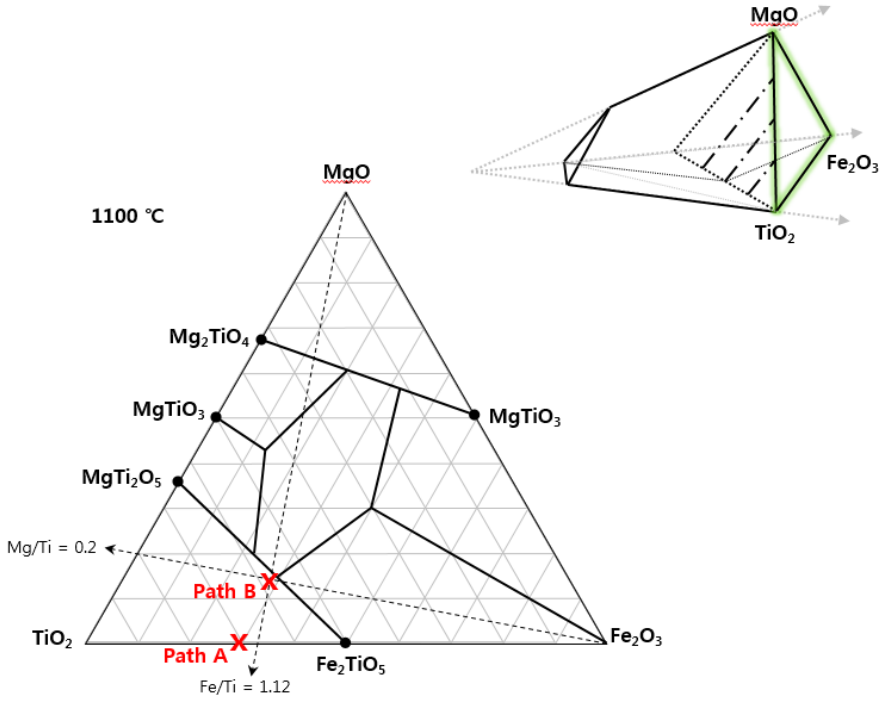

Figure 2.9 The Fe_2O_3-TiO_2-MgO system at 1100 ℃ [15]

According to the Norwegian ilmenite, the ratios Mg/Ti and Fe/Ti are 0.2 and 1.12, respectively. The end product for "Path B" is assumed to be a mixture of rutile, ferric pseudobrookite, and magnesium dititanate ($MgTi_2O_5$). Magnesium dititanate has a relativity high thermal stability among pseudobrookite-type phases [46], and it is assume to have detrimental impact towards reduction. More details concerning the impact of Mg in reduction will be explained in **Section 2.4.3**.

2.4 Reduction

2.4.1 The pre-reduction step in the Tyssedal Process

In this section, the pre-reduction step in the Tyssedal Process from **Section 1.2.3** will be further explained prior to the theoretical reduction of ilmenite. This part is mentioned to give a broad, yet clear understanding of the ilmenite reduction process.

After the ilmenite pellets have been harden by heat treatment, they are fed into a rotary kiln for pre-reduction. The pre-reduction of ilmenite in a rotary kiln is a solid-state reaction. This means the reaction proceeds as a gas-solid reaction between gases through the Boudouard reaction [47] where the gasification of coal is required. The Boudouard reaction is given by **Reaction (10)**.

$$CO_{2\,(g)} + C = 2CO_{\,(g)} \qquad \textbf{(10)}$$

The reaction mechanism of ilmenite pre-reduction can be described with the Boudouard reaction and **Reaction (11)**: The CO gas diffuses into the pellet and reduces ilmenite to metallic iron, rutile and CO_2 gas. The CO_2 gas then diffuses out of the pellet and into a coal particle, where it reacts with carbon to form new CO gas (Boudouard reaction). The combination of these two reactions yields the total reaction, which is shown in **Reaction (12)** [18].

$$FeTiO_3 + CO_{\,(g)} + Fe + TiO_2 + CO_{2\,(g)} \qquad \textbf{(11)}$$

$$FeTiO_3 + C = Fe + TiO_2 + CO_{\,(g)} \qquad \textbf{(12)}$$

The net CO gas produced in the reaction is of importance. Since the conversion degree, which is the amount of iron oxide that is reduced to metallic iron, is dependent on the amount CO_2 and CO gas, it is crucial to have a low CO_2 / CO ratio. This implies that the Boudouard reaction is influential in the pre-reduction step. The temperature in the pre-reduction step is above 1100 ℃, and the Boudouard reaction is almost completely shifted to the right side. In this thesis, the author will assume low CO_2 / CO ratio and will not consider factors influencing this ratio such as coal reactivity, age, origin, composition and etc. since pure CO gas was used in the experiment instead of coal. Considering the reduction method in this thesis, more details are explained in **Section 3.3**.

2.4.2 Reduction of ilmenite

The reduction of ilmenite with gaseous reductants, such as CO or H_2 gas, takes place in a number of stages. For pre-oxidized ilmenite, the starting point of reduction will be the ferric iron in pseudobrookite. According to previous studies, reduction begins by reducing ferric iron to ferrous iron and then reduction of ferrous iron to metallic iron [21, 22, 44]. The related reactions are shown by **Reactions (13)** and **(14)**. R represents the reductant gases, CO and H_2.

$$Fe_2TiO_5 + TiO_2 + R_{(g)} = 2FeTiO_2 + RO_{(g)} \quad \textbf{(13)}$$

$$FeTiO_3 + R = Fe + TiO_2 + RO_{(g)} \quad \textbf{(14)}$$

The first stage of reduction is expressed in **Reaction (13)**, where the ferric iron (Fe^{3+}) in pseudobrookite reduces to ferrous iron (Fe^{2+}) in ilmenite. This indicates that ilmenite is being reformed by a recombination-reduction mechanism, and the net result is described by **Reaction (13)**. Also, it has been reported previously by Jones that pseudobrookite reacts with the reductant, R (CO or H_2), to form ilmenite and the off-gas, RO (CO_2 or H_2O), according to **Reaction (13)** [44].

The second stage of reduction is described in **Reaction (14)**, where the ferrous iron (Fe^{2+}) in ilmenite reduces to metallic iron (Fe). In this stage, ilmenite reacts further with the reductant, R (CO or H_2), and assuming complete reduction of iron oxides, the final products are metallic iron and rutile according to **Reaction (14)**. This was also previously reported by Jones [44].

Beyond **Reaction (14)**, a third stage can be considered relating to the reduction of titanium oxide species. In prolonged reduction time or the use of higher H_2 content in reductant gases, reduction of rutile can reduced to reduced rutile species according to **Reaction (15)**.

$$TiO_x + R = TiO_{x-1} + RO_{(g)} \quad \textbf{(15)}$$

However, the mechanism of reduced rutile species is still ambiguous and there only have been few studies. In this thesis, details relating to this will not be further handled, but some facts and assumptions will be considered in **Section 2.4.4**.

2.4.3 Reduction of Mg-rich ilmenite

The starting point for pre-oxidized Mg-rich ilmenite is similar with pre-oxidized ilmenite but with an additional mixture of magnesium dititanate ($MgTi_2O_5$) according to **Figure 2.9**. Unlike the theoretical reduction of ilmenite, where the end product of complete reduction is metallic iron and rutile, the end product for the reduction of Mg-rich ilmenite is not likely to have the same result.

Previous studies show indications that impurity elements, such as Mg and Mn, allow the formation of other end products besides metallic iron and rutile. Lobo and colleagues have reported armalcolite, $(Fe,Mg)Ti_2O_5$, besides metallic iron and rutile after reduction of Norwegian ilmenite ores [21]. Grey and colleagues also have shown incomplete reduction due to the presence of Mg or Mn, which was thought to be the stabilization of the M_3O_5 phase [33]. These indications of incomplete reduction by impurity elements had been predicted by Jones before. Jones predicted that these impurity elements diffuse ahead of the reaction interface and displace iron in the oxide phase. Eventually, the thermodynamic activity of iron becomes so low that further reaction is not possible [48].

The impurity elements are believed to influence the reduction behavior of the ilmenite ore, but the exact reduction mechanism and effect of these impurities are not completely isolated due to the use of natural ilmenite ores. In this thesis, synthetic ilmenite ores are prepared and the comparison of the reduction behavior between natural ilmenite ore and synthetic ilmenite ore is mentioned. Then, it might be possible to isolate the impact of Mg in ilmenite during reduction.

2.4.4 Influence of H_2 gas as reductant

Although CO gas is mostly used for solid-state reduction, such as DRI (Direct Reduced Iron) production [18, 49], the addition of H_2 gas can enhance the reduction rate. In case of solid-state reaction, there have been many studies indicating that H_2 gas is a better reducing agent than CO gas [21-23].

The reduction of synthetic ilmenite with reductant gases, H_2 and CO, was previously executed by Canaguier [31]. **Figure 2.10** shows the reduction results of synthetic ilmenite with two different reductant gases. The red line indicates the reduction with CO gas, and the black line

indicates the reduction with H_2 gas. Both reduction trials were done for 4 hours. The value "0" in terms of conversion degree corresponds to no mass loss, whereas a conversion degree of "1" corresponds to all oxygen loss from the iron oxide ($Fe_2O_3 \cdot TiO_2$ or Fe_2TiO_5) in ilmenite.

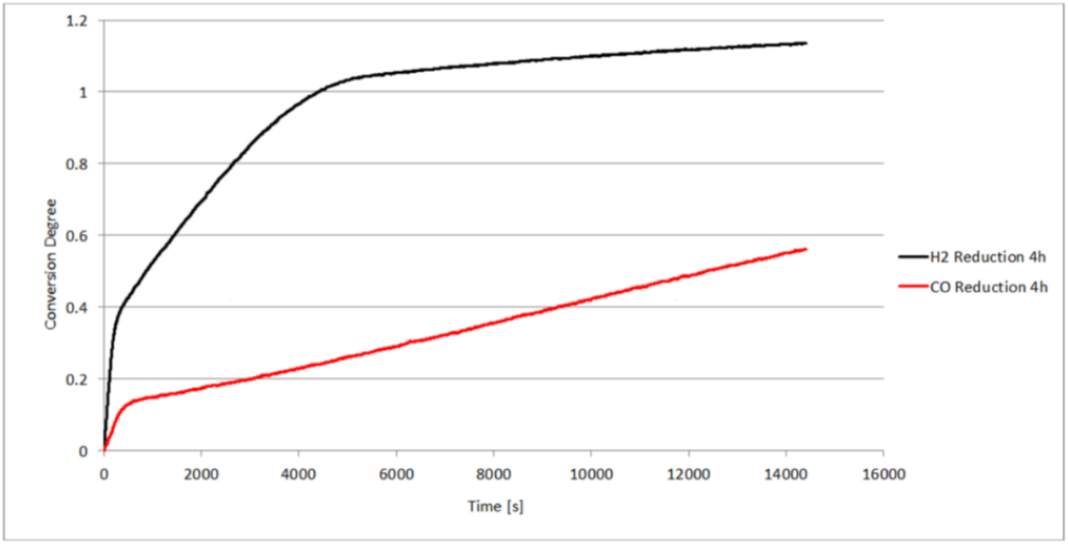

Figure 2.10 Conversion degree curve for CO and H_2 gas reduction [31]

There is a significant difference in the conversion degree between the two results. The conversion degree is approximately "0.58" for the reduction with CO gas, whereas the conversion degree is more than "1.0" for the reduction with H_2 gas after 4 hours of reduction. This indicates that H_2 gas is a far better reductant than CO gas when reducing ilmenite. For using a combination of CO and H_2 gas, the conversion curve is assumed to be between the two curves if executed.

However, when it comes to Mg-rich ilmenite, it is not clear whether the use of H_2 gas with different amount will influence the reduction rate. Assuming that the Mg in ilmenite strongly hinders the reduction degree, it is ambiguous if H_2 gas is likely to give further reduction. The impact of Mg content verses the impact of H_2 gas content is still in question.

Nevertheless, the related thermodynamic data gives indication for the question above. **Figure 2.11** shows the standard Gibbs free energy change as the function of temperature for reduction reactions of $MgTiO_3$, TiO_2, $FeTiO_3$ and FeO by H_2 gas. From **Figure 2.11**, two expectations can be noticed.

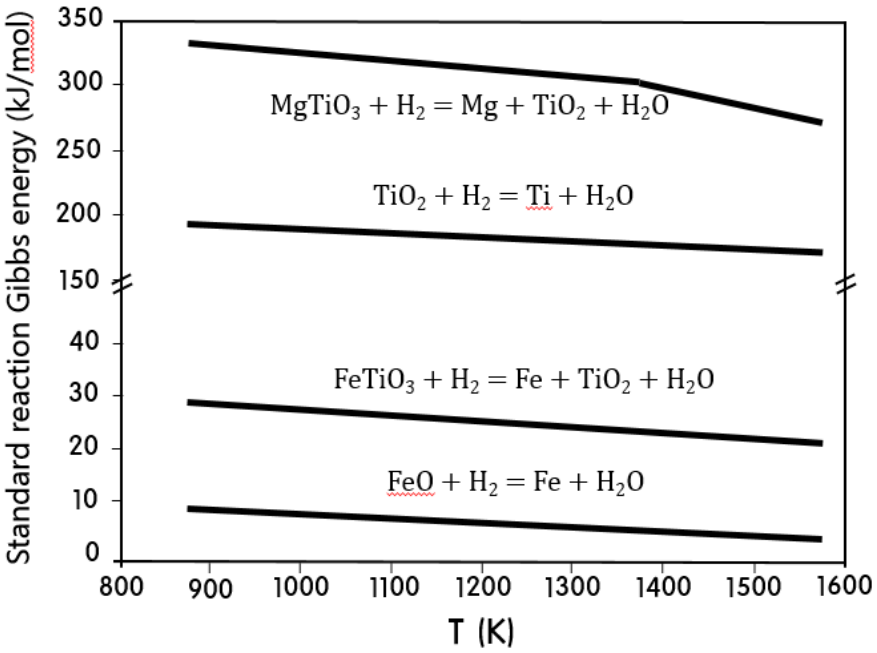

Figure 2.11 The standard Gibbs free energy change as the function of temperature for reduction reactions of $MgTiO_3$, TiO_2, $FeTiO_3$ & FeO by H_2 gas

First, the standard reaction Gibbs energies for $FeTiO_3$ and FeO with H_2 gas are relatively lower than $MgTiO_3$ and TiO_2. Not considering the iron in armalcolite, $(Fe,Mg)TiO_3$, this means that iron oxides will reduce rather easily compared to the other compounds. This is in a good correlation with the theoretical reduction of ilmenite in **Section 2.4.2**, where iron oxide is reduced with two main stages.

Second, the standard reaction Gibbs energy for reduction of $MgTiO_3$ with H_2 gas is higher than the reduction of TiO_2 with H_2 gas at the given temperature range. This gives a rough idea that the Mg content is seemingly more influential than the H_2 gas content in reduction. The Mg in ilmenite is likely to overpower the effect of H_2 reduction, but the author has no knowledge or known previous experiments to confirm this.

In addition, the reduced rutile species should also be considered. When using H_2 gas as reductant, the further reduction of rutile has been reported previously. Lobo and coworkers reported reduced rutile phase, TiO_{2-x}, from reduction of Norwegian ilmenite with H_2 gas [21]. Dang also showed indications of reduced rutile species and the maximum reduced rutile specie

was reported to be Ti_2O_3 [50]. However, it is not clear if the reduced rutile species will react with Mg. For example, after rutile is reduced to reduced rutile, TiO_{2-x}, it can have interaction with Mg to form magnesium titanium oxide spices such as $Mg_xTi_{3-x}O_5$ solid solution ($0 \leq x \leq 1$).

Chapter 3 Experimental

The experimental details considering the synthesis, oxidation and reduction of synthetic ilmenite and Mg-rich ilmenite are explained in this chapter. Also, proper analyzing methods are mentioned to verify each analysis of the synthesis, oxidation and reduction step.

In the synthesis step, the use of the CCIF (Cold Crucible Induction Furnace) for synthesizing ilmenite will be the main focus. Materials packing into the crucible for optimized induction and temperature profile during the synthesis are explained. Prior to synthesis, material preparation and sample parameters will be also briefly mentioned.

In the next step, the method of pelletization and oxidation of synthetic ilmenite pellets is described. The pelletization part consists of grounding and pelletizing with a brief explanation. In the oxidation part, a muffle furnace is used for oxidation and the time-temperature profile is considered.

Lastly, the reduction step was done by using a TGA (Thermo-Gravimetric Analyzer) vertical retort furnace. Both synthetic ilmenite and Mg-rich ilmenite were reduced with a mixture of CO and H_2 gas. Then, another reduction for synthetic Mg-rich ilmenite was experimented with different amount of H_2 gas to identify the question, which was mentioned in **Section 2.4.4**.

In addition, analysis tools, such as XRD (X-Ray Diffraction) and EPMA (Electron Probe Micro-Analysis), were used after each step of synthesis, oxidation and reduction. XRD was used after every step for the confirmation of phase analysis. EPMA was mainly used for pellets after oxidation and reduction to find the mapping of elements.

3.1 Synthesis

3.1.1 Material preparation

For the preparation of synthetic ilmenite and Mg-rich ilmenite, high purity powder and sintered pieces of hematite (Fe_2O_3), rutile (TiO_2), magnesia (MgO) and iron (Fe) were used. The form, size and purity of these materials are shown in **Table 3.1**.

Table 3.1 Material form, size and purity for synthesizing ilmenite

Material		Form	Size	Purity (%)
Hematite	**Fe_2O_3**	Powder	≤ 5 μm	99.99
Rutile	**TiO_2**	Powder / Sintered pieces	≤ 5 μm / 3.0-6.0 mm	99.9
Magnesia	**MgO**	Powder	≤ 5 μm	≥ 99.9
Iron	**Fe**	Irregularly shaped	3.2-6.4 mm	99.99

More precautions were considered when using the powder materials. Initially, the powder materials had to be compressed into briquettes of acceptable size. When using the mixture of powder and sintered pieces, such as powder hematite and sintered pieces of rutile, the mixture volume was less than the volume of the crucible. However, when mixing only powder materials, the volume of the mixture exceeded the volume of the crucible. The volume of the crucible was limited to about 283 cm^3 (Height: ~10 cm, Width: ~6 cm). In order to have a mixture volume less than 283 cm^3, a compressor was used to decrease the mixture volume. The compressor used with its simple sketch is shown in **Figure 3.1**.

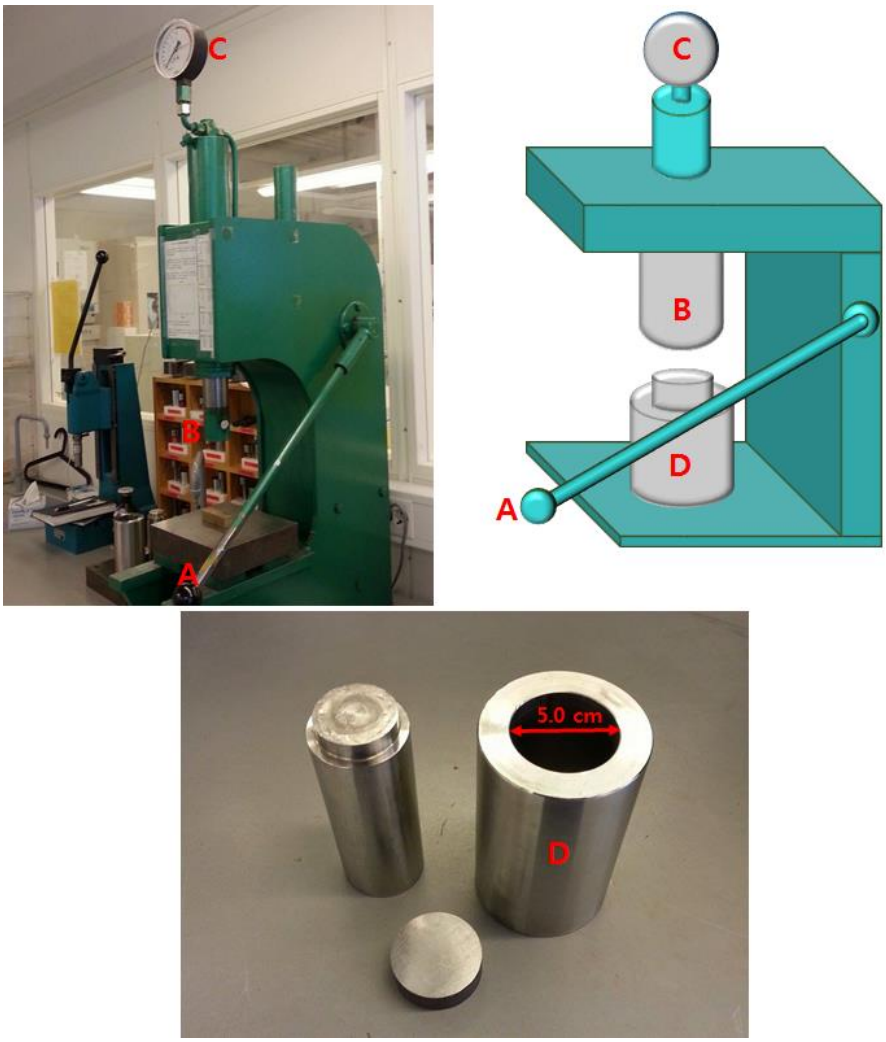

Figure 3.1 Compressor (left-top), sketch of compressor (right-top) and compress container (bottom)

The name of the compressor is "C-presse", and it's a hydraulic press type with maximum pressure of 10 tons. The compressor simply consists a compressor lever (A), compress point (B), barometer (C) and compress container (D). Considering the width of the crucible, which was approximately 6 cm, the compress container of inner diameter size 5.0 cm was used.

Another precaution for using powder materials was to avoid voids within the briquettes. If the briquettes were not steadily compressed, it can leave internal voids. These voids are filled up with air and they have a high possibility to cause splashing of melt during the high temperature synthesis. To avoid these voids, high pressure was applied to the compress container for more

than 90 seconds. The pressure applied was approximately 6 tons for the 5.0 cm diameter compress container.

In addition, improper packing of these briquettes into the crucible can also make voids within the packed crucible. More description about crucible packing is further explained in **Section 3.1.3**.

3.1.2 Sample parameters

Each batch of synthetic ilmenite and Mg-rich ilmenite were considered based on the Fe_2O_3-TiO_2-MgO system, which was previously mentioned in **Section 2.2.2**. The molar composition of each batch in the Fe_2O_3-TiO_2-MgO system and sample parameters are shown in **Figure 3.2** and **Table 3.2**, respectively.

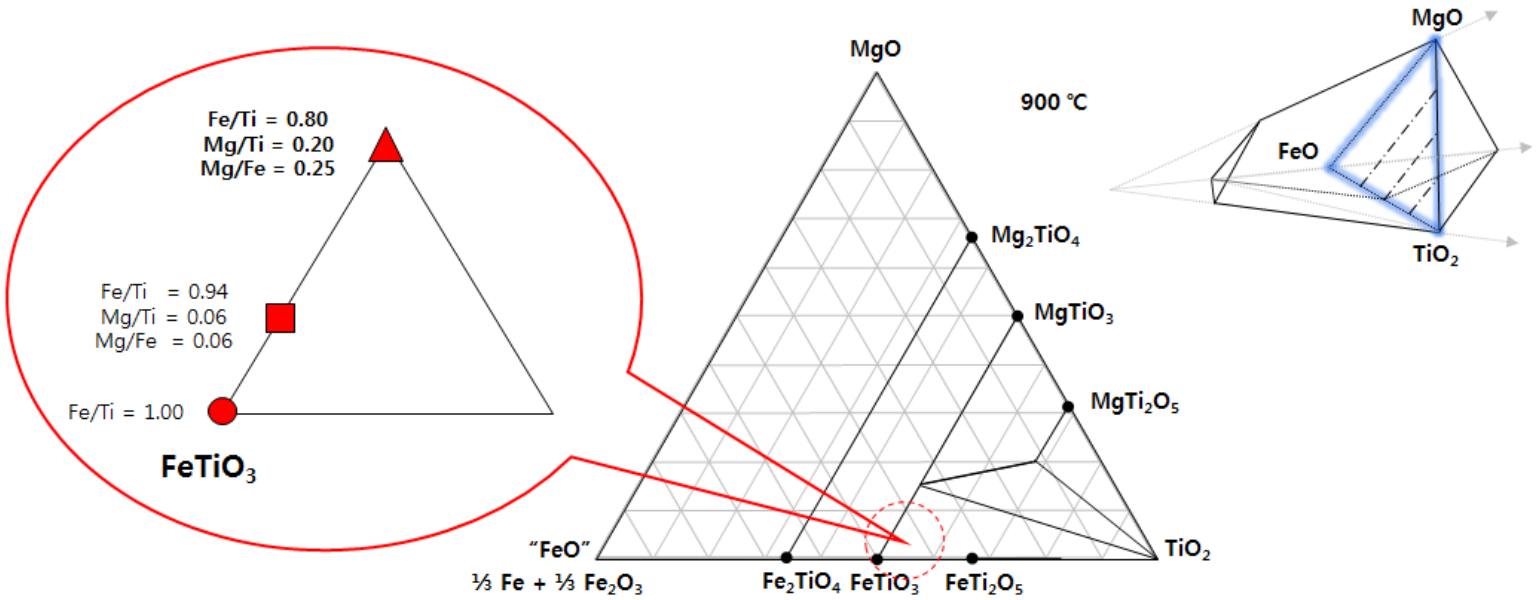

Figure 3.2 The Fe_2O_3-TiO_2-MgO system at 900℃ with synthetic ilmenite and Mg-rich ilmenite composition

Table 3.2 Synthetic ilmenite and Mg-rich ilmenite mass amount [g]

	Symbol	Fe_2O_3	TiO_2	Fe	MgO	Total mass	Note
Batch 1	●	105.25	157.95	36.8	0.0	300.0	Synthetic ilmenite (**No Mg**)
Batch 2	■	100.61	159.76	35.19	4.84	300.4	Mg-rich ilmenite (Mg/Ti = 0.06, **Low Mg**)
Batch 3							
Batch 4	▲	89.43	167.75	31.28	16.93	305.39	Mg-rich ilmenite (Mg/Ti = 0.20, H**igh Mg**)
Batch 5							

For synthetic ilmenite, the mass of each material was calculated according to the molar composition in the Fe_2O_3-TiO_2-MgO system (Detailed calculations can be found in Appendix A). Considering the volume of the crucible, approximately 300 g for one batch was adequate. The synthetic ilmenite was used as a reference ilmenite (No Mg) to compare with the synthetic Mg-rich ilmenite.

For synthetic Mg-rich ilmenite, 4 batches with two different amounts of Mg were considered. Batch 2 and 3 have Mg amount of 4.84 g (Low Mg) and 16.93 g (High Mg), respectively. This was considered to find the increasing impact of Mg in ilmenite. The Mg amount in batch 3 have the same Mg/Ti ratio of 0.2 regarding the Norwegian ilmenite, which was mentioned in previous chapters. Batches 4 and 5 have the same composition with batch 3. These batches were reduced with different amount of H_2 gas to find the effect between Mg and H_2 gas. More details regarding the reductant ratio of CO and H_2 gas in reduction is further described in **Section 3.3.1**.

3.1.3 Synthesis: CCIF (Cold Crucible Induction Furnace)

The CCIF was used for the synthesis of each ilmenite. A picture of the furnace and crucible (with sketch) is shown in **Figures 3.3** and **3.4**, respectively.

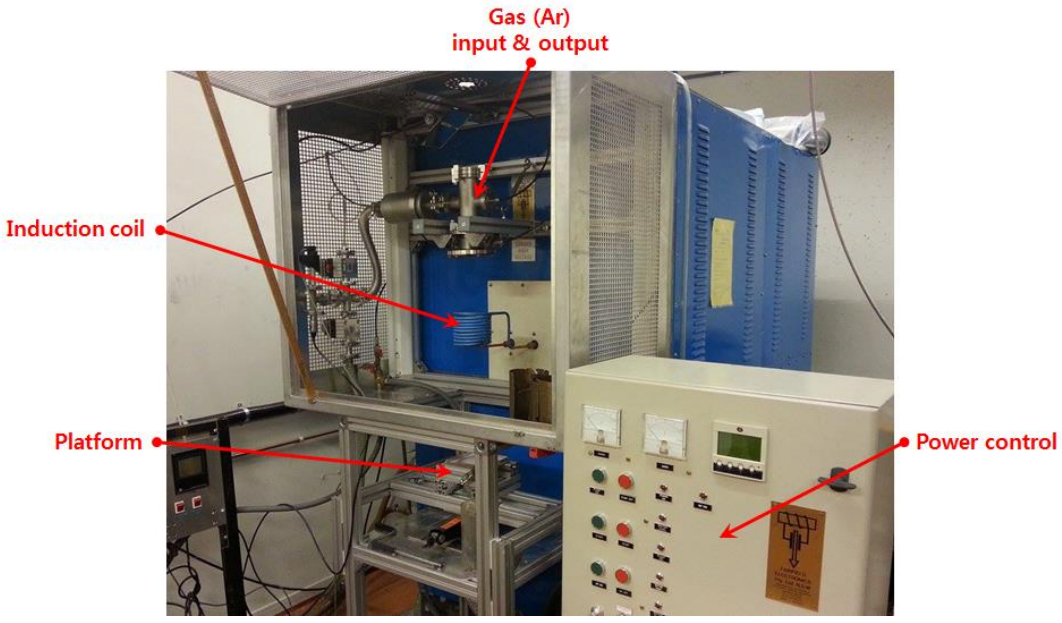

Figure 3.3 CCIF (Cold Crucible Induction Furnace)

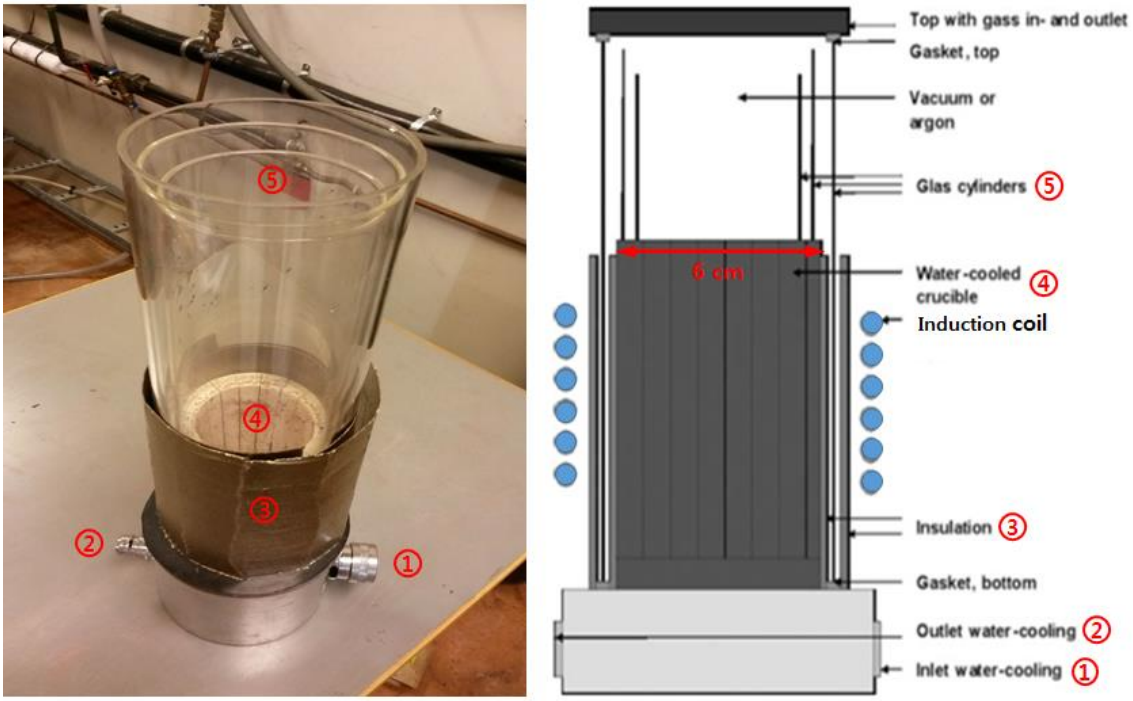

Figure 3.4 Picture of crucible setup (left) and sketch (right) [51]

The CCIF is a high frequency induction furnace and consists of a power supply from Farfield Electronics PTY Ltd and a water-cooled copper crucible from ANSTO (Australian Nuclear Science and Technology Organization). The high frequency generator operates at 750 kHz and has a power capacity of 75 kVA. The power control on the furnace consists of a radio tube where the acceleration current is applied. This results in a current running through the induction coil. The power control for the experiments was the measured current running through the induction coil and all synthesis were kept at equal power setting of 70 % of maximum current. This current input corresponds to approximately 1650 ℃ and was sufficient for a complete melt.

The water-cooled copper crucible is vertically segmented in order to prevent induction in the crucible. The gaps between the segments are filled with boron nitride (BN) to prevent raw materials falling out during packing, and the melt to flow into the gaps. The inside of the crucible has also been treated with boron nitride coating [52]. This coating will limit the wear and tear on the crucible as well as making the extraction of the sample from the crucible easier. The coating is assumed not to contaminate the samples due to its relatively high thermal stability (stable up to

2800 ℃ with inert atmosphere). The crucible has one water inlet and one outlet connection, thus the cooling is internal. Detailed procedures of using the CCIF can be found in Appendix B.

The material packing into the cooper crucible was carefully executed during the synthesis. Two main aspects were considered: prevention of melt splashing and optimized induction effect.

First, all possibilities which cause splashing of melt during the high temperature synthesis were anticipated. The causes of splashing of melt during high temperature were mainly due to the leftover moisture in the raw materials and the unintended void generated during the material packing.

Raw materials, such as Magnesia (MgO), were tested for hydroxylation before use. The moisture absorbed Magnesia is Magnesium hydroxide, $Mg(OH)_2$, and it starts to decompose at approximately 300 ℃ by giving off water vapor according to **Reaction (16)**.

$$Mg(OH)_{2\,(s)} = MgO_{\,(s)} + H_2O_{\,(g)} \qquad \textbf{(16)}$$

The temperature in the crucible increases to approximately 1650 ℃ within few seconds. At this temperature, decomposed moisture from Magnesium hydroxide is extremely likely to give splashing of the melt (See pictures of melt splashed protection glass in Appendix B) due to the huge volume expansion (approximately 1600x) of $H_2O_{\,(l)}$ to $H_2O_{\,(g)}$. For prevention of splashing, the magnesia should go through a chemical analysis such as XRD to find if it is moisture absorbed. In case of moisture absorbed, it should be pre-heated in an oven of temperature more than 300 ℃, or should be replaced by a moisture free new source. In this experiment, new magnesia powder was used instead of the former one which contained moisture.

Unintended void generated during the material packing into the crucible should be avoided also. These voids contain air, which are entrapped during the packing of raw material briquettes. For example, the gap between the crucible wall and the briquettes should be filled up with leftover raw material powder, but it might not be filled up completely. Also, if too fragile, briquettes can break into several pieces and air can be trapped between these gaps. The entrapped air will cause splashing of melt during the high temperature synthesis. To prevent this, careful packing of briquettes and powder was done. Powder was first applied to the bottom to establish a certain layer. Then a briquette was put on the top of it, and the gaps between the crucible wall

and briquette were filled carefully by using a small spoon. After the powder and briquette layer were firmly established, the same procedure was done with the rest of the power and briquettes. None of the briquettes were broken due to careful handling.

Second, the material packing order was considered to ensure an optimized induction effect. The material packing order was studied by Canaguier previously [31]. Since the furnace is an induction furnace, the raw materials should contain metal to have induction effect. The heat is applied by induction heating of the metal where the Eddy currents are generated within the metal and resistance leads to heating of the metal [53]. **Figure 3.5** shows the packing order of the raw materials. The iron pieces were placed on the top. As the induction effect goes on, the iron is melted and mixed with the oxides. If the iron was packed in the bottom, the iron will be melted only in the bottom part, leaving unreacted oxides above.

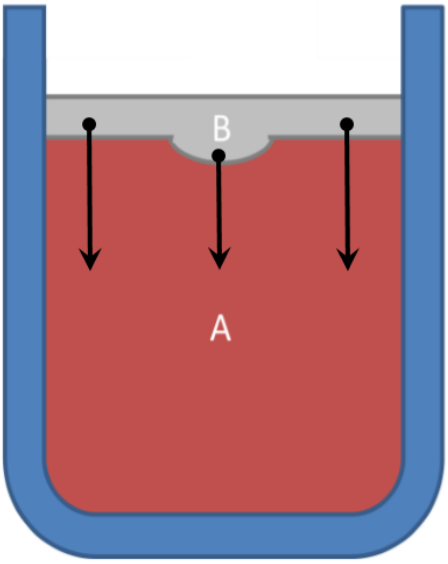

Figure 3.5 Packing of materials. A: Fe_2O_3 + TiO_2 (+ MgO) / B: Fe

The temperature profile during the synthesis was also another important aspect to consider. When synthesizing Mg-rich ilmenite, it was very important not to have the ferrous pseudobrookite ($Fe^{2+}Ti_2O_5$) phase because they tend to be stabilized with Mg during reduction with CO and H_2 gas. This was previously documented in **Section 2.2.2**. In order to prevent this, a slow cooling of the melt was suggested. This was done by gradually decreasing the power supply

after a period of time. The temperature measurement during the synthesis was conducted by using a spectro-pyrometer (See Appendix B).

Synthetic ilmenite was cooled rapidly by killing the power supply, and synthetic Mg-rich ilmenite was cooled slowly by decreasing the power supply by 5 % after every 3 minutes. The initial power supply was 70 %, and it was gradually decreased until the temperature of the melt was below 800 ℃.

In addition, Ar gas was used to prevent unnecessary reaction of the melt with air, and the holding time of the melt at temperature of approximately 1650℃ was kept for 3-4 minutes to ensure complete melt. The argon flow was maintained at a flow of 1 L/min from the starting of the synthesis to complete cooling of the melt.

3.2 Oxidation

3.2.1 Pelletization

Each synthetic ilmenite and Mg-rich ilmenite bulk was crushed into small pieces by using a steel mortar. Then the small pieces were ground into fine ilmenite powder by a crushing machine. A picture of the crushing machine and the container with its sketch is shown in **Figure 3.6**. The steel crusher container consist two crusher parts, which are shaped as a ring (B) and a cylinder (A). They crush the small ilmenite pieces into fine powder by using the vibration from the machine. The vibration speed was 960 vibration per minute. For each batch, 24 seconds were measured for crushing.

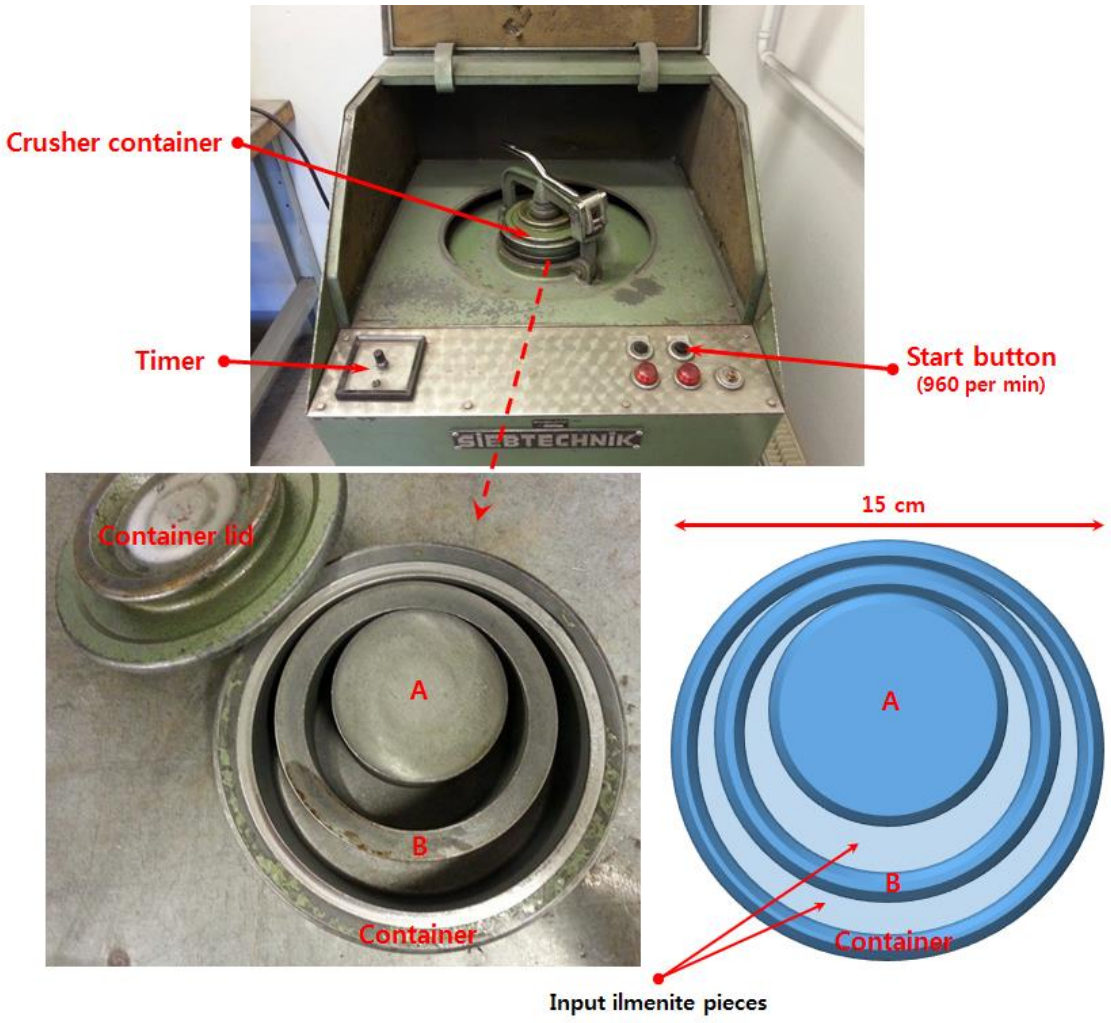

Figure 3.6 Crushing machine (top), crusher container (left) and its sketch (right)

Next the synthetic ilmenite powder was put into a pelletizing drum for pelletization. The pelletizer with its simple sketch is shown in **Figure 3.7**. Initially, a small amount of ilmenite powder was put into the pelletizing drum at a high rotation speed of 70 rpm to produce small seeds. Then, water was used as a binder by using a water sprayer (note that bentonite as binder was not used in this work for prevention of further contamination of synthetic ilmenite). Controlled amount of water and ilmenite powder were added into the pelletizing drum as the seeds grew. After achieving a pellet size of approximately 3 mm, the rotation speed of the drum has been lowered to 50 rpm. Then, as the pellets increase in size by adding more ilmenite powder and water, the rotation speed was gradually decreased to 30 rpm. When the pellets were

approximately 9 mm in size, sieves of mesh size 10, 9 and 5 mm were used to collect the pellets. Pellets of size 9 and 10 mm were collected and put into a dryer of temperature of 100℃ to be dried for 24 hours. Pellet sizes less than 9 mm were collect separately and were crushed into powder to be used again for pelletizing. An informal know-how for successful pelletizing is described in Appendix C.

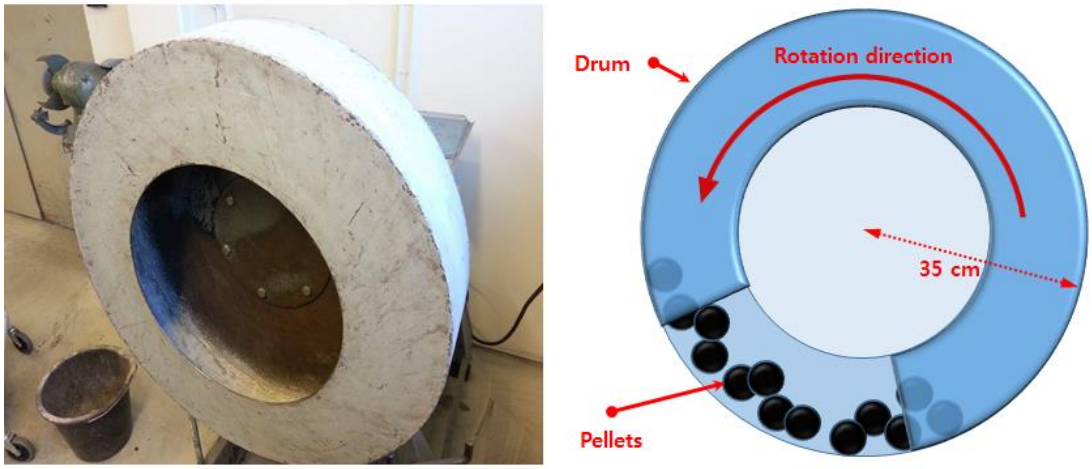

Figure 3.7 Pelletizer drum with its sketch

3.2.2 Oxidation: Muffle furnace

The dried synthetic ilmenite pellets were carefully retrieved from the dryer and were oxidized. The ilmenite pellets were put into a steel pan, and oxidation was done by using a muffle furnace of type Nabertherm N17/HR Controller C290. The picture of the muffle furnace with its sketch is shown in **Figure 3.8**. Each synthetic ilmenite and Mg-rich ilmenite pellets were heated for 2 hours at 1000℃ to ensure complete oxidation. Then the pellets were air-cooled after 2 hours of heating. The time-temperature profile for the oxidation of ilmenite pellets is shown in **Figure 3.9**.

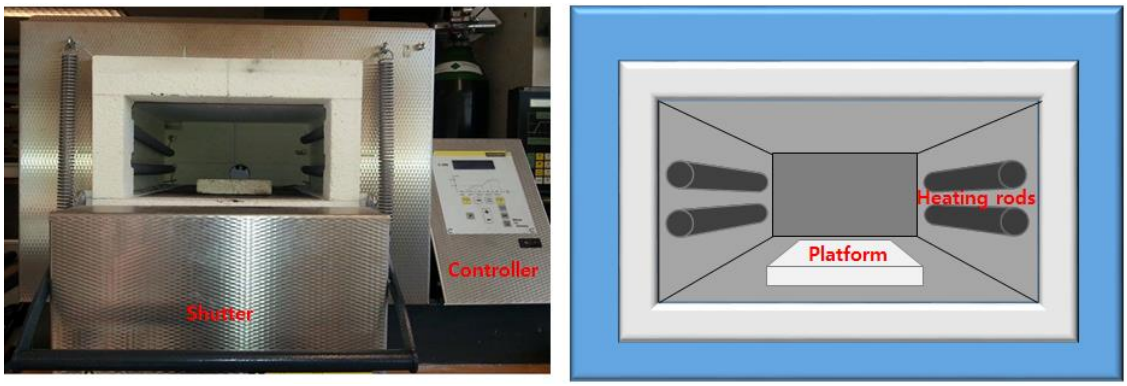

Figure 3.8 Muffle furnace with its sketch

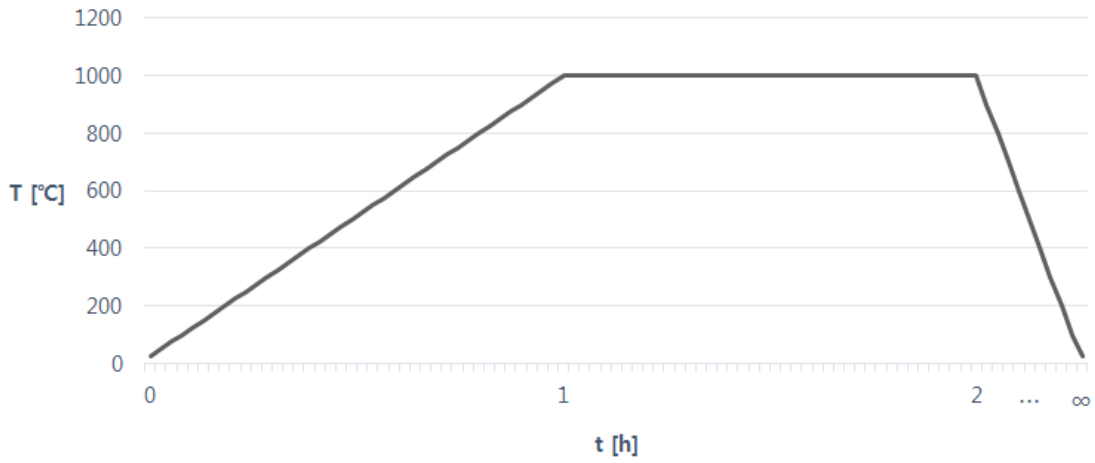

Figure 3.9 Time-temperature profile for oxidation

3.3 Reduction

3.3.1 Reduction parameters

The aim of reduction was to find the impact of Mg and H_2 gas in ilmenite. Batches 1, 2 and 3, which have different Mg amount in the increasing order, were reduced with a mixture of 50 % CO and 50 % H_2 gas to find indication of Mg impact in ilmenite during reduction. Batches 3, 4 and 5 have the same Mg amount, which was the amount considering the Norwegian ilmenite [15], and were reduced with different amount of H_2 gas to find the competing relation between Mg

and H_2 gas. Batches 4 and 5 were reduced with 25 % CO + 75 % H_2 gas and 100 % H_2 gas, respectively.

The initial mass for all batches were 200 g of 9-10 m pellets, and the reduction temperature was 1000℃ for 4 hours. The mass loss was recorded, and data were logged for every 2 seconds during the reduction. It was assumed that the mass loss was initially due to oxygen removal from iron oxides (Fe_2TiO_5 or $Fe_2O_3 \cdot TiO_2$) and further oxygen removal from rutile. For example, the conversion degree between "0" to "1" is due to the oxygen loss from iron oxides while rutile is considered as inert. When the conversion degree is above "1", all the oxygen from the iron oxides have been remove and oxygen is being removed from rutile. Calculations of conversion degree were based on this assumption:

$$\text{Conversion Degree} = \frac{-\Delta m}{\kappa \cdot m}$$

M [g] is the initial amount of oxygen tied to the iron oxides before reduction, and Δm is the oxygen loss from the reduction. The constant, κ, is the oxygen to iron oxide ratio. The values for κ were based on the calculations in Appendix A and were 31.6, 30.2 and 26.8 for batch 1, batch 2 and batches 3-5, respectively. The reduction parameters and plot for each batch is shown in **Table 3.3** and **Figure 3.10**, respectively.

Table 3.3 Reduction parameters for each batch

	MgO amount [g]	Gas [%]	Temperature	Time	Initial mass	Pellet size	Note
Batch 1	-						Synthetic ilmenite
Batch 2	4.84	50 CO + 50 H_2					Mg-rich ilmenite (Mg/Ti = 0.06)
Batch 3			1000 ℃	4 h	200 g	9-10 mm	
Batch 4	16.93	25 CO + 75 H_2					Mg-rich ilmenite (Mg/Ti = 0.20)
Batch 5		100 H_2					

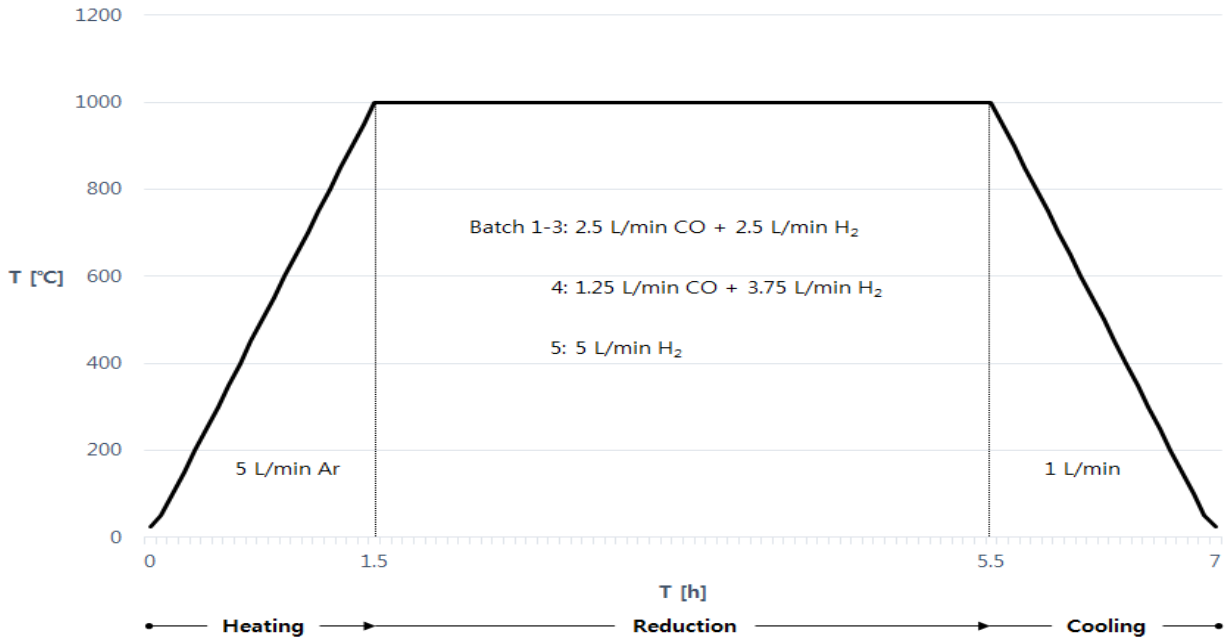

Figure 3.10 Reduction Plot

3.3.2 Reduction: TGA (Thermo-Gravimetric Analyzer) vertical retort furnace

The TGA (Thermo-Gravimetric Analyzer) vertical retort furnace was used for the reduction of ilmenite. A picture of the crucible with its sketch is shown in **Figure 3.11**.

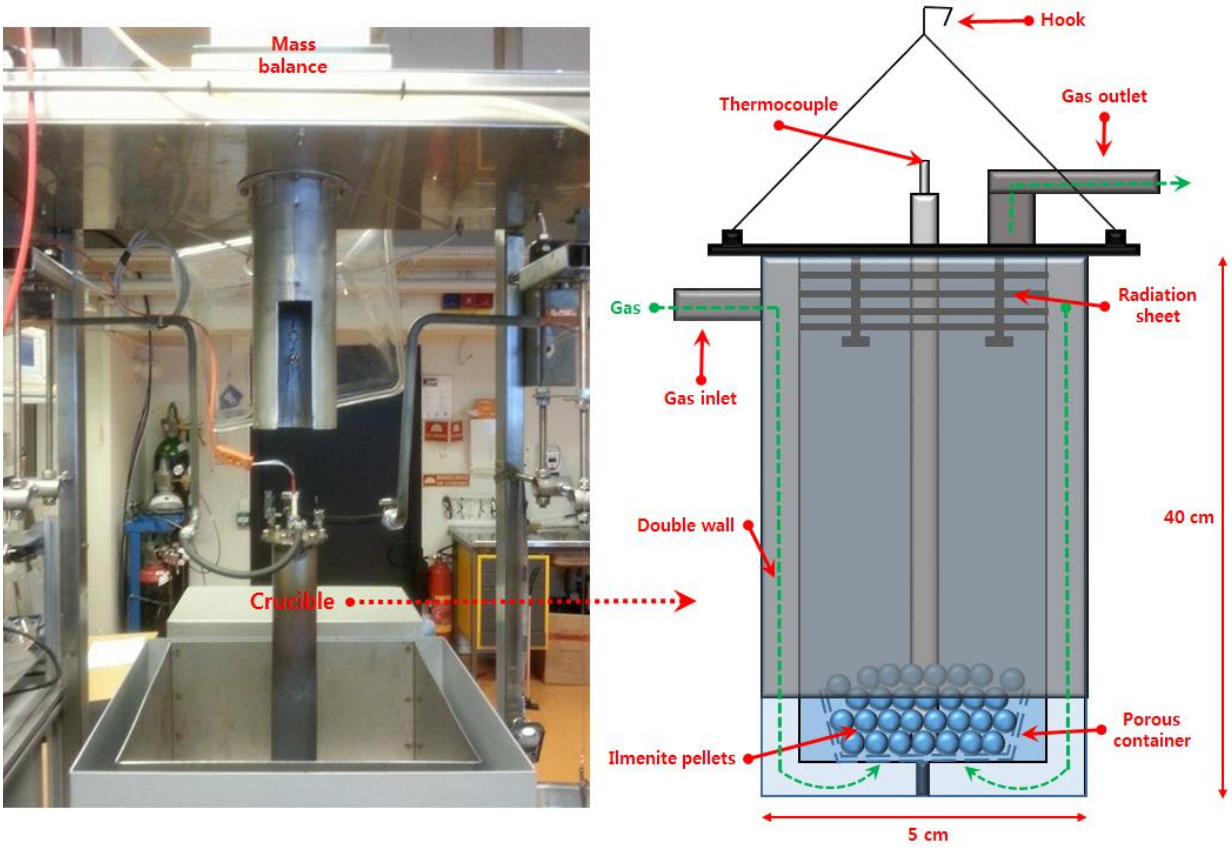

Figure 3.11 TGA vertical retort furnace (left) and sketch of crucible (right)

The furnace is an Entech resistance furnace (Model VTF 801/12) with a kanthal element, and the gas flow is controlled by Bronkhorst model F201c mass flow controllers. The mass balance is a model PR2003DR by Mettler Toledo. The crucible has a double wall for gas inlet and is suspended with wire to the mass balance, which is not to contact with the furnace. Also, it is connected with two gas tubes, which are free of movements in order to minimize their impact on the mass balance. The thermocouple is inserted through the center of the graphite gasket and placed in the pile of ilmenite pellets.

The pellets were placed on a porous container at the bottom of the crucible, and the top part was sealed by using a graphite gasket. The reduction experiment of each batch was executed according to **Table 3.3** and **Figure 3.10**. The procedures of the TGA vertical retort furnace are described in Appendix B.

3.4 Analysis

3.4.1 XRD (X-Ray Diffraction)

The XRD (X-Ray Diffraction) investigations were done at the Department of Material Science and Engineering, NTNU. The equipment used was D8 DaVinci diffractometer. Each sample powder from synthesis, oxidation and reduction was prepared by grounding and was placed in a sample holder. The scan range was set from 10° to 60°, and the V6 parameter was enabled. Each sample was analyzed for 15 minutes. After the analysis, the software, Diffrac.Eva, was used to match the result peaks. The database, PDF -4+ 2013 RDB, was used.

3.4.2 EPMA (Electron Probe Micro-Analysis)

The EPMA (Electron Probe Micro-Analysis) was used for the mapping of elements in pellets after oxidation and reduction. The equipment used was the JEOL JXA-8500F. The JEOL JXA-8500F is a high performance thermal field emission electron probe micro analyzer combining high SEM (Scanning Electron Microscope) resolution with high quality X-ray analysis of submicron areas. It is also equipped with 5 wavelength dispersive X-ray spectrometers and an EDS (Energy Dispersive x-ray Spectrometer).

Each pellet sample from oxidation and reduction was mounted in epoxy and then polished down to 1 μm prior to analysis. Then, the images of each sample were taken considering three continuous regions according to **Figure 3.12**. This was considered to see the whole area between the center and the end boundary of a pellet. Next, the mapping of elements was done for each sample with the same area.

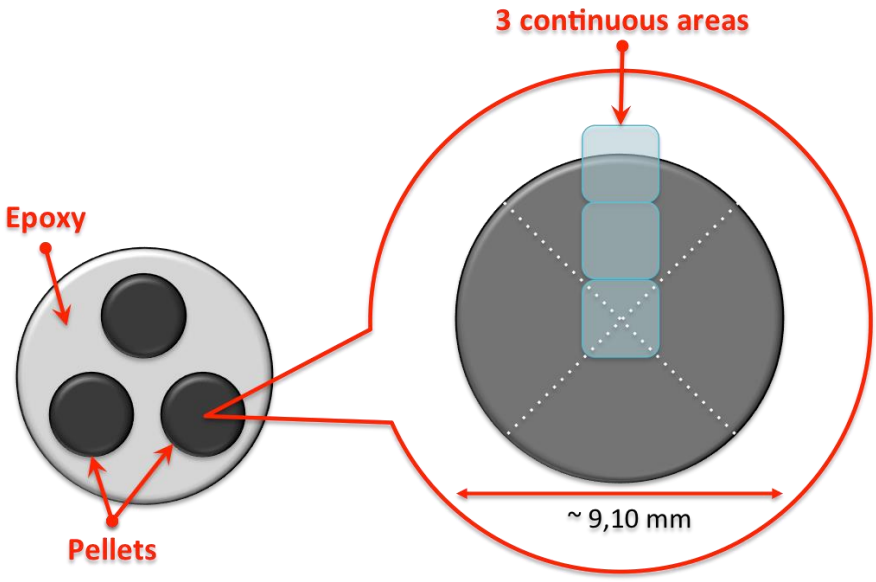

Figure 3.12 A sketch of an EPMA sample

Chapter 4 Results

In this chapter, the results from the synthesis, oxidation and reduction step of synthetic ilmenite and Mg-rich ilmenite are given. The synthesis part consists pictures of bulk appearance and cross-section of each ilmenite. XRD analysis was done to verify the synthetic ilmenite phase. Also, the temperature profiles are shown for each synthetic ilmenite and Mg-rich ilmenite. In the oxidation step, both results of XRD and EPMA analyses are shown. The EPMA results show SEM images of three continuous areas. The mappings of elements (Fe, Ti, O, Mg) are also shown. The results from the reduction step show the reduction curves, which were calculated into conversion curves, according to the reduction plot (**Figure 3.10**). XRD and EPMA analyses after reduction are also given.

4.1 Synthesis

4.1.1 Synthetic ilmenite

The pictures of bulk appearance and cross-section of synthetic ilmenite (batch 1) are shown in **Figure 4.1**. The synthetic ilmenite bulk had an upper and lower width of approximately 5.0 and 4.5 cm, respectively. The height was approximately 5.0 cm.

Figure 4.1 Bulk appearance (left) with sketch (right) & cross-section (bottom) of synthetic ilmenite

The synthetic ilmenite bulk was easily taken out of the crucible by applying force with a rubber hammer and had a volume of approximately ⅓ of the crucible volume. The remaining boron nitride and other residuals on the synthetic ilmenite bulk were blown off by using an air compressor, and a steel hammer was used to break the bulk. The cross-section of the bulk is shown in **Figure 4.1**, and the visual appearance showed a dense homogeneous oxide structure.

XRD analysis was done after preparing ilmenite powder. The ilmenite bulk was broken into several small pieces and further ground into fine powder by using a steel mortar and crusher (**Figure 3.6**). The XRD analysis is shown in **Figure 4.2**.

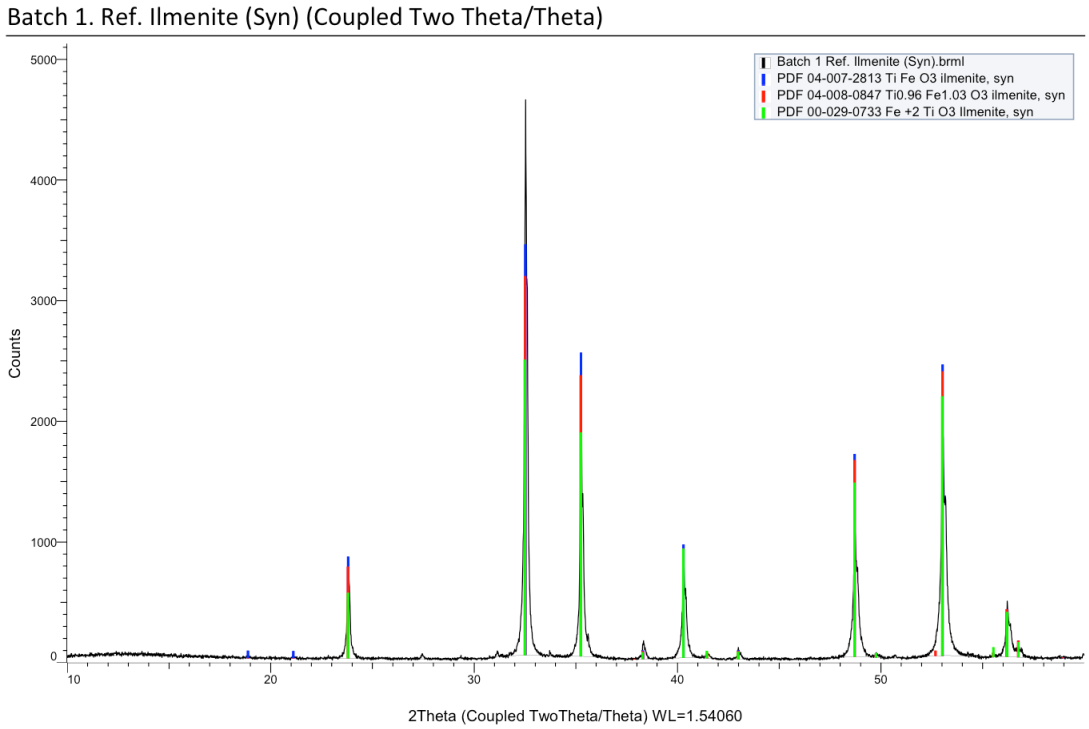

Figure 4.2 XRD analysis for synthetic ilmenite (Batch 1)

From the XRD analysis, ilmenite ($FeTiO_3$) of reference PDF 04-007-2813, PDF 04-008-0847 and PDF 00-029-0733 were detected. These references indicated synthetic ilmenite peaks. Quantitative information was not given by the XRD analysis, but the peaks showed that synthetic ilmenite with only insignificant amount of impurities was the dominating phase in batch 1.

4.1.2 Synthetic Mg-rich ilmenite

The bulk appearance for synthetic Mg-rich ilmenites (batches 2-5) was similar with **Figure 4.1** (left). However, the cross-sections of synthetic Mg-rich ilmenites were rather porous compared to the dense synthetic ilmenite. The pores were more concentrated at the rear and bottom rather

than the center in the bulk. **Figure 4.3** shows the cross-section of the synthetic Mg-rich ilmenite bulk (batch 2) with its simple sketch.

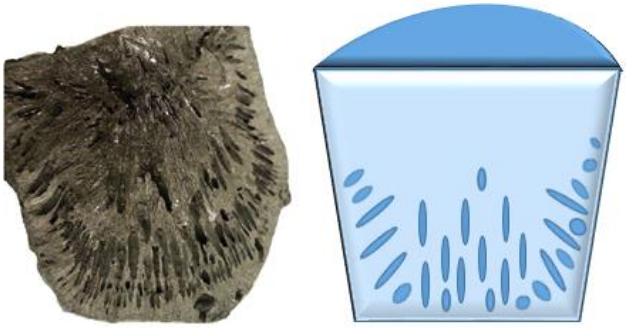

Figure 4.3 Cross-section of Mg-rich ilmenite bulk (batch2) with its simple sketch

The temperature profile of synthetic Mg-rich ilmenites was different compared to the temperature profile of synthetic ilmenite. Synthetic ilmenite was cooled instantly after complete melt, and synthetic Mg-rich ilmenites were cooled slowly. The temperature profiles of both batch 1 and batch 2 for synthesis are shown in **Figure 4.4**.

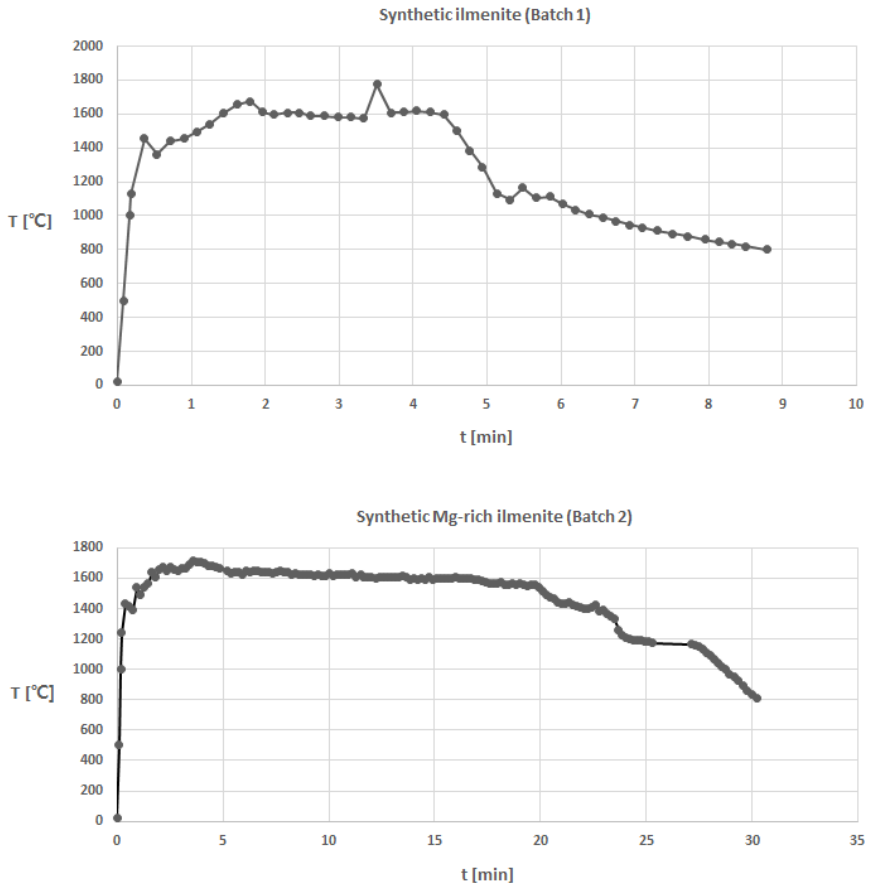

Figure 4. 4 The temperature profile for batches 1 and 2

When the temperature of the melt was over 1600 ℃, the temperature was hold for approximately 3-4 minutes to ensure complete mixture. Then the temperature decreased rapidly by killing the power supply. For synthetic Mg-rich ilmenites, approximately 3-4 minutes was also used for holding the melt after the temperature was over 1600 ℃. However, the temperature decreased slowly after gradually decreasing the power supply. The power supply was gradually decreased by 5 % after every 3 minutes until the temperature was below 800 ℃. Batches 3-5 showed similar temperature profiles with batch 2 (see Appendix D).

XRD analysis of Synthetic Mg-rich ilmenites were also done by following the same procedure with synthetic ilmenite, and the result of batch 2 is shown in **Figure 4.5**.

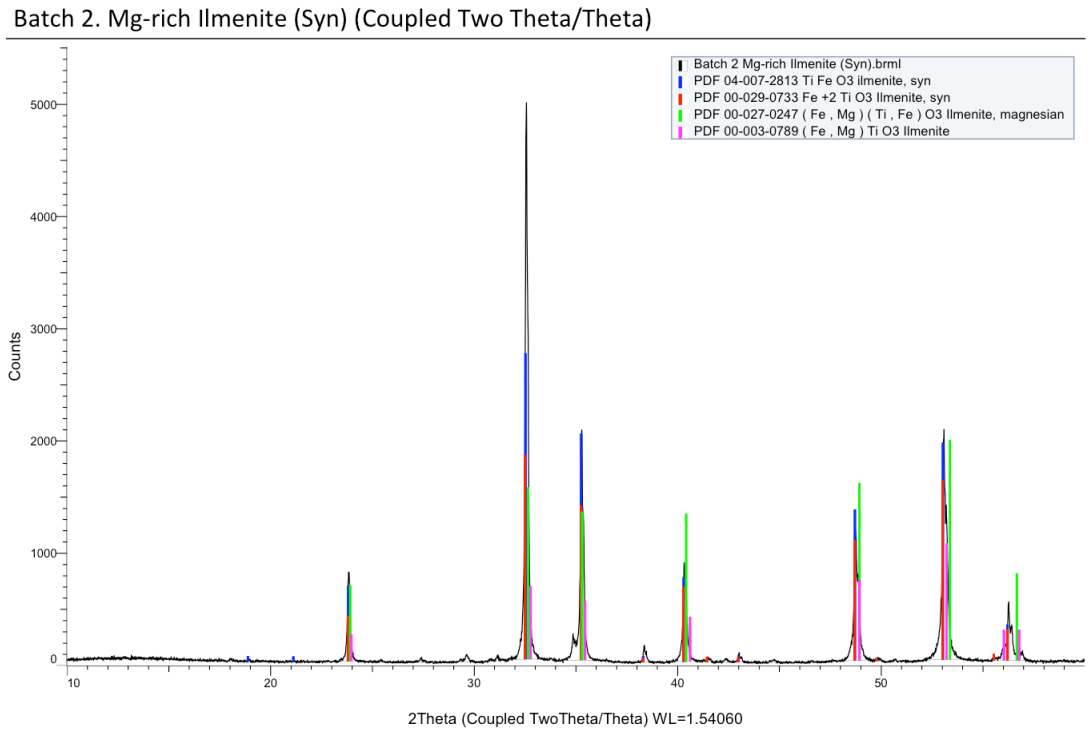

Figure 4.5 XRD analysis for synthetic Mg-rich ilmenite (Batch 2)

From the XRD analysis of batch 2, references of PDF 04-007-2813 and PDF 00-029-0733 were detected for the ilmenite ($FeTiO_3$) phase, and references of PDF 00-027-0247 and PDF 00-003-0789 were detected for the M_2O_3 ($FeTiO_3$-$MgTiO_3$) solid solution phase. The references of ilmenite peaks showed indication of synthetic ilmenite, and references of M_2O_3 solid solution peaks showed indication of M_2O_3 solid solution. The quantitative information was not known, but the XRD result shows that the dominating phases were synthetic ilmenite and M_2O_3 solid solution with only insignificant amount of impurities. The XRD analyses of batches 3-5 (batches 3-5 are the same composition) had similar results with batch 2 (See Appendix E). The dominating phases were also synthetic ilmenite and M_2O_3 solid solution.

4.2 Oxidation

4.2.1 Synthetic ilmenite

The oxidation of synthetic ilmenite (batch 1) was done according to **Figure 3.9**. The XRD analysis of oxidized synthetic ilmenite is given in **Figure 4.6**.

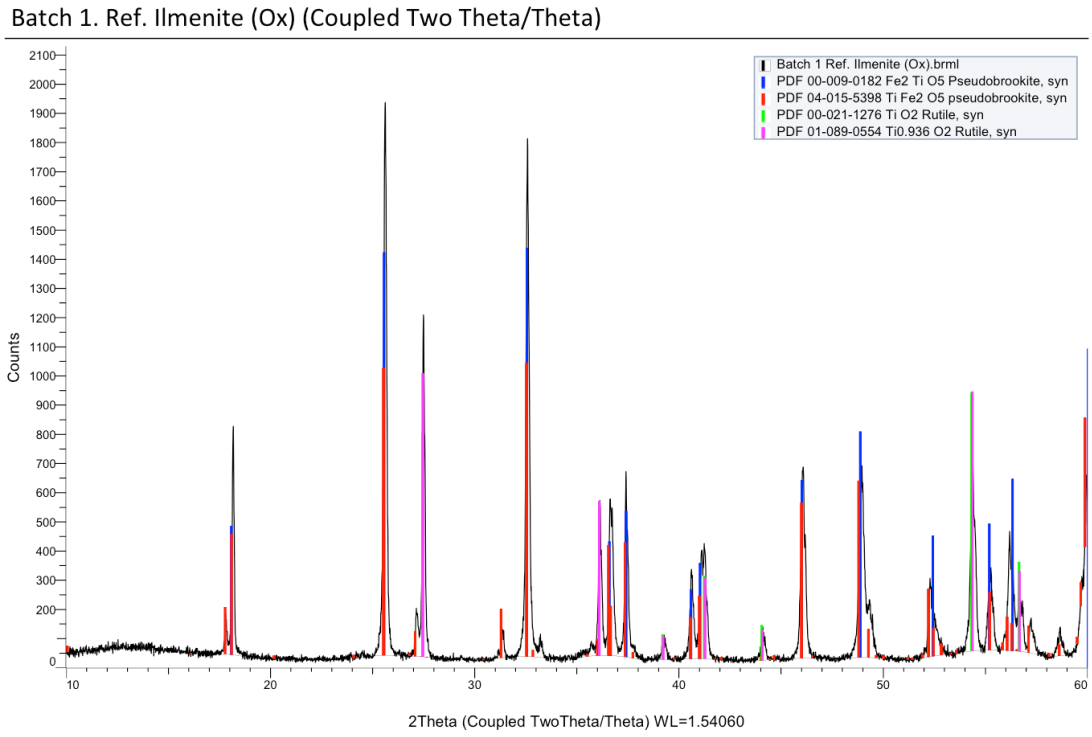

Figure 4.6 XRD analysis for synthetic ilmenite after oxidation (Batch 1)

From the XRD analysis of oxidized synthetic ilmenite, two main phases were detected. First, high intensity peaks of ferric pseudobrookite ($Fe^{3+}{}_2TiO_5$) with references of PDF 00-009-0182 and PDF 04-015-5398 were detected. Next, peaks of rutile (TiO_2) with references of PDF 00-021-1276 and 01-089-0554 were seen. The quantitative amount of these phases was not known, but the analysis indicated that the major phases after oxidation of synthetic ilmenite were mainly ferric pseudobrookite and rutile.

The EPMA analysis was also done for the oxidized synthetic ilmenite according to **Figure 3.12**. **Figures 4.7** and **4.8** show the SEM image and element mappings (Fe, O and Ti) of batch 1 after oxidation, respectively.

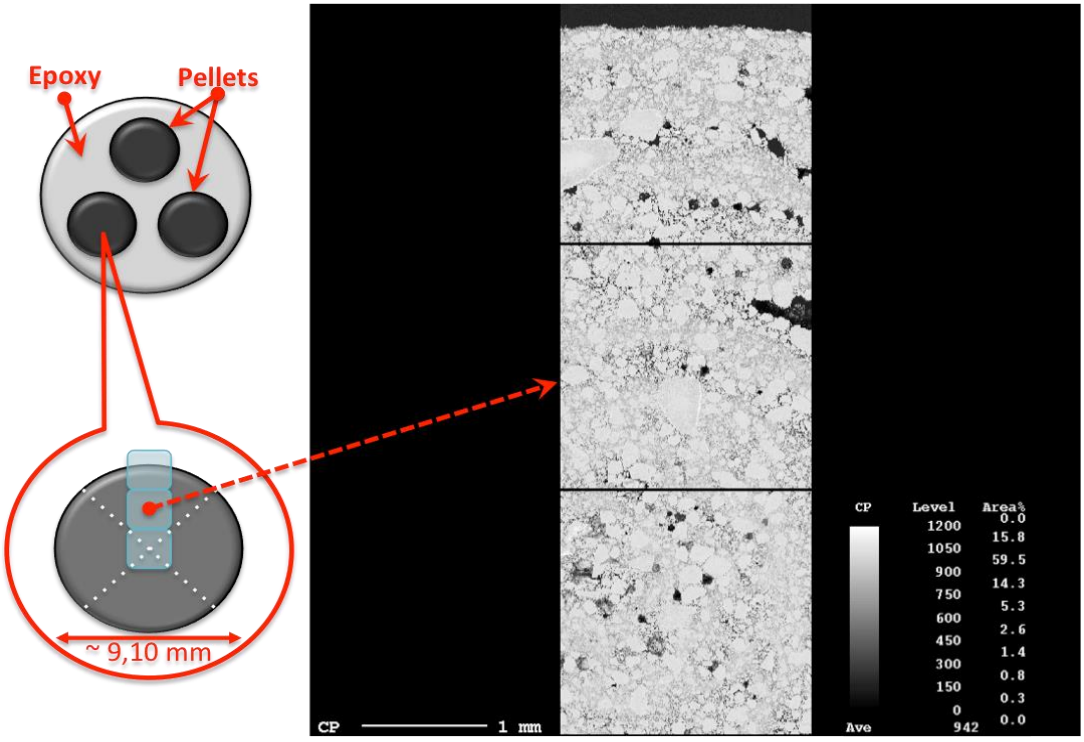

Figure 4.7 SEM image of batch 1 after oxidation

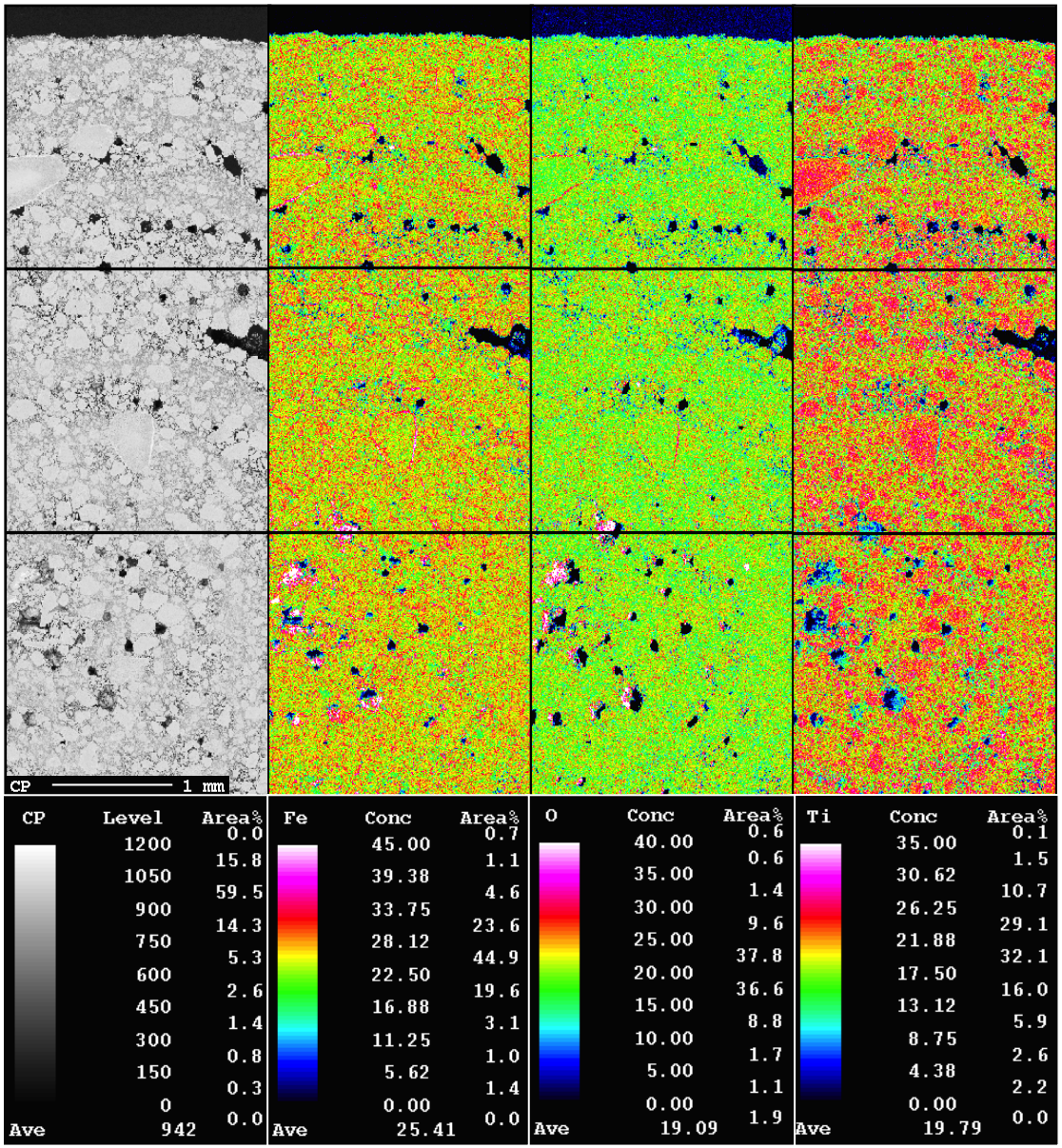

Figure 4.8 SEM image and element mappings (Fe, O, Ti) of batch 1 after oxidation

The different colors on the scale bars indicate the different kinds of phases and the concentration of each element. For example, from **Figure 4.8**, there are three different phases, which has the colors white, grey and black. The SEM image showed mostly two phases, which are white and grey. The black phases are assumed to be epoxy or internal voids.

From **Figure 4.9**, the concentration of each element is shown according to its scale, which shows different colors (white > purple > red > yellow > green > light blue > dark blue > black). Besides the black area (which is assume to be epoxy or internal voids), iron and oxygen showed a rather homogeneous distribution within the pellet with a majority of colors of yellow and green, respectively. Iron mapping showed a tendency of more iron concentration on the edges of each grain with the color red, but the iron concentration within the grains was homogeneous with colors of yellow and green. For titanium, two major colors of red and yellow were shown. The concentration of titanium was higher within the grains (red).

4.2.2 Synthetic Mg-rich ilmenite

The oxidation of synthetic Mg-rich ilmenites was also executed according to **Figure 3.9**. The XRD analysis of batch 2 and batches 3-5 (batches 3-5 are the same Mg-rich ilmenites), is shown in **Figure 4.9** and **Figure 4.10**, respectively.

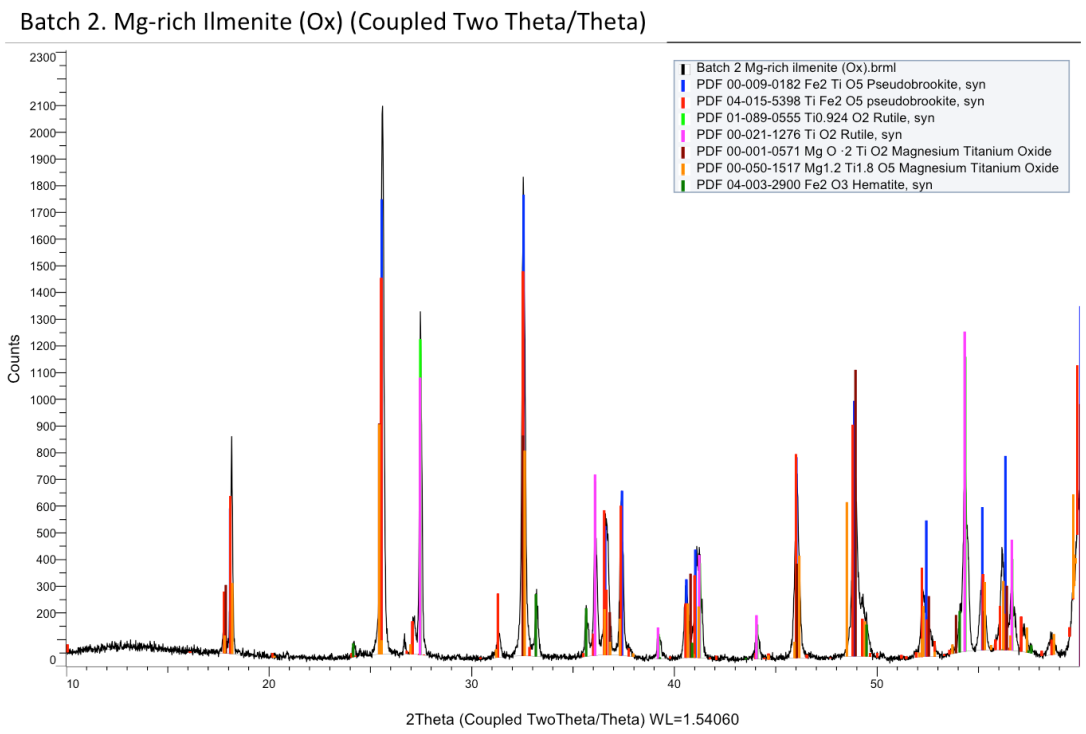

Figure 4.9 XRD analysis for synthetic Mg-rich ilmenite after oxidation (Batch 2)

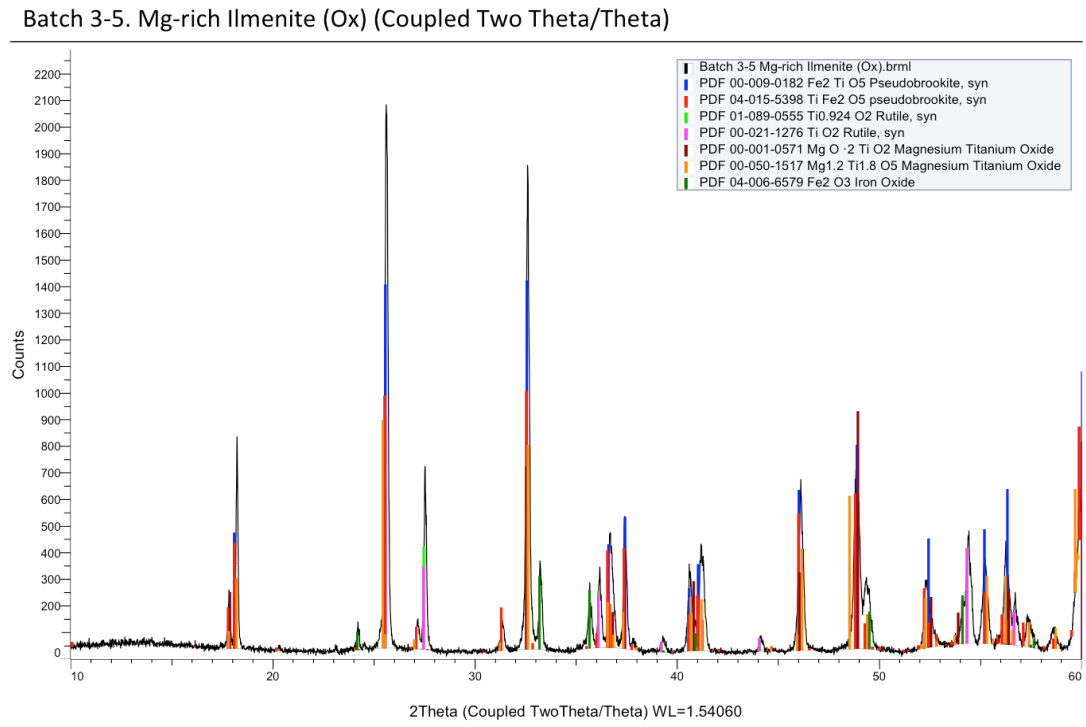

Figure 4.10 XRD analysis for synthetic Mg-rich ilmenite after oxidation (Batch 3-5)

Three main phases were detected in oxidized batch 2. First, the ferric pseudobrookite ($Fe^{3+}{}_2TiO_5$) peaks of references PDF 00-009-0182 and PDF 04-015-5398 were detected. Second, the rutile (TiO_2) peaks of references PDF 01-089-0555 and PDF 00-021-1276 were seen in the result. Lastly, the peaks of magnesium titanium oxide (magnesium dititanate, $MgTi_2O_5$) with references PDF 00-001-0571 and PDF 00-050-1517 were included in the analysis. In addition, a small amount of hematite (Fe_2O_3) of reference 04-003-2900 was also seen. Although the quantitative information was not given, the XRD analysis showed that the major phases after oxidation of synthetic Mg-rich ilmenite were ferric pseudobrookite, rutile and Magnesium dititanate. Batches 3-5 had similar XDR results to batch 2.

The EPMA analysis was also done for the oxidized synthetic Mg-rich ilmenites according to **Figure 3.12**. **Figures 4.11** and **4.12** show the SEM image and element mappings (Fe, O, Ti and Mg) of batch 2 and batches 3-5 after oxidation, respectively.

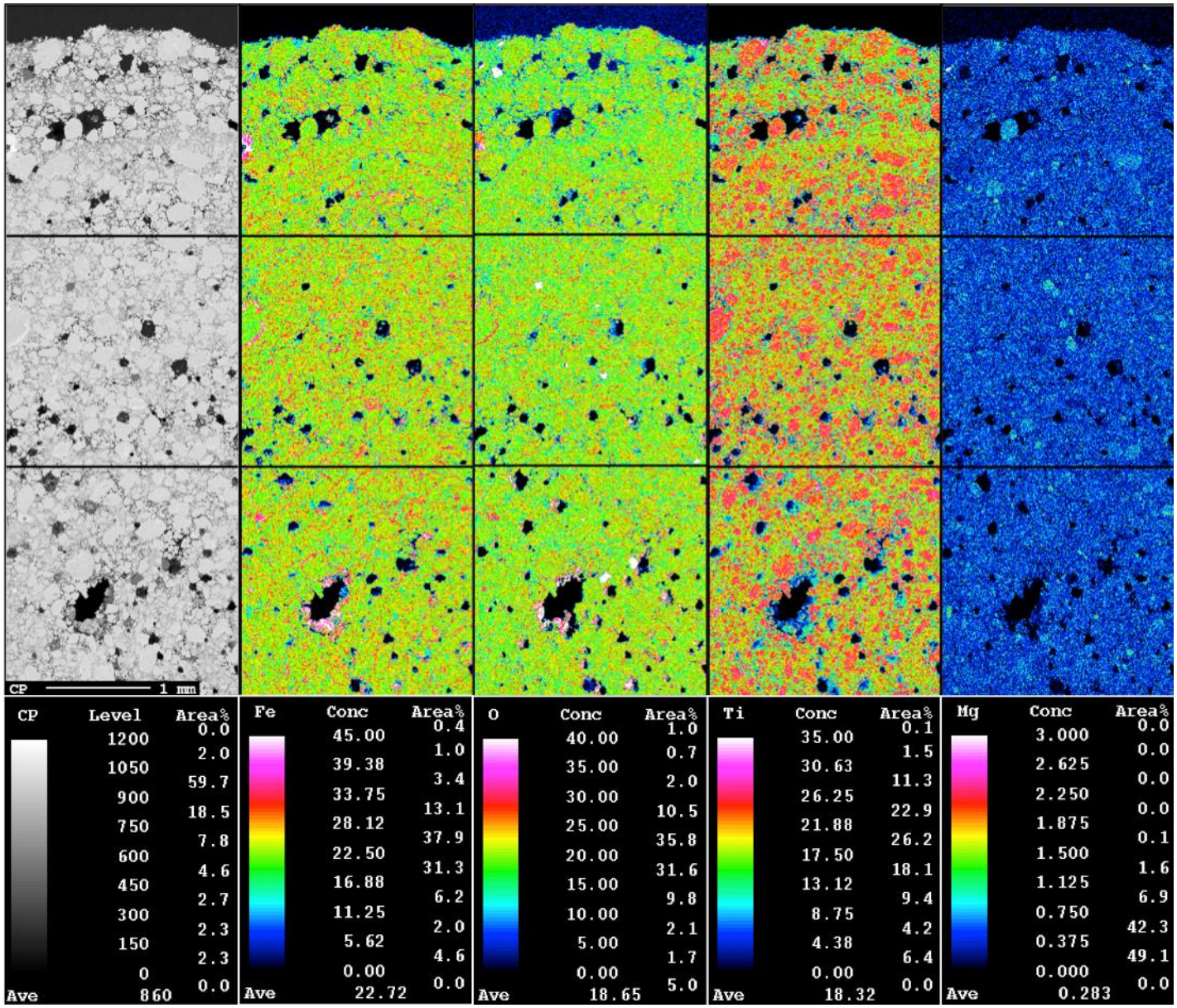

Figure 4.11 SEM image and element mappings (Fe, O, Ti, Mg) of batch 2 after oxidation

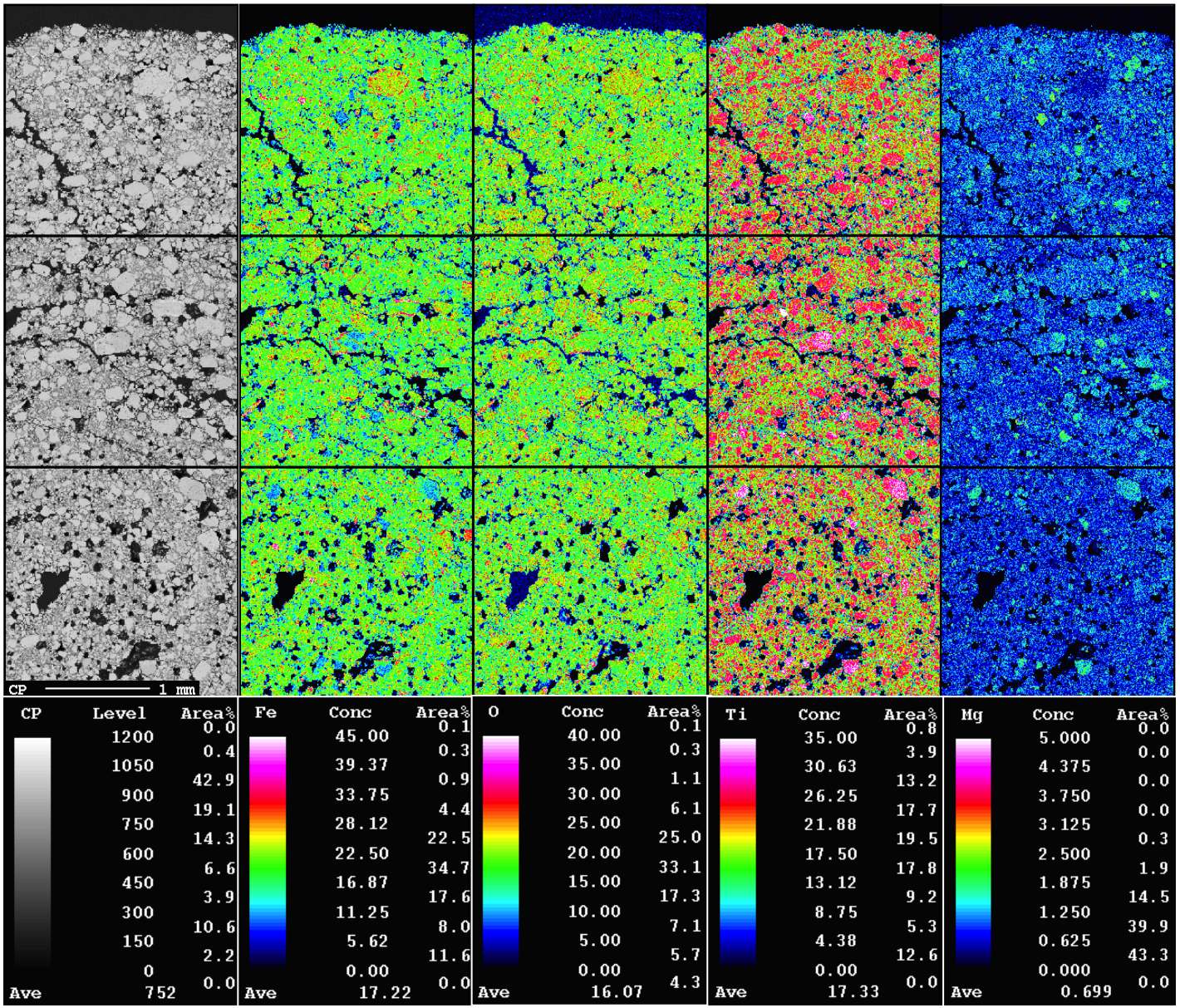

Figure 4.12 SEM image and element mappings (Fe, O, Ti, Mg) of batches 3-5 after oxidation

The analyses showed similar results with oxidized batch 1 from **Figure 4.8** and **4.9**. The SEM images for both batch 2 and batches 3-5 showed mainly 2 phases: white and grey phases. The black phases are also assumed to be epoxy or voids. The mappings of iron and oxygen for both batch 2 and batches 3-5 were similar with only minor difference. Batch 2 had an iron and oxygen concentration of color yellowish green, and batches 3-5 had an iron and oxygen concentration of color greenish yellow. Despite the minor difference, both results showed a homogeneous distribution of iron and oxygen within the pellet. For titanium mapping, both analyses showed similar results with oxidized batch 1. They showed a concentration of two main colors of red and yellow, and the concentration of titanium was higher within the grains. The mapping of magnesium showed a rather homogeneous distribution of color dark blue for both results. However, batch 2 showed a lower concentration of magnesium compared to batches 3-5. Since Batches 3-5 had more magnesium content, it showed more light blue regions.

4.3 Reduction

4.3.1 Synthetic ilmenite

The reduction of synthetic ilmenite, batch 1, went accordingly to **Table 3.3** and **Figure 3.10**. The conversion curve is shown in **Figure 4.13** (See Appendix F for mass loss curve).

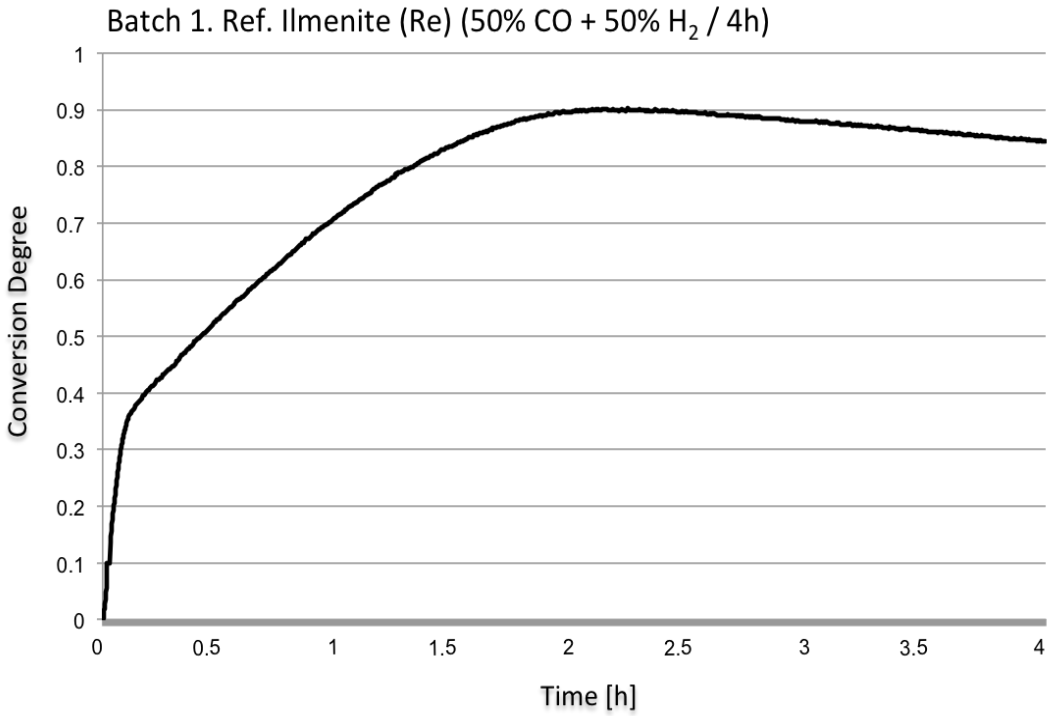

Figure 4.13 Conversion degree curve of batch 1 after 4 hours of reduction with 50% CO + 50% H_2

The conversion curve of batch 1 showed three different slopes. Between the time of 0 to approximately 0.1 hour, the conversion curve increased rapidly from "0" to approximately "0.36". Then the conversion curve began to increase slowly from "0.36" to "0.9" until approximately 2.25 hour. After the conversion curve reached its peak, it slowly began to decrease from "0.9" to approximately "0.85" until 4.0 hour. Since the conversion curve is based on mass loss of oxygen, the decreasing region between 2.25 to 4.0 hour indicates mass gain during reduction.

The XRD analysis for the reduction of synthetic ilmenite, batch 1, is given in **Figure 4.14**. When synthetic ilmenite was reduced with a mixture of 50 % CO + 50 % H_2 gas for 4 hours at temperature of 1000℃, the resulting phases were mainly metallic iron (Fe), rutile (TiO_2) according to the XRD analysis. Iron peaks of references PDF 00-003-1050 and PDF 04-007-9753 were detected. For rutile peaks, references of PDF 01-089-0554 and PDF 01-089-0555 are shown. However, additional peaks of pseudorutile of reference PDF 00-047-1777 and

unidentified peaks were also among the XRD analysis. The unidentified peaks are shown as red checkmarks in the analysis.

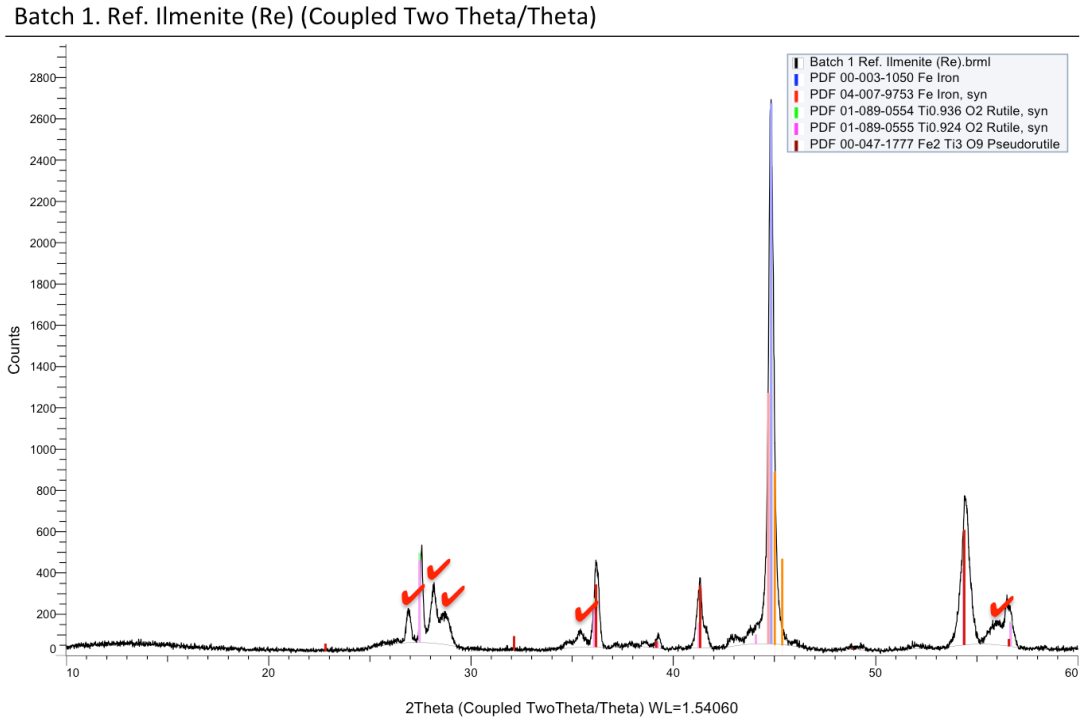

Figure 4.14 XRD analysis for synthetic ilmenite after reduction (Batch 1)

The reduced synthetic ilmenite pellets were also mounted in epoxy according to **Figure 3.12** for EPMA analysis. The EPMA analysis for the reduced synthetic ilmenite is shown in **Figure 4.15**, which show a SEM image and element mappings (Fe, O and Ti).

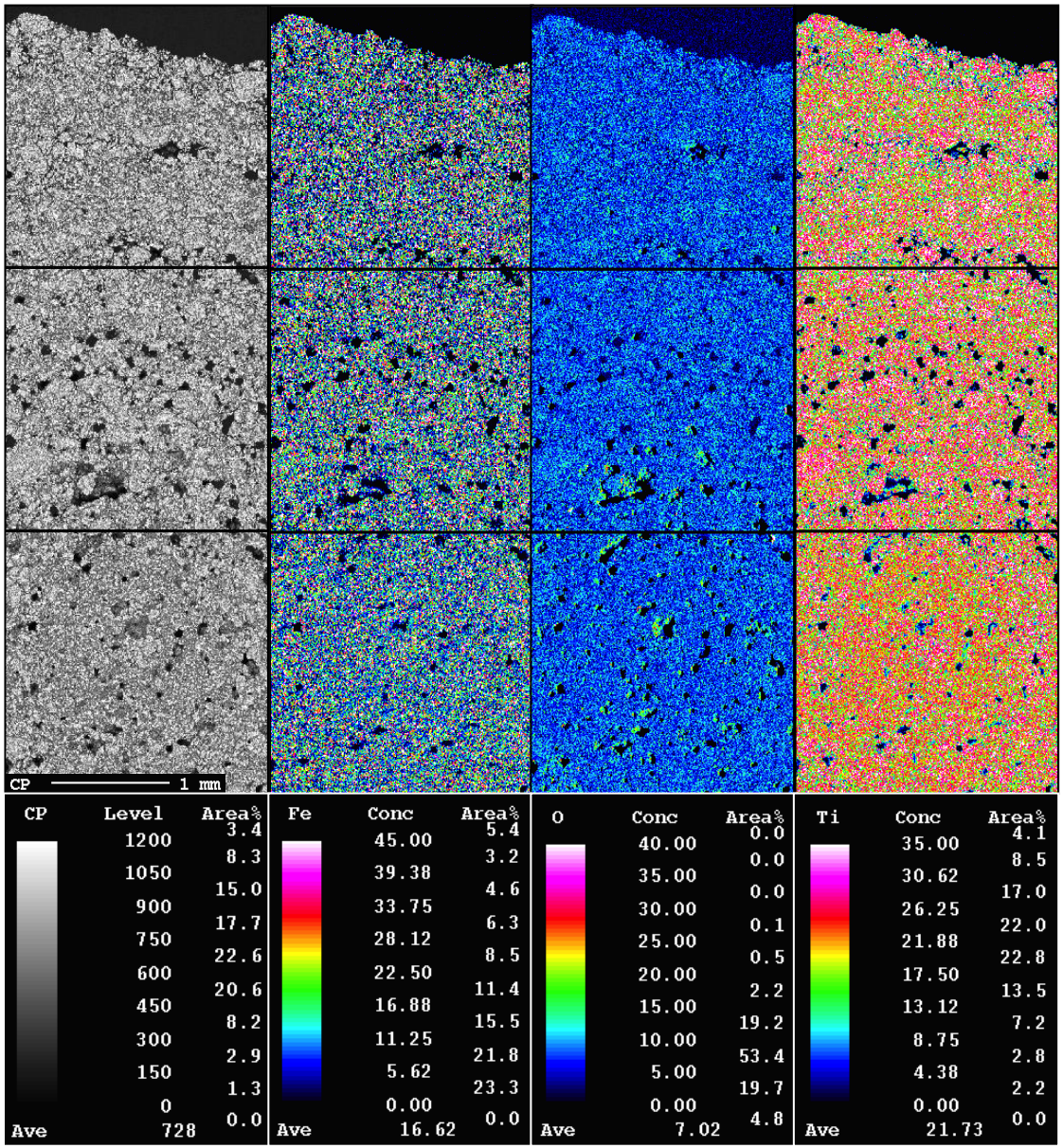

Figure 4.15 SEM image and element mappings (Fe, O, Ti) of batch 1 after reduction

The SEM image for reduced batch 1 showed two main phases of colors of white and grey. The black phases are also assumed to be epoxy and internal voids.

For element mappings, iron mapping showed a mixed concentration of colors of white, purple, light blue and dark blue. However, judging from the XRD analysis of batch 1, where the main phases were iron and rutile, iron concentration of color white seems to be the basis in the mapping where the other colors are rather homogeneously distributed on it. Oxygen mapping showed a mixed oxygen concentration of colors light blue and dark blue with dark blue being more dominant. For titanium, it showed a mixed titanium concentration of colors white, red and yellow. All three colors were rather homogeneously distributed within the pellet, but concentration of red is more focused within the grains.

4.3.2 Synthetic Mg-rich ilmenite

The reduction of synthetic Mg-rich ilmenites, batches 2-5, was also done according to the reduction plot, **Table 3.3** and **Figure 3.10**. The conversion degree curves for each synthetic Mg-rich ilmenite are shown in **Figures 4.16-19**, and the comparisons of the conversion degree curves for all batches (comparison between batches 1-3, batches 3-5 and batches 1-5) are shown in **Figures 4.20-22**. (See Appendix F for mass loss curves)

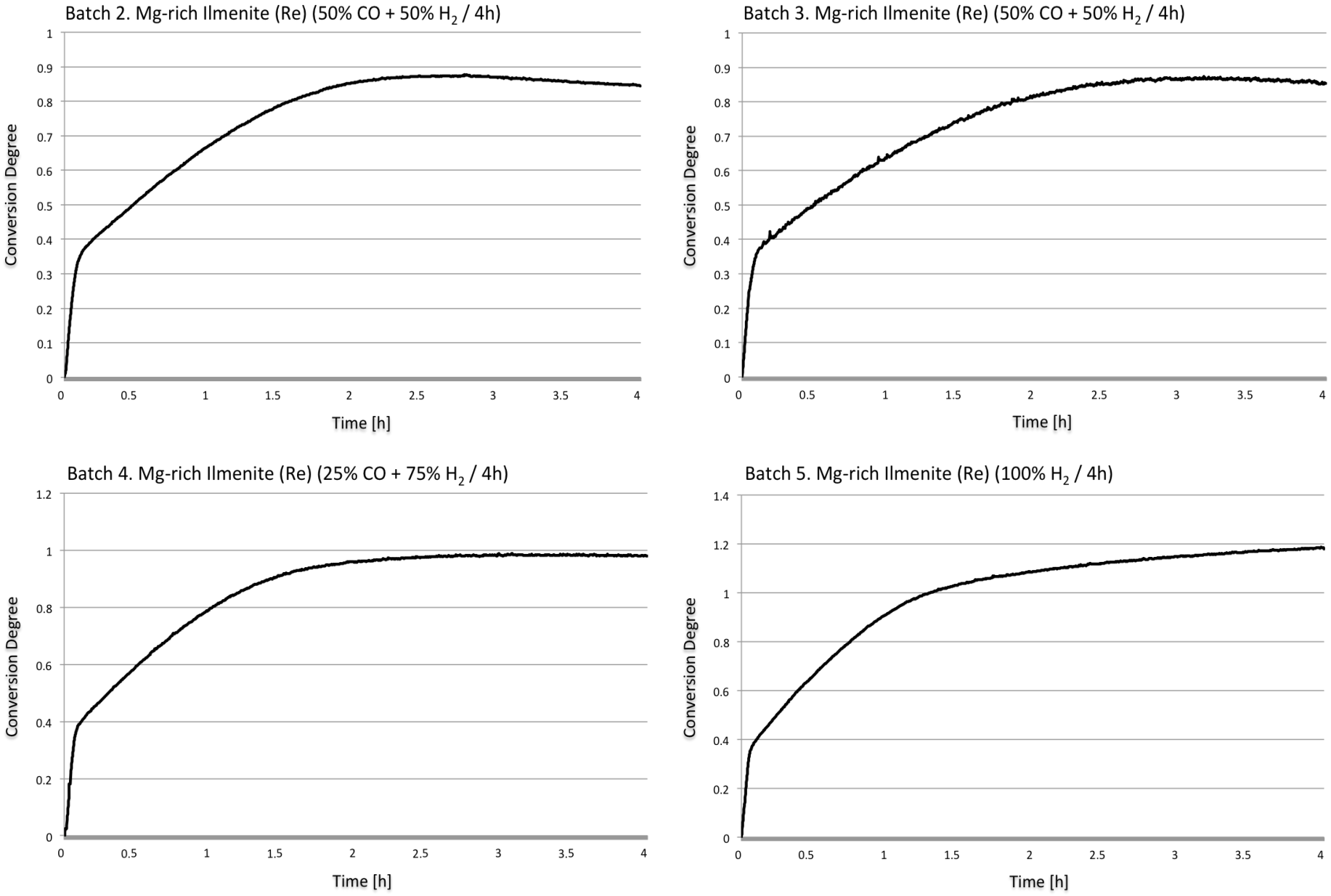

Figure 4.16-19 Conversion degree curves: Batch 2 (top-left), Batch 3 (top-right), Batch 4 (bottom-left) & Batch 5 (bottom-right) after 4 hours of reduction

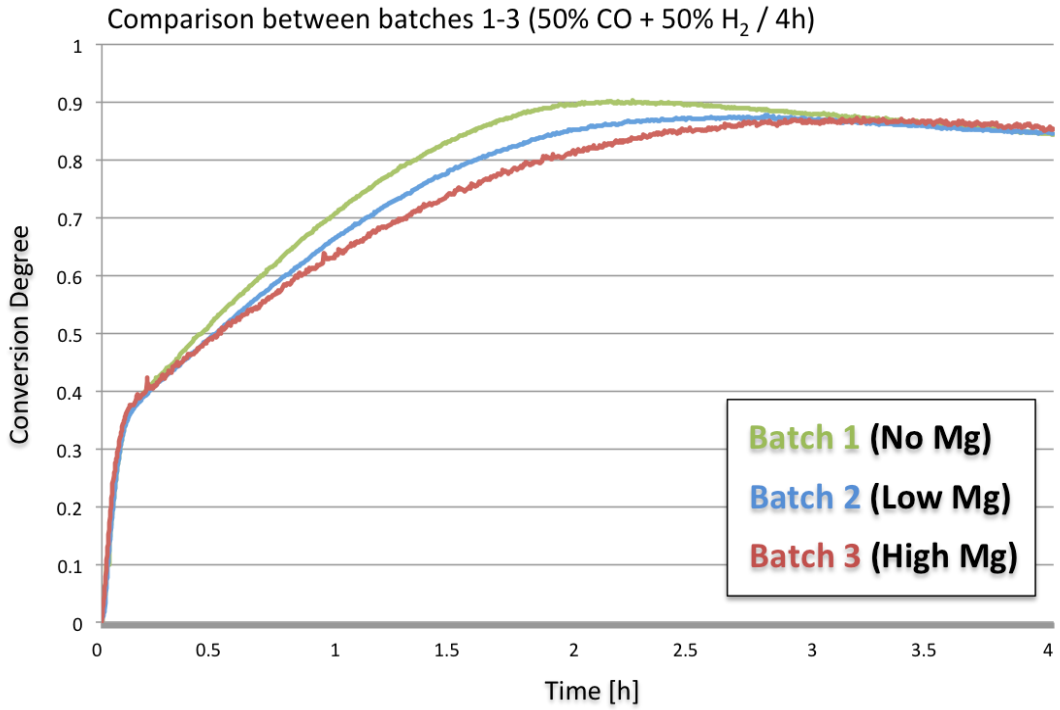

Figure 4.20 Comparison of conversion degrees between batches 1-3
(Mg amount is simply expressed as "No Mg, Low Mg, High Mg" according to **Table 3.2**)

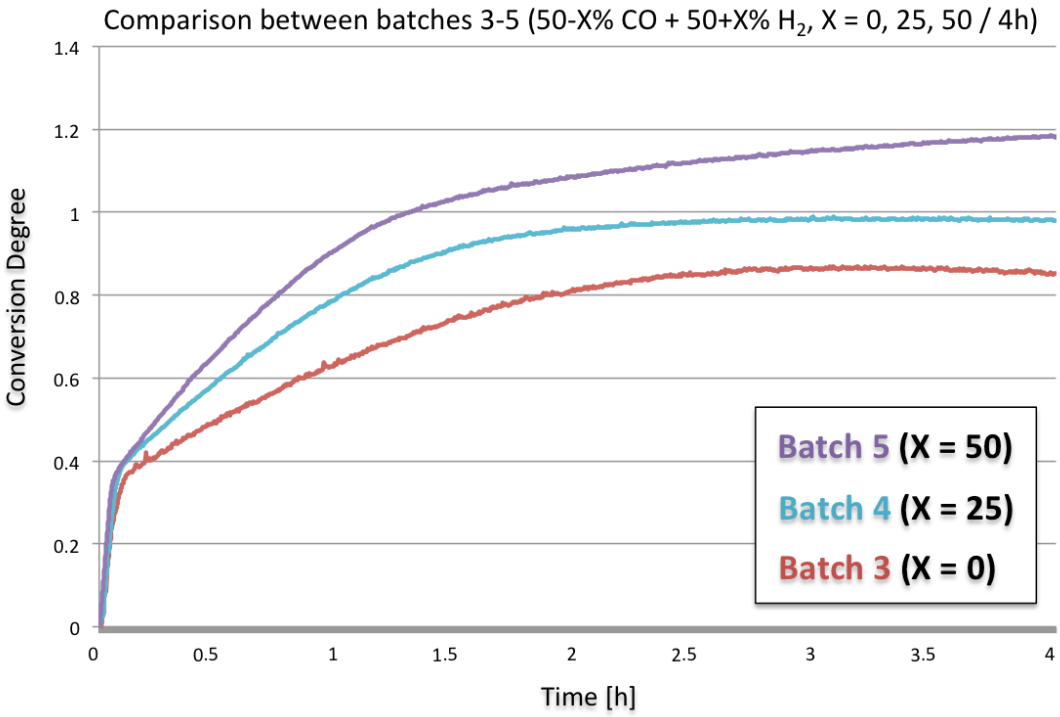

Figure 4.21 Comparison of conversion degrees between batches 3-5
(Batches 3-5 have the same amount of Mg: High Mg)

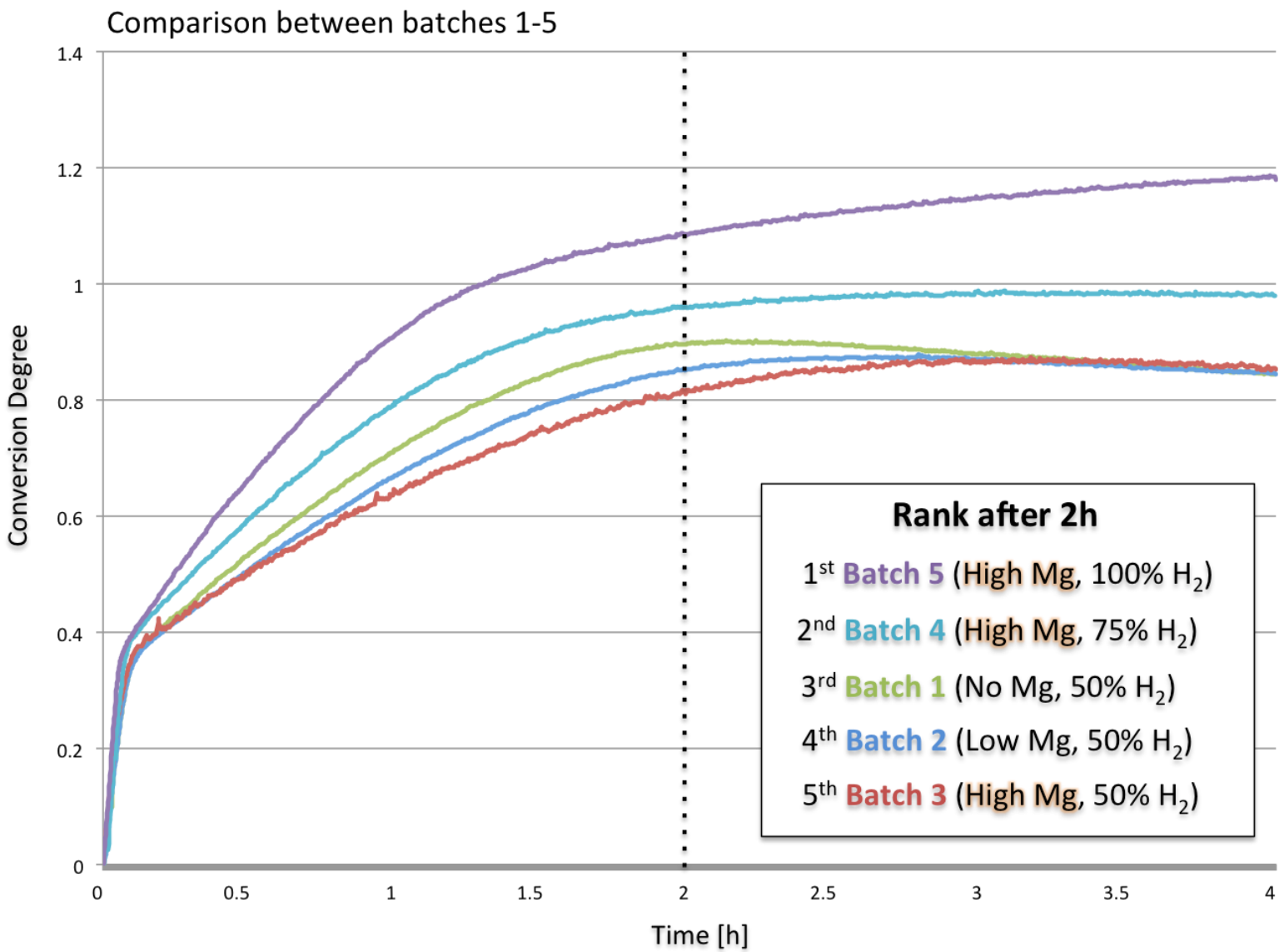

Figure 4.22 Comparison of conversion degrees between batches 1-5
(The conversion degrees of batches 1-5 are ranked after a certain amount of time: 2h)
(Note that "High Mg" is highlighted)

From **Figures 4.16-19**, the different conversion degree of each batch is shown. The maximum conversion degree for batches 2 and 3 was approximately “0.88” and “0.86”, respectively. Also, similar with batch 1, both batches showed a minor decrease in conversion degree after reaching their peaks. This also indicates mass gain since the conversion degree is based on mass loss of oxygen. The peak conversion degree for batch 4 was approximately “0.98” and it remain constant until the end of reduction. The conversion degree for batch 5 was exceeding “1” after 1.5 hour and was continuously increasing during the whole reduction. The conversion degree of batch 5 was approximately “1.18” after 4.0 hour.

The comparison of conversion degrees between batches 1-3 and batch 3-5 in **Figures 4.20** and **4.21** shows the conversion degree of synthetic ilmenite regarding the amount of magnesium or hydrogen. In **Figure 4.20**, the magnesium amount in each ilmenite is simply expressed as “No Mg”, “Low Mg” and “High Mg” considering **Table 3.2**. From the comparison, the more amount of magnesium in ilmenite resulted in lower conversion degree after a certain time. For example, the conversion degree of each ilmenite, batch 1, batch 2 and batch 3, after 2.0 hour was approximately “0.9”, “0.85” and “0.81”, respectively. From **Figure 4.21**, batches 3-5 (batch 3 in **Figures 4.20** and **4.21** are the same) had the same amount of magnesium (High Mg), but they were reduced with different amount of hydrogen gas. The more use of hydrogen gas in reduction showed higher degree of conversion after a certain time. For example, batch 5, which was reduced with only hydrogen gas, showed the highest conversion degree compared to other batches. It was already exceeding “1” after 1.5 hour. Batch 4 was reduced with 75% hydrogen gas, and the conversion degree was near to “1” after 2.0 hour but did not exceed “1”. Batch 3 was reduced with 50% hydrogen and it showed the lowest conversion degree among the comparison. It was approximately “0.81” after 2.0 hour.

The comparison of all batches is also given in **Figure 4.22** to see the integrated relation of synthetic ilmenite with magnesium and hydrogen gas. The conversion degrees after a certain time (2.0 hour) were ranked: 1st Batch 5, 2nd Batch 4, 3rd Batch 1, 4th Batch 2 and 5th Batch 3. From the ranking, the results were same with **Figures 4.20** and **21**, but the ranking gap between the used of hydrogen content in reduction was greater than the ranking gap of the magnesium content in ilmenite. For example, when considering only batches 1-3, the result was the same in **Figure 4.20**. However, when considering only batches 3-5 (where the “High Mg” is highlighted

in **Figure 4.22**), there was a big gap between batch 4 and 3. Also, the ranking gaps between batches 3-5 were bigger than the ranking gaps between batches 1-3.

The XRD analyses for reduction of synthetic Mg-rich ilmenites, batches 2-5, are also given in **Figures 4.23-26**, and the summary of these results are described in **Table 4.1**.

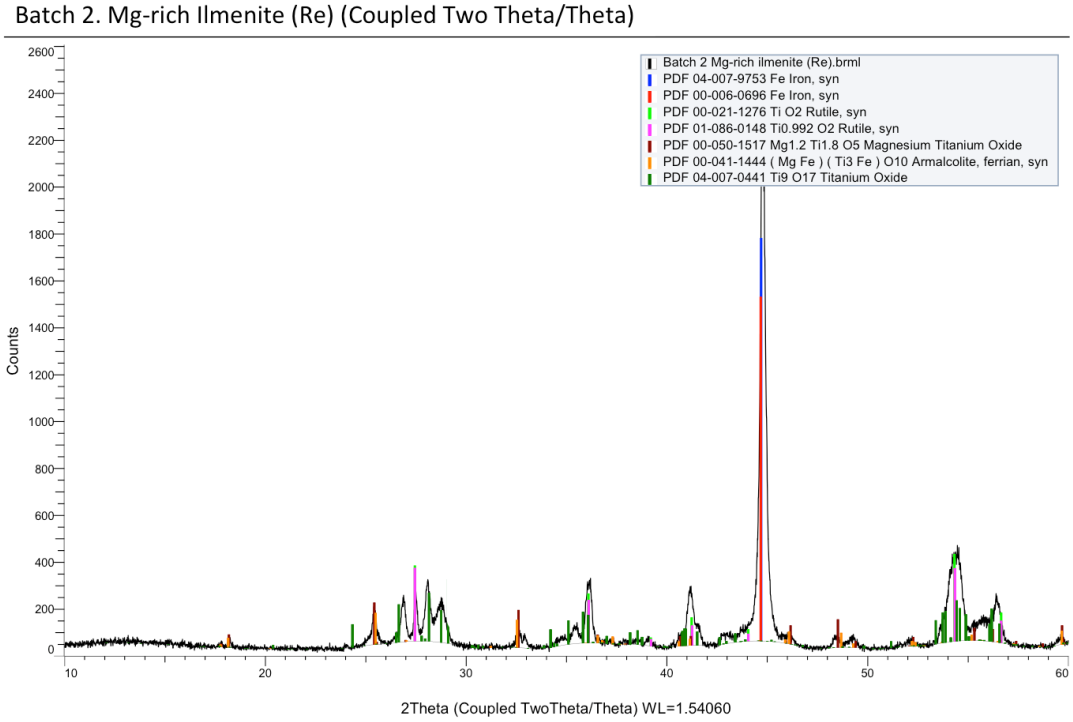

Figure 4.23 XRD analysis for synthetic Mg-rich ilmenite after reduction (Batch 2)

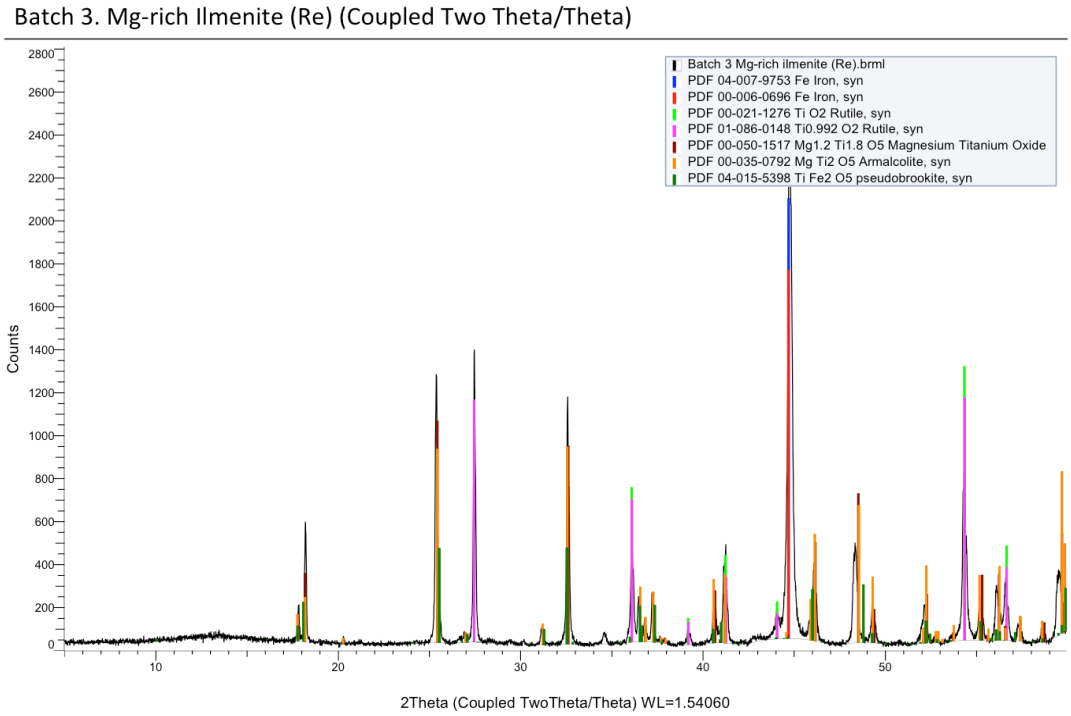

Figure 4.24 XRD analysis for synthetic Mg-rich ilmenite after reduction (Batch 3)

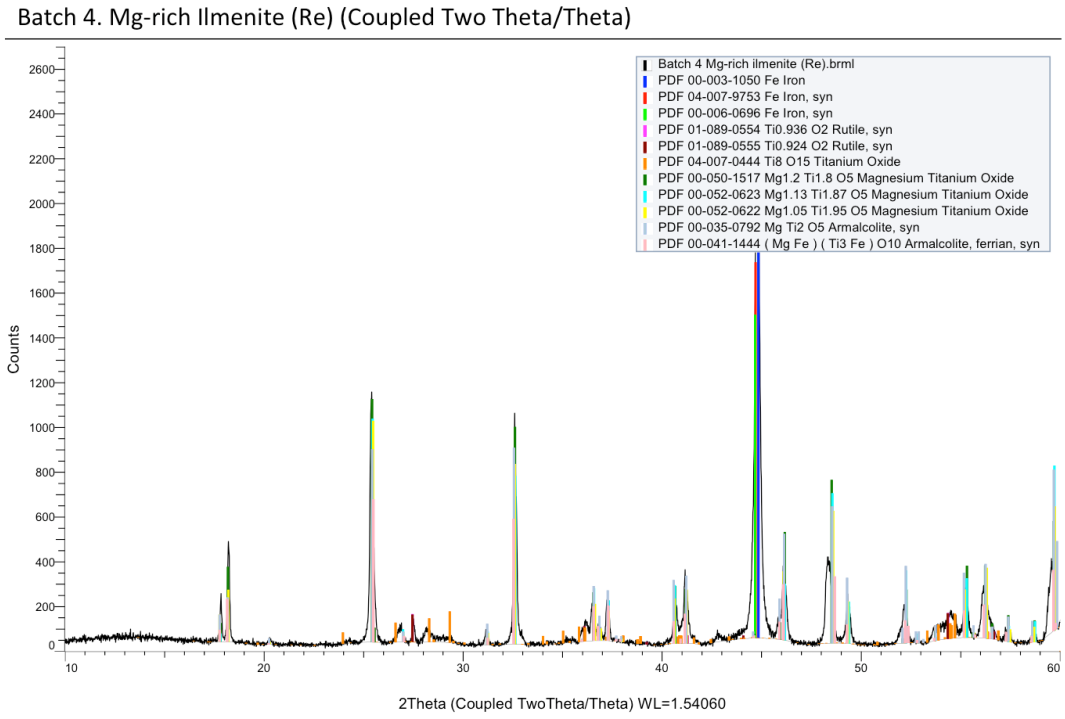

Figure 4.25 XRD analysis for synthetic Mg-rich ilmenite after reduction (Batch 4)

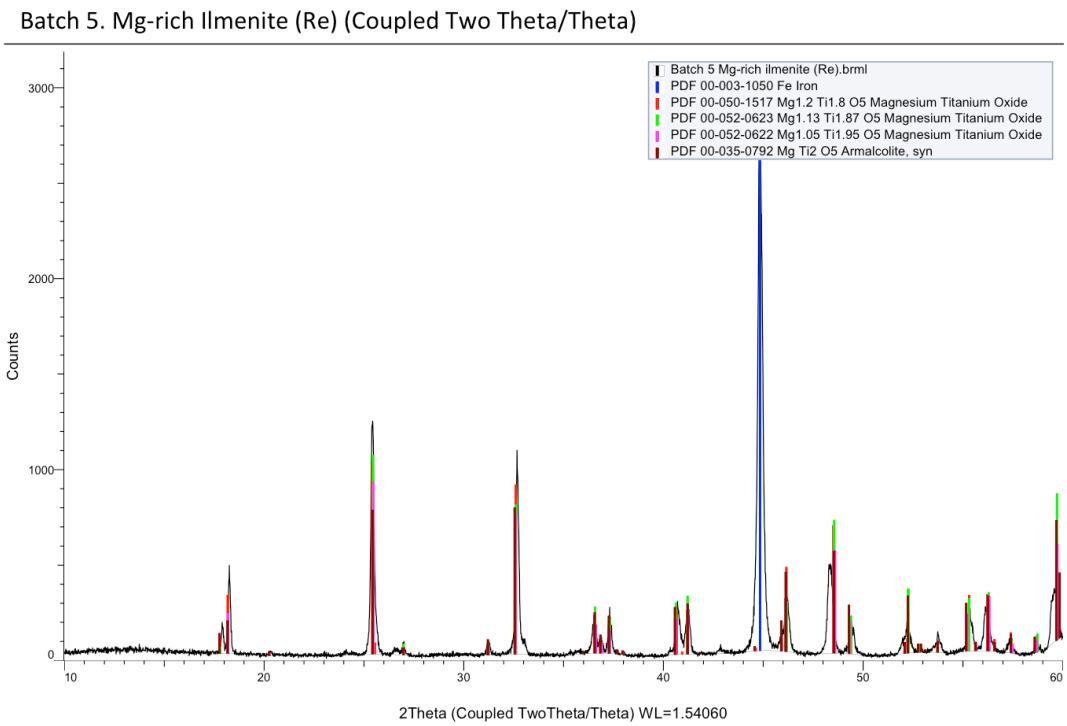

Figure 4.26 XRD analysis for synthetic Mg-rich ilmenite after reduction (Batch 5)

Table 4.1 Summary for reduction of batches 2-5

Batch	Common	Difference	Mg	Reductant
2	Iron		Low Mg	50% CO + **50% H_2**
3	Pseudobrookite			
4	Rutile		High Mg	25% CO + **75% H_2**
5	Mg, Ti oxide Species Armalcolite	No (Reduced) Rutile No Pseudobrookite		**100% H_2**

The main phases from batch 2 were iron and rutile according to the XRD analysis in **Figure 4.23**. It showed an iron peak of references PDF 04-007-9753 and PDF 00-006-0696. For rutile, there were peaks of references PDF 00-021-1276 and PDF 01-086-0148. A reduced rutile phase (Ti_9O_{17}) was also seen with reference of PDF 04-007-0441. There were also detection of Mg, Ti oxide specie and armalcolite with reference of PDF 00-050-1517 and PDF 00-041-1444, respectively.

The XRD analysis of batch 3 in **Figure 4.24** showed similar results with batch 2. The main phases were iron and rutile. Iron peak of references PDF 04-007-9753 and PDF 00-006-0696, and rutile peaks of references PDF 00-021-1276 and PDF 01-086-0148 were detected. Also peaks of pseudobrookite, Mg, Ti oxide specie and armalcolite were seen. The references of these peaks were PDF 04-015-5398, PDF 00-050-1517 and PDF 00-035-0792, respectively.

Batch 4 in **Figure 4.25** was similar with batches 2 and 3 but with more references of Mg, Ti oxide species and armalcolite. References of iron peaks were PDF 00-003-1050, PDF 04-007-9753 and PDF 00-006-0696, and references of rutile peaks were PDF 01-089-0554 and PDF 01-089-0555. Also, an additional reduced rutile phase (Ti_8O_{15}) was seen with the reference of PDF 04-007-0444. For the Mg, Ti oxide species, the references were PDF 00-050-1517, PDF 00-052-0623 and PDF 00-052-0622. Armalcolite with references of PDF 00-035-0792 and PDF 00-041-1444 were also included in the XRD analysis.

Batch 5 in **Figure 4.26** showed a different result. It showed only iron, Mg,Ti oxide species and armalcolite peaks but no detection of rutile or pseudobrookite peaks. The reference of iron peak was PDF 00-003-1050, and the references of Mg, Ti oxide species peaks were PDF 00-050-1517, PDF 00-052-0623 and PDF 00-052-0622. Armalcolite peaks had the reference PDF 00-035-0792.

Summarizing the XRD analyses from batches 2-5, the common phases detected were iron, rutile, pseudobrookite, Mg, Ti oxide species and armalcolite. However, batch 5, which was reduced with only hydrogen gas, showed no detection of rutile or reduced rutile (since the conversion degree exceeded "1") and pseudobrookite peaks in the XRD analysis.

The reduced synthetic Mg-rich ilmenite pellets (batches 2-5) were also mounted in epoxy according to **Figure 3.12** for EPMA analysis. The EPMA analysis for the reduced batch 2 and 5 are shown in **Figure 4.27** and **28**, respectively. They show a SEM image and element mappings (Fe, O, Ti and Mg). The EPMA analyses for batches 3 and 4 were quite similar with batch 2 (See Appendix G for EPMA analyses for batch 3 and 4).

The SEM images for reduced batch 2 and 5 showed two main phases of colors white and grey, which were similar with reduced batch 1 in **Figure 4.15**. The black phases were also assumed to be epoxy and internal voids.

For element mappings, iron mapping for both batch 2 and 5 was similar with the previous iron mapping of reduced batch 1 in **Figure 4.15**. It also showed a mixed concentration of colors white, purple, light blue and dark blue. Since the XRD analysis for both reduced batches 2 and 5 had

detected iron as the dominating phase, the iron concentration of color white seems to be the basis in both mappings where the other colors are rather homogeneously distributed. The oxygen mappings for both batches showed very similar color concentration with the oxygen mapping in reduced batch 1. Both batches 2 and 5 had a mixed light blue and dark blue color concentration. The titanium mapping for batches 2 and 5 also had the similar results compared to the titanium mapping of batch 1 in **Figure 4.15**. The dominating colors were white, red and yellow with red more concentrated within the grains.

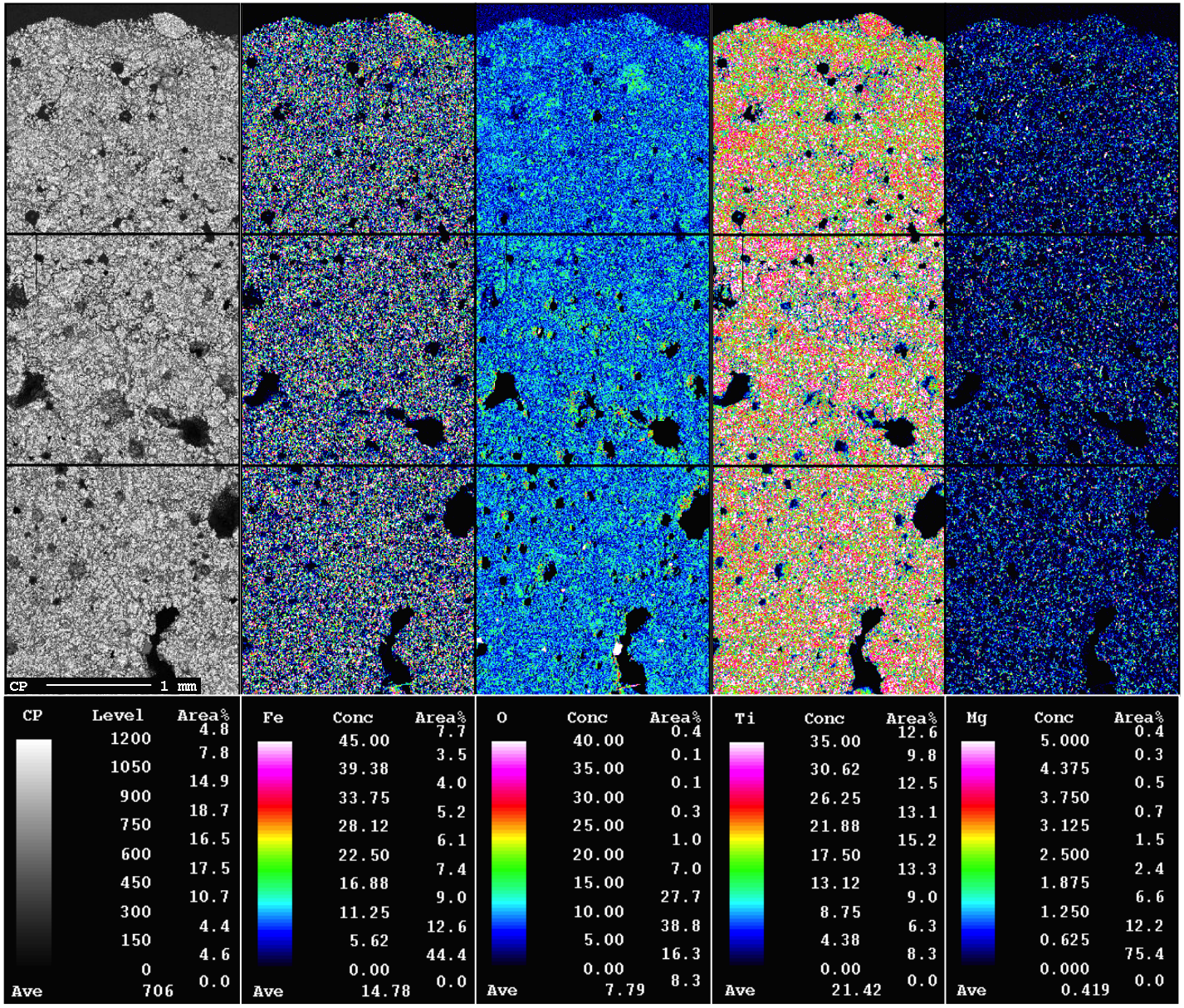

Figure 4.27 SEM image and element mappings (Fe, O, Ti, Mg) of batch 2 after reduction

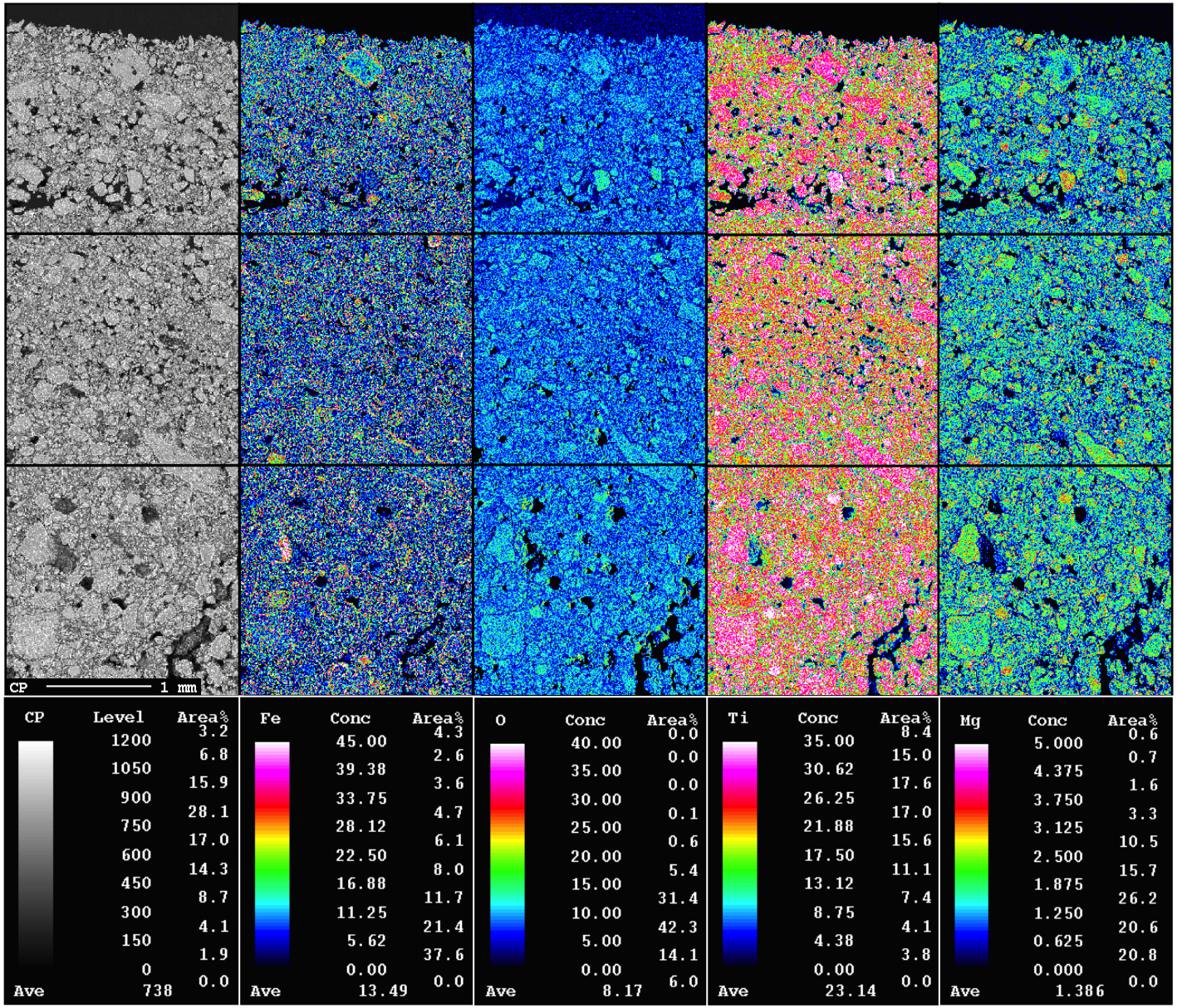

Figure 4.28 SEM image and element mappings (Fe, O, Ti, Mg) of batch 5 after reduction

Chapter 5 Discussion

The discussion part aims at the interpretation of the results from the previous chapter. Interpretation of each experimental result (synthesis, oxidation and reduction) is asserted based on the documentation from chapter 2, theory.

In the synthesis part, the meaning of successful ilmenite synthesis is explained along with the porous structure of synthetic Mg-rich ilmenite, which was observed in this work. The oxidation part focuses on the oxidation mechanism of ilmenite and how magnesium in ilmenite affects it. The Fe, Ti, Mg and O quaternary system from chapter 2 is also mentioned to describe the comparison of the oxidation path between synthetic ilmenite and Mg-rich ilmenite. The reduction part mainly consists the interpretation of the conversion curve of each batch and the influence of magnesium and hydrogen gas in gaseous reduction of synthetic Mg-rich ilmenite. Also, the comparison of the reduction behavior between natural ilmenite and synthetic ilmenite is described to conclude the impact of magnesium in ilmenite pre-reduction. In addition, possible future works considering kinetic modeling and surface characteristics of ilmenite reduction are briefly introduced as further objectives.

5.1 Synthesis

5.1.1 Meaning and possibilities of synthetic ilmenite ore

The successful synthesis of ilmenite ores (bulk in **Figure 4.1** and **4.3**) in this work has an appealing fact that they are relatively very pure compared to natural ilmenite ores. This advantage can open many opportunities where impurity elements in question can be added. It can use to isolate of the impact of a single impurity element by applying controlled amount into the synthesis, or even adding multiple impurity elements to see how they influence each other in the ilmenite host during gaseous reduction. Magnesium was the impurity element added into pure ilmenite in this work, and the impact of magnesium in ilmenite during gaseous reduction was clearly observed due to the pureness of synthesized ilmenite. More details of magnesium in synthetic ilmenite reduction are described in **Section 5.3**. The results of synthetic ilmenite experiments can be considered well founded compared to the obscure indications of natural ilmenite experiments, which has various impurities with different amounts.

5.1.2 Porous structure of synthetic Mg-rich ilmenite

The cross-section of the synthetic Mg-rich ilmenite bulks (batches 2-5) showed a porous structure compared to the dense structure of synthetic ilmenite (batch 1). This comparison can be easily seen between **Figures 4.1** and **4.3**. There are three assertions, which can be thought to explain the porous structure of the synthesized Mg-rich ilmenite bulk.

First, the different lattice parameters between ilmenite and geikielite (the partially replaced ilmenite by magnesium in the ilmenite crystal structure, -$MgTiO_3$) can give an explanation for the porous structure of synthetic Mg-rich ilmenites. The lattice parameters and ideal cell volume of ilmenite and geikielite were mentioned previously in chapter 2: the lattice parameters were a = 5.088 Å, c = 14.092 Å for ilmenite and a = 5.086 Å, c = 14.093 Å for geikielite. The ideal cell volume was 315.839 $Å^3$ and 315.573 $Å^3$ for ilmenite and geikielite, respectively. The porous structure in the synthetized Mg-rich ilmenite bulk can be created due to the difference in the cell volume. However, this is a poor assertion since the difference of lattice parameters and cell volume were insignificant to create a porous structure visible to a naked eye. Also, the pores

observed were more concentrated near the rear and bottom edges of the bulk. This indicates that the generated pores have close relation with temperature difference because the copper crucible used for the synthesis was a water-cooled system (see **Section 3.1.3**).

Second, the porous structure could have been created due to the leftover moisture in the raw materials or boron nitride coating. For example, raw material such as magnesium oxide (MgO) easily absorbs moisture when exposed at air in room temperature (explained in **Section 3.1.3**). Incompletely dried boron nitride coating on the crucible walls can also contain moisture. These moisture cause expansion during the cooling of the synthesis and can create pores in the synthesized material. However, this is also a weak assertion. During the high temperature synthesis, there were no observations of liquid melt splashing, which are caused by the extreme volume expansion of moisture. The possibility of leftover moisture in the cooling of the melt is very unlikely to be found if there was no liquid melt splashing during the high temperature melt. Also, the magnesium oxide used was examined for absorbed moisture before the high temperature synthesis to prevent lethal accidents, and the boron nitride coating was dried more than three days before use.

Third, the density change of the liquid melt due to the slow cooling method could have been a possibility to create pores in the synthetic Mg-rich ilmenite bulk. The copper crucible used was an internal water-cooled container, and the liquid melt in the crucible is cooled instantly when killing the power supply. For example, synthetic ilmenite (batch 1) was cooled rapidly after killing the power supply and its cross-section showed a dense homogeneous oxide structure. However, for synthetic Mg-rich ilmenites, slow cooling was done so that the rear and bottom edges of the melt solidify first. Since the density of the melt depends on the temperature, there could have been a possibility of separation between solid and fluid, which could have generated the pores. The density-temperature relation of liquid oxides is a complicated concept but the general idea is that density decreases with increasing temperature (exception such as water or silicon at low temperature):

$$PV = nRT, \qquad \frac{n}{V} = \frac{P}{RT}$$

$$\frac{m}{V} = \rho = \frac{PM}{RT} \qquad \left(n = \frac{m}{M} \right)$$

$$\rho \propto \frac{1}{T}$$

Where P = pressure, V = volume, n = mole, R = ideal gas constant, T = absolute temperature, ρ = density, m = mass and M = molar mass.

This is an affirmative assertion because the pores observed in **Figure 4.3** were rather concentrated on the rear and bottom edges than the upper edge where the temperature cooling was the slowest.

Of course, there can be other explanations of the porous structure of synthetic Mg-rich ilmenite and an integrated theory should be considered. Nevertheless, among the three assertions above, the pore generation due to the separation of solid and fluid from density-temperature relation seems the most convictive explanation.

5.2 Oxidation

5.2.1 Homogeneous distribution of iron

The homogeneous distribution of iron during oxidation of ilmenite was observed in both synthetic ilmenite and Mg-rich ilmenite samples. The iron mappings of the EPMA results in **Figures 4.9, 4.12** and **4.13** show a homogeneous iron concentration of colors yellow and green within the pellet. Also, when considering the grains, the concentration of iron was higher at the grain boundaries, which showed a concentration of color red. This suggests that the iron is more mobile towards the grain boundaries or interface layers where it is oxidized. **Figure 2.7** in **Section 2.3.2** shows the appropriate illustration of this mechanism. At the grain boundaries or interface layers, it seems that the crystal lattices of rutile, hematite and pseudorutile disintegrate and form the new phase, ferric (Fe^{3+}) pseudobrookite. This is in a good agreement since the main stable phase at the oxidation temperature of more than 800 ℃ was ferric pseudobrookite, which was previously mentioned in chapter 2. The XRD analysis in **Figure 4.6**, which shows only pseudobrookite and rutile peaks, also supports the tentative mechanism illustrated in **Figure 2.7**.

5.2.2 Phases after oxidation of synthetic ilmenite and Mg-rich ilmenite

The impurity, magnesium, during ilmenite oxidation tends to form other phases besides ferric (Fe^{3+}) pseudobrookite and rutile. The other phases are magnesium dititanate ($MgTi_2O_5$) and hematite (Fe_2O_3), which were observed in **Figures 4.10** and **4.11**.

The theoretical phases after oxidation of ilmenite (T > 800℃) are only ferric pseudobrookite and rutile as mentioned in **Section 2.3.2**. The oxidation of synthetic ilmenite (batch 1) in this work follows the theory where the oxidation results were only ferric pseudobrookite and rutile. However, when Mg-rich ilmenites (batches 2-5) were oxidized, they gave additional phases such as magnesium dititanate and hematite. According to the quaternary and ternary phase diagram in **Figures 2.8** and **2.9**, magnesium dititanate was expected after the oxidation of synthetic Mg-rich ilmenites but not hematite. The detection of hematite indicates that ferrous iron (Fe^{2+}) in ilmenite has not completely all oxidized into ferric pseudobrookite but into other ferric oxides such as hematite.

The formation of hematite seems to be from the lack of pseudobrookite-type formation for iron because of magnesium. As the ionic radius of magnesium was similar with iron (**Section 2.1.2**), magnesium also tends to form the thermodynamically stable pseudobrookite-type phase such as magnesium dititanate at a relatively high temperature (T > 800℃). The formation rate of magnesium dititanate is assumed to be more faster than the formation rate of ferric pseudobrookite because the specific gravity of magnesium is approximately 4.5 times lighter than iron (**Section 2.1.2**). Before all iron in ilmenite oxidized into ferric pseudobrookite, magnesium is likely to be stabilized first into a pseudobrookite-type form by forming magnesium dititanate. Then the leftover iron, which could not form pseudobrookite, oxidizes into the next stable phase, hematite. The following **Figure 5.1** describes the reason for hematite formation in synthetic Mg-rich ilmenite oxidation. The parentheses in the figure are the amount of iron in ilmenite before and after oxidation, and the numbers are examples. The exact amount was not known in this work.

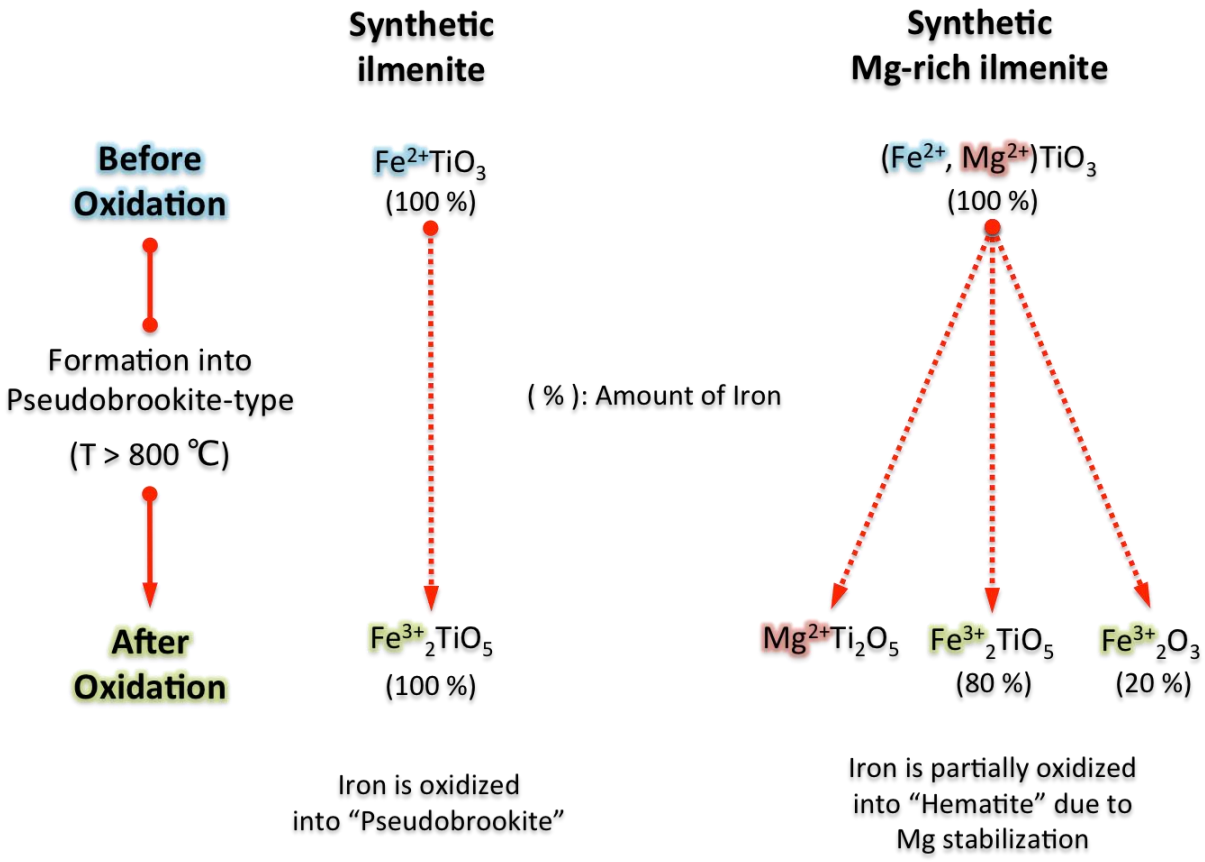

Figure 5.1 Illustration of synthetic ilmenite and Mg-rich ilmenite oxidation

Assuming the hematite formation due to magnesium, the oxidation paths, A and B, in **Figures 2.8** and **2.9** should now consider the results from **Figure 5.1**. While path A, which is the oxidation of synthetic ilmenite, shares no argument, path B should have an auxiliary path to explain the unexpected hematite formation. **Figures 5.2** and **5.3** shows the suggested revision of **Figures 2.8** and **2.9**. The added auxiliary path, B2, is assumed to be on the right side of the main path, B1, following the ratio, Mg/Ti = 0.2. This is only alleged considering the constant Mg/Ti ratio and the small amount of hematite. The accurate revision should require additional theoretical work and experiments.

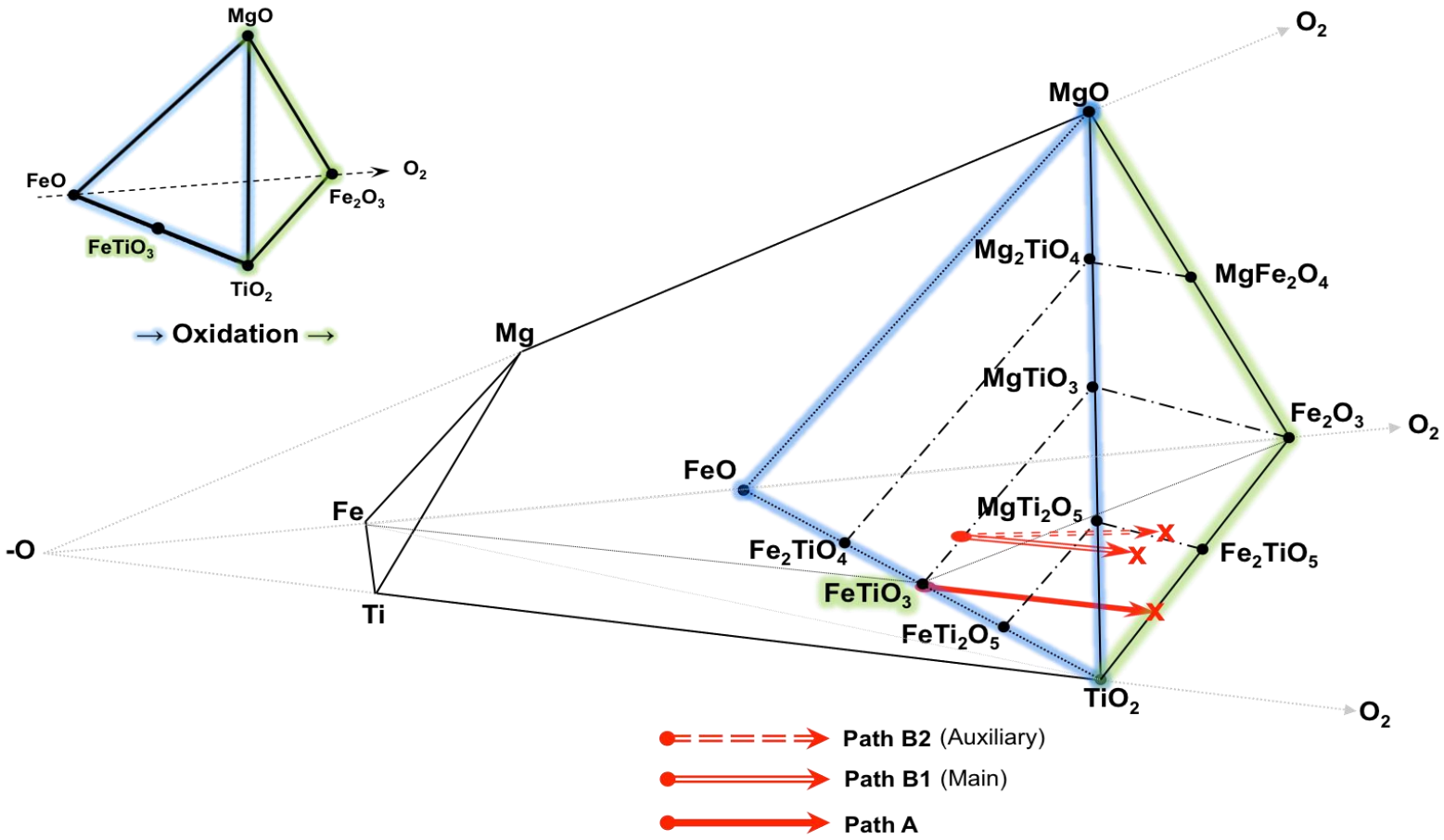

Figure 5.2 The suggested revision of Figure 2.8

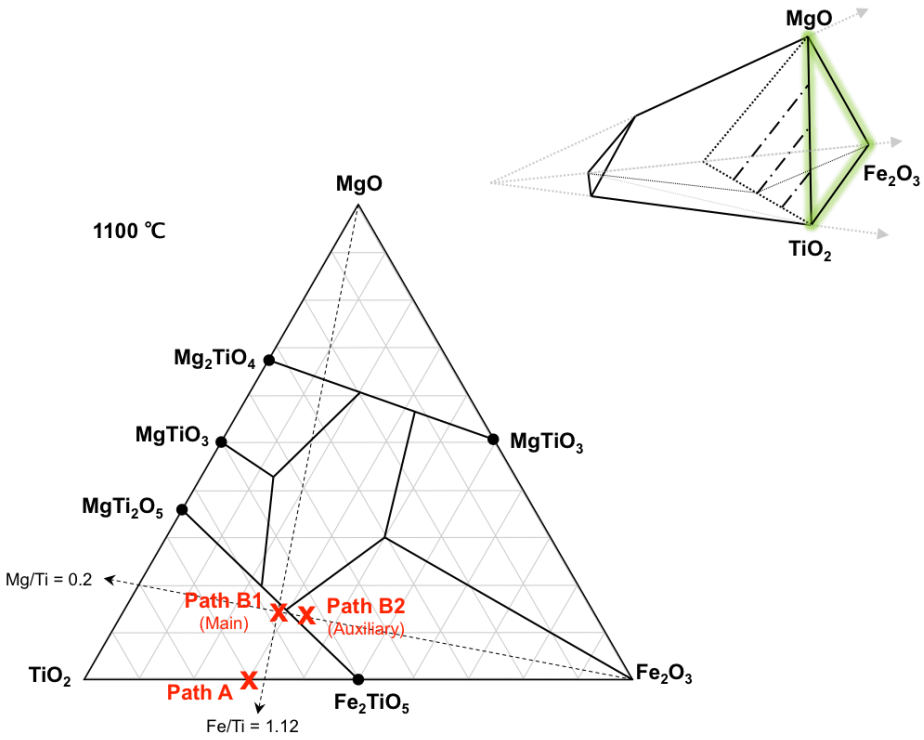

Figure 5.3 The suggested revision of Figure 2.9

5.3 Reduction

5.3.1 Comparison between natural ilmenite and synthetic ilmenite gaseous reduction

The comparison of gaseous reduction between natural ilmenite and synthetic ilmenite shares clear indications of how an impurity behaves in the ilmenite host. The indications from natural ilmenite experiments were ambiguous due to complicated relations of various kinds of impurities with different amounts. Previously, there were some suggestion of how an impurity behaves in the ilmenite host during gaseous reduction and affects the reduction rate, but not conclusive.

However, the results from synthetic ilmenite experiments were much more convincing due to its relatively high purity. Synthesized ilmenite ores were oxidized and reduced with controlled amount of impurity in this work. With no other foreign elements affecting, the behavior of the impurity in question in ilmenite reduction was very clear. It was not only the impact of the impurity itself, but also the results from different amount of impurity and reductant gases were

comprehensible. For example, batches 1-3 had different amount of magnesium but were reduced with 50% CO + 50% H_2 in this work. Batches 3-5 had the same amount of magnesium but were reduced with different percentage of hydrogen gas. The results from these experiments were clear enough to give an idea of how magnesium and hydrogen gas influences the reduction rate during gaseous reduction of ilmenite.

5.3.2 The impact of Mg and H_2 gas in ilmenite reduction

The magnesium in ilmenite as impurity clearly hinders the reduction rate in ilmenite reduction. The increasing amount of magnesium in ilmenite had gave lower conversion degree for ilmenite reduction and was well observed with batches 1-3 in **Figures 4.20** and **4.22**. Without other foreign impurities interfering, the fact that increasing amount of magnesium in ilmenite giving lower conversion degree clearly indicates that magnesium had hindered the reduction rate in ilmenite reduction. For example, the different slopes of conversion degrees in **Figures 4.20** and **4.22** show the different reduction rates according to the amount of magnesium in ilmenite. The first rapidly increasing slopes of bathes 1-3 between 0 to approximately 0.1 hour were the expected first stage iron reduction (ferric, Fe^{3+} to ferrous, Fe^{2+}) from **Section 2.4.2**. The curves from these slopes were similar and had no significant difference in the conversion degree. However, the slopes start to change after approximately 0.1 hour where the expected second stage of iron reduction (ferrous, Fe^{2+} to metallic, Fe) begins, and they increased slowly according to the magnesium amount in ilmenite. The slope of each conversion curve was lower with increasing amount of magnesium.

Since the final phases detected after reduction were Mg, Ti oxide species and armalcolite ($(Fe,Mg)Ti_2O_5$) besides metallic iron and rutile for batches 2 (low Mg) and 3-5 (high Mg), it is assumed that the iron oxide reduction in ilmenite is being hindered by armalcolite formation due to magnesium. The armalcolite phase still carries the iron oxides even after the slopes of conversion curves become parallel, and this is in a good agreement because the conversion degrees were below "1" for batches 2-4. The exact amount of armalcolite in batches 2-4 were not known but it is assumed that more amount of armalcolite was formed with increasing amount of magnesium in ilmenite. This assumption is also in a good agreement because the conversion degree was lower with increasing amount of magnesium in ilmenite.

In addition, the minor decrease of conversion degree in batches 1-3 indicates mass gain after peak conversion since the conversion degree was calculated based on the mass loss of each batch. The carbon deposition from the Boudouard Reaction (**Reaction 10** in **Section 2.4.1**) seems to explain the mass gain of batches 1-3 because the reductant gas had considerable amount of CO gas (50% CO + 50% H_2). The CO gas initially tackles the iron oxides in ilmenite and produces CO_2 gas. After the conversion degree stops increasing, which further reduction is hindered by magnesium, the amount of CO gas reducing the iron oxides becomes less. Then the partial pressure of CO gas increases while the partial pressure of CO_2 gas decreases inside the crucible. According to the Boudouard reaction, the CO gas formation side at higher temperatures (reduction temperature: 1000 ℃) is more favorable. However, carbon deposition had occurred, and it is thought to be from the high CO gas concentration. Most of the deposited carbon was found near the top part of the crucible wall near the radiation sheets (**Figure 3.11**), and the top part of the crucible is assumed to have relatively lower temperature than the lower part of the crucible where the pellets are being reduced. To support this assumption, traces of carbon elements were not found within the pellets or the surfaces of pellets. Nevertheless, additional work should be required before a complete understanding of carbon deposition in ilmenite reduction.

The use of hydrogen as additional reductant gas in ilmenite reduction clearly enhanced the reduction rate. The more amount of hydrogen used for the reductant gas showed higher conversion degree in ilmenite reduction as it was seen with batches 4 and 5 in **Figures 4.21** and **4.22**. Batch 4, which was a 25 percent increase of hydrogen amount from batch 3, showed a conversion degree close to "1", and batch 5, which was reduced with only hydrogen gas, showed a conversion degree near to "1.2" after 4.0 hour. The relatively high conversion degree of batches 4 and 5 compared to batch 3 indicates hydrogen gas has clearly enhanced the reduction rate of ilmenite.

The combined impact of magnesium and hydrogen gas in ilmenite reduction should also be mentioned to interpret the results in batch 5. The XRD result of batch 5 in **Figure 4.26** shows phases of metallic iron, Mg, Ti oxide species and armalcolite but not rutile or reduced rutile. According to **Figure 4.19**, the conversion degree of batch 5 after 4.0 hour was exceeding "1", which indicates that all iron oxides have been reduced and oxygen was being removed from rutile. However, **Figure 4.26** shows no indication of rutile or reduced rutile. Also the presence of

armalcolite indicates unreduced iron oxides are still incorporated in the armalcolite phase. There can be two assumptions to explain these indications.

First, as it was anticipated in **Section 2.4.4**, magnesium as impurity in ilmenite seems to immediately stabilized the reduced rutile species after they are produced. For impurity-free ilmenite, the theoretical phases are metallic iron, rutile and reduced rutile species above the conversion degree of "1". However, for Mg-rich ilmenite (batch 5), only phases of metallic iron, Mg, Ti oxides species and armalcolite were observed above the conversion degree of "1". The absence of rutile or reduced rutile species indicates magnesium had possibly stabilized the thermodynamically less stable reduced rutile species by forming Mg, Ti oxides species or armalcolite. The standard Gibbs energy data of $MgTiO_3$ and TiO_2 reduction by H_2 gas in **Figure 2.11** gives a hint to this possibility, and the fact that pure synthetic Mg-rich ilmenite used in this work supports the first assumption. **Figure 5.4** shows the illustration of the first assumption explained above. Hydrogen reduction of synthetic ilmenite is added in the illustration for comparison with synthetic Mg-rich ilmenite (batch5), and "X" are the values found in the XRD results for Mg-rich ilmenites (batches 2-5).

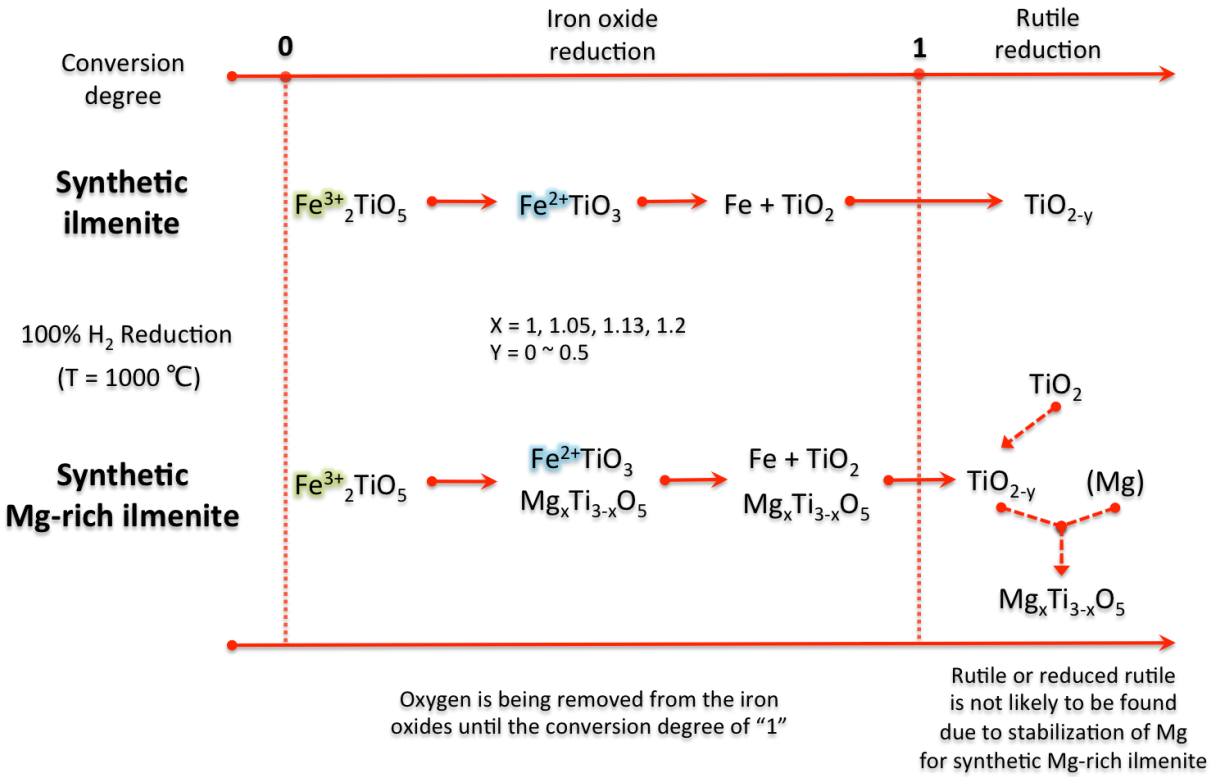

Figure 5.4 Illustration of synthetic Mg-rich ilmenite (batch 5) reduction result

Second, the iron oxides are assumed to be incompletely reduced even after the conversion degree exceeds “1” due to formation of armalcolite. Below the conversion degree of “1”, the pseudobrookite or armalcolite phase can explain the unreduced iron oxides in ilmenite. Pseudobrookite is the unreduced version of ilmenite and armalcolite still contains iron oxides, which are incorporated within. This can be seen clearly in the XRD results of batches 2-4, **Figures 4.23-25**. However, the conversion degree was above “1” when the reduction of batch 5 was finished and it showed armalcolite phase. This means there were still iron oxides incorporated within armalcolite after the conversion degree exceeded “1”. It can be thought that magnesium had strongly hindered the iron oxide reduction by capturing them in the armalcolite phase, and the assumptions, which were used to calculate the conversion degree of ilmenite reduction, should be revised.

It is necessary to revise the assumptions of conversion degree calculation for ilmenite reduction. One of the initial assumptions, which were explained in **Section 3.3.1**, was that rutile during reduction is assumed to be inert so that only iron oxide reduction is in progress until the conversion degree of “1”. After the conversion degree of “1”, all the iron oxides has been reduced to metallic iron and oxygen is being removed from rutile. But to explain the presence of armalcolite (which incorporates iron oxides) above the conversion degree of “1” in batch 5, the assumption that rutile is considered to be inert until the conversion degree of “1” needs to be reconsidered. One suggestion is that the reduction of phases in ilmenite is thought to be spontaneous throughout the whole time rather than in distinct stages. The reduction of rutile seems to start not after all the iron has been reduced but at the same time when the two iron oxide reduction stages begins. The reduction of phases can seem separated only because of their different rate of reduction. During the first two iron oxide reduction stages, the reduction rate of iron oxide is relatively much more dominate than the reduction rate of rutile so that rutile reduction does not seems to occur. To support this revised assumption, reduced rutile was actually observed before the conversion degree reached “1”. The XRD result of batches 2 and 4 in **Figures 4.23** and **4.25** showed small peaks of reduced rutile species, Ti_9O_{17} and Ti_8O_{15}. **Figure 5.5** illustrates the revised assumption for conversion degree and explains the presence of reduced rutile and armalcolite (which incorporates iron oxides) before and after the conversion degree of “1”, respectively. The magnitude of each reduction rate is loosely based on the slopes in the conversion degree curves.

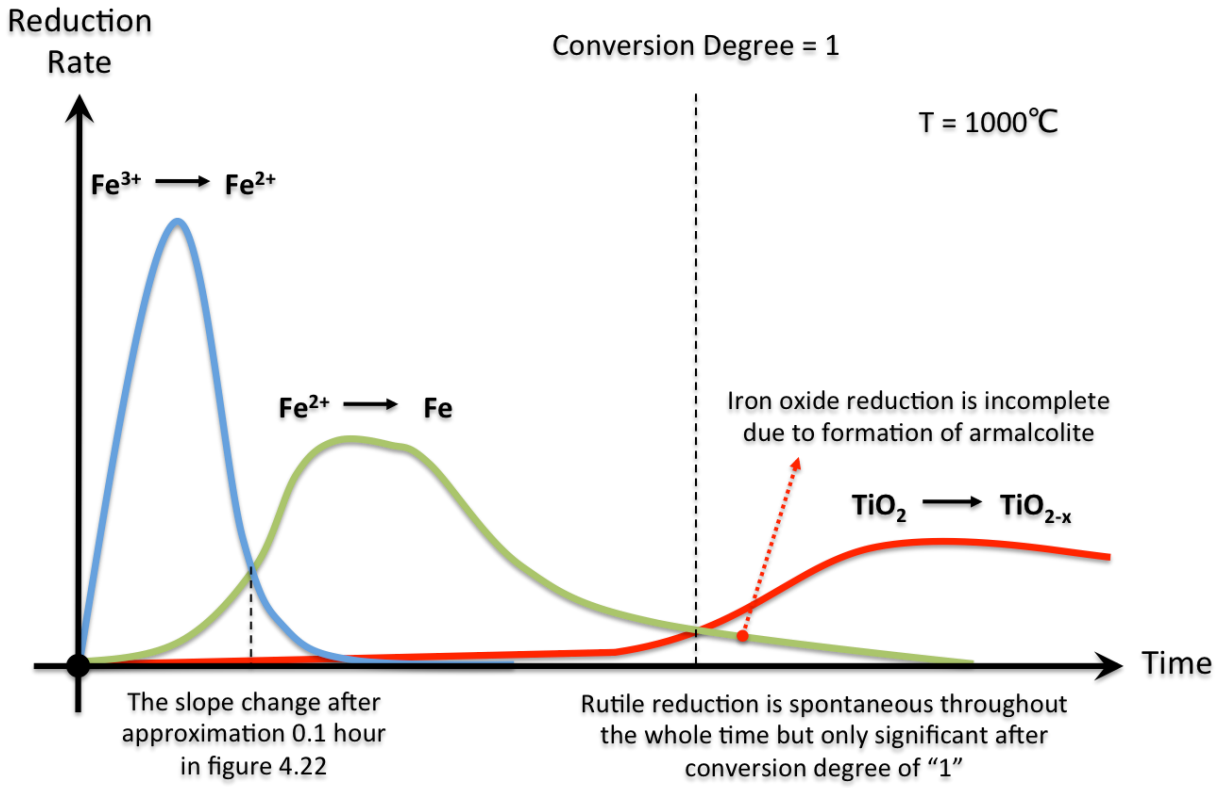

Figure 5.5 Illustration of ilmenite reduction with revised assumption for conversion degree

5.4 Future work

5.4.1 Necessary of future work

Although the main objective, which was to isolate the impact of impurity (Mg) in ilmenite reduction, was achieved in this thesis work, additional experimental and theoretical work is necessary to support documentation. For example, further examination on the surface of reduced ilmenite pellets can share different surface properties according to experiment conditions. Also, ilmenite reduction with different reduction time can share certain data, which can be useful for kinetic modeling of ilmenite reduction. These two examples of further work will only be briefly introduced in this section.

5.4.2 Surface properties of reduced ilmenite pellets

Examining the surface properties of reduced ilmenite pellets can share how different experimental conditions influence the iron oxide reduction in ilmenite. Since the conversion degree for each batch in this work was different due to the magnesium amount and gas composition, it is easy to see that iron oxides reduce to metallic iron with different rate. This rate can determine the surface properties of ilmenite pellets, and the amount of impurity (magnesium) and gas composition possibly controls it.

To support this need of additional work, an experiment of DRI (Direct Reduced Iron) production in a fluidized bed can be related [54]. **Figure 5.6** describes the structural change of an iron ore particle during reduction with reductant gases.

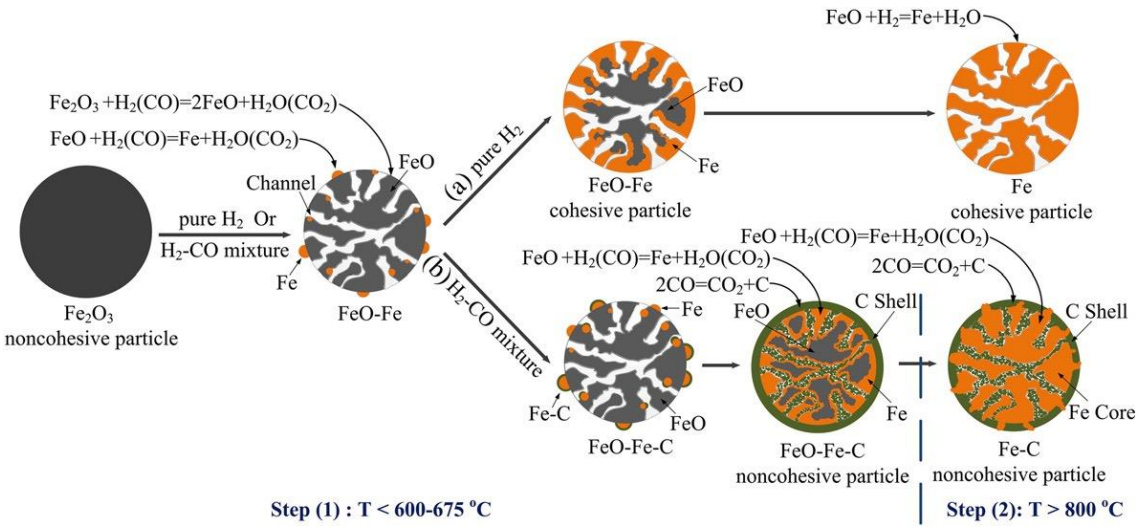

Figure 5.6 Diagrammatic sketches of the structure change of an iron ore particle during reduction by (a) H_2 and (b) H_2-CO mixture [54]

Iron ore particles in Step (1) are reduced with pure H_2 gas (a) or a mixture of H_2-CO gas (b). The structure of iron ore particles behave differently according to each reduction, and the reduction results are illustrated in Step (2). When iron ore particles were reduced with pure H_2 gas, iron oxide reduction was the only dominating reaction. It gave a cohesive surface property and eventually de-fluidization had occurred in the fluidized bed furnace. However, unlike the results with pure H_2 gas (a), when iron ore particles were reduced with a mixture of H_2-CO gas

(b), carbon deposition on the particles was also among the reactions. It had formed noncohesive carbon shell on the particles, which prevented de-fluidization in the fluidized bed furnace [54].

Although traces of carbon were not found with ilmenite pellets when reducing with a mixture of 50% CO + 50% H_2 in this thesis work, examining the surface structures of reduced ilmenite pellets can reveal how impurity (magnesium) or different reductant gas composition affects the surface properties and further reduction rate of ilmenite.

5.4.3 Kinetic modeling of ilmenite reduction

An additional work considering kinetics can also be done to complete the impact of impurity (magnesium) and hydrogen gas in ilmenite reduction. The EPMA images from chapter 4 were from relatively prolonged reduction time, where reductant gases had reached the pellet core. These images share less kinetic data such as layer boundaries showing reduction progress. However, **Figure 5.7** shows the image of synthetic ilmenite reduction for relatively short reduction time [55]. From the iron and oxygen mapping, layers with different colors can be seen. These different layers indicate how far the reductant gases had progressed in ilmenite reduction. The radius from the cord to each layer can be measured, and relation with other variables such as time, temperature, Mg amount, gas composition, grain size, etc. can be served as raw data for building an accurate SCM (Shrinking Core Model) for ilmenite reduction:

$$f(t) = g(R) \cdot h(T) \cdot k(Mg) \cdots z(etc.)$$

where t =time, R = layer radius, T = temperature, Mg = Mg amount and etc. = other variables.

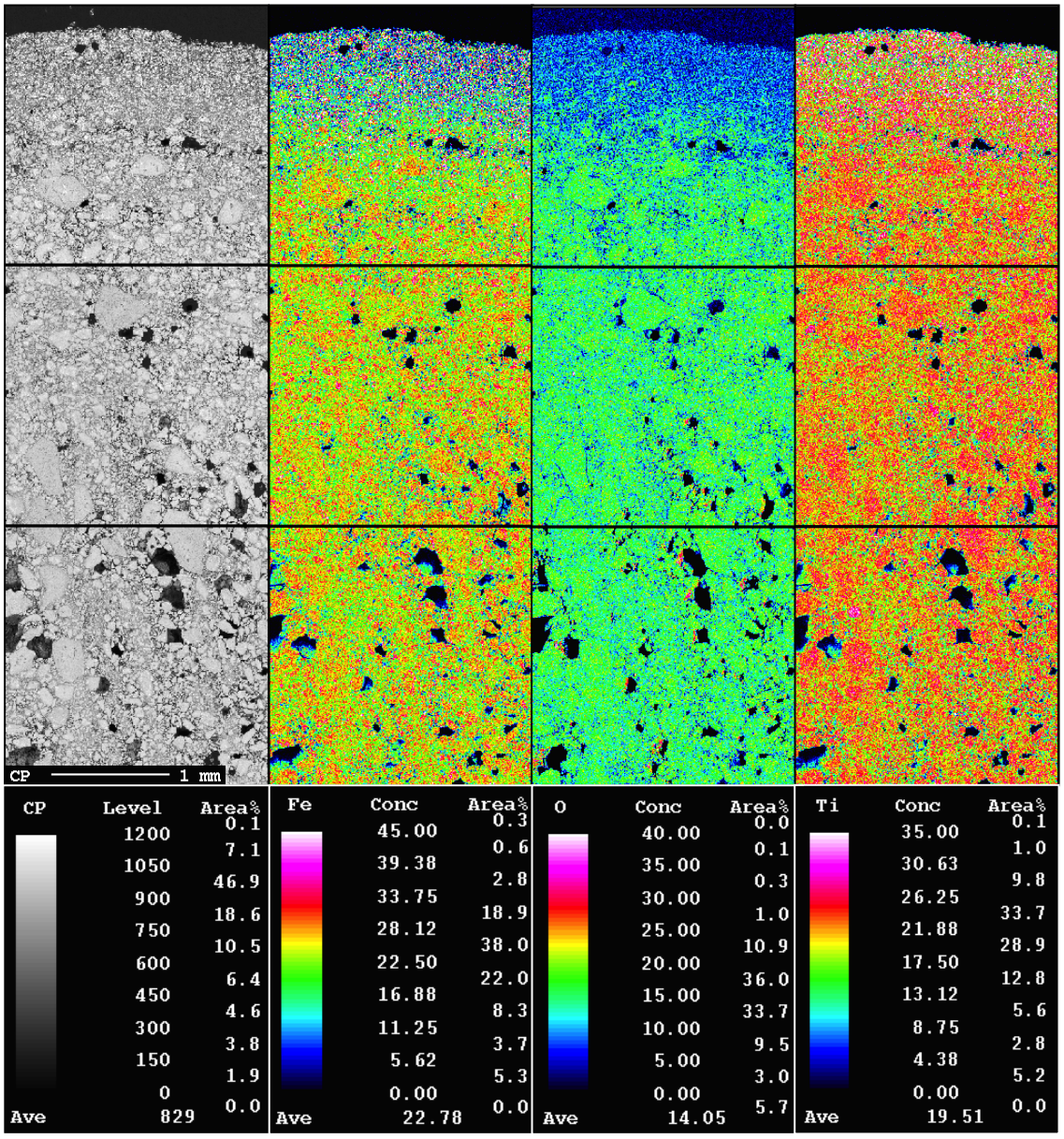

Figure 5.7 SEM image and element mappings (Fe, O, Ti) of synthetic ilmenite after reduction (50% CO + 50% H2 / 34 min) [55]

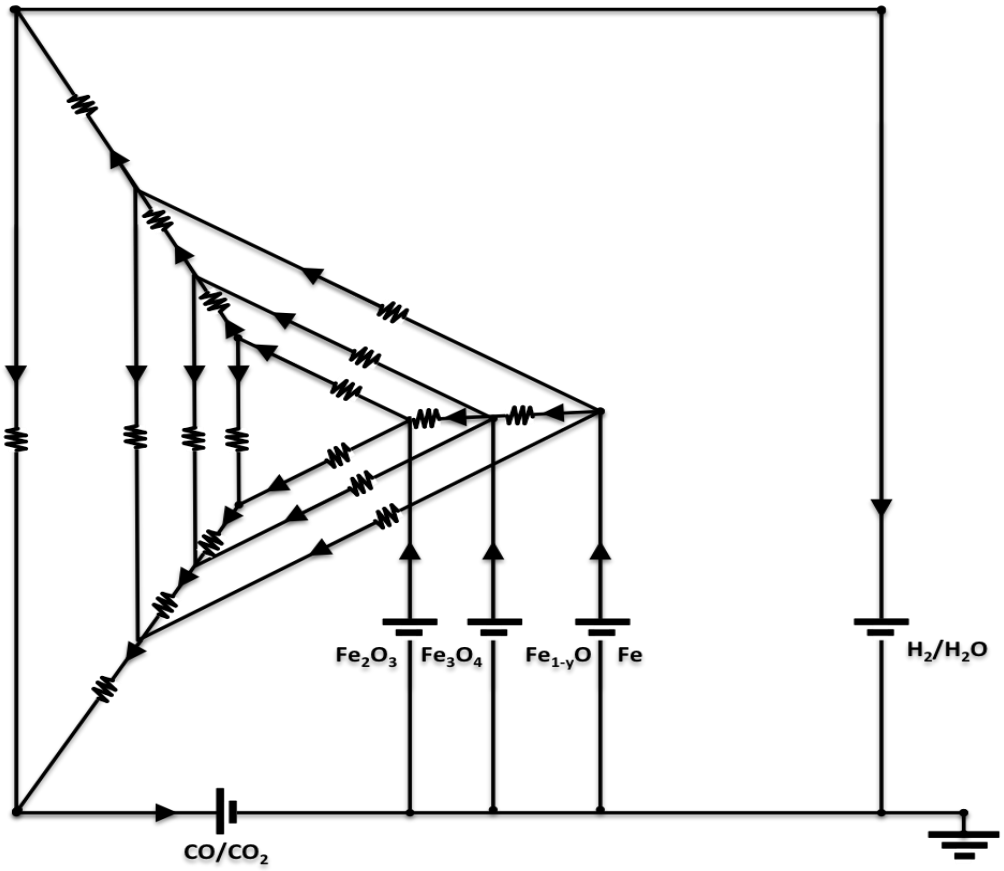

Figure 5.8 Electric circuit analogy for iron ore shrinking core model [56]

Currently, Lobo is developing a model for pre-reduction of ilmenite with natural gas based on Kolbeinsen's "Electrical Circuit Analogy For Iron Ore Shrinking Core Model" [22, 56]. The electrical circuit analogy uses the shrinking core model as a basis. **Figure 5.8** shows the electrical circuit for iron ore shrinking core model. Each controlling step is a resistance, and diffusion (both gas film and solid product layer) and chemical reactions are resistant to the current (current is the flow of oxygen in the circuit). By using these methods from electrical circuit analysis, the model can be solved with oxygen flow acting similarly to current and Gibbs energy providing a driving force.

In case of ilmenite, the reduction generally only takes into account the reduction of the iron oxides when rutile is assumed to be inert until the conversion degree of "1". However, rutile have shown to be reduced before and after the conversion degree of "1" in this work, and challenges in the future work will be to incorporate the effects of rutile into the shrinking core model for ilmenite reduction.

Chapter 6 Conclusion

The final chapter summarizes the experimental work and discussion of magnesium in ilmenite. Key points from each synthesis, oxidation and reduction are briefly described in bulleted list.

6.1 Synthesis

- Synthetic ilmenite and Mg-rich ilmenite were successfully made in a laboratory scale by using a CCIF (Cold Crucible Induction Furnace) in Ar atmosphere.
- The synthesis of $FeTiO_3$-$MgTiO_3$ (M_2O_3) solid solution was possible without having the $FeTi_2O_5$-$MgTi_2O_5$ (M_3O_5) solid solution by slow cooling method.
- The porous structure of synthetic Mg-rich ilmenite seems to be formed from the temperature difference when slow cooling, which caused density difference between the rear and center part of the melt.
- Precautions considering liquid melt splashing during the high temperature synthesis were studied: moisture absorbed raw material (MgO), briquetting powder raw materials and raw material packing in crucible.

6.2 Oxidation

- Oxidation of synthetic ilmenite and Mg-rich ilmenite pellets were oxidized in a muffle furnace at 1000℃ for 2 hours.
- The Fe-Ti-Mg-O quaternary system was useful for predicting the phases after oxidation of synthetic ilmenite and Mg-rich ilmenite.
- Homogeneous distribution of iron in ilmenite during oxidation was confirmed by the iron mapping in EPMA results.
- While synthetic ilmenite follows the expected oxidation path in the Fe-Ti-Mg-O quaternary system, synthetic Mg-rich ilmenite showed an additional phase, hematite, besides the expected oxidation path.
- Mg as impurity in ilmenite tends to hinder the pseudobrookite-type formation of ilmenite when oxidized at 1000℃ by forming magnesium dititanate ($Mg^{2+}Ti_2O_5$).

6.3 Reduction

- The TGA (Thermo-Gravimetric Analyzer) vertical retort furnace was used for the reduction. Synthetic ilmenite and Mg-rich ilmenite pellets were reduced with a mixture of CO + H_2 gas for 4 hours at 1000℃.
- Magnesium as impurity in ilmenite clearly hindered the reduction rate: increasing amount of magnesium in ilmenite gave lower conversion degree.
- The addition of hydrogen gas in ilmenite reduction clearly enhanced the reduction rate: more percentage of hydrogen in reductant gas gave higher conversion degree.
- The carbon deposition from the Boudouard reaction is thought to be the reason for mass gain during the reduction for 50% CO + 50% H_2 gas composition.
- When Mg-rich ilmenite was reduced with only hydrogen gas, rutile or reduced rutile species were not detected after the conversion degree had exceeded "1". Magnesium is thought to immediately stabilize the reduced rutile species by forming Mg, Ti oxide species or armalcolite.
- Armalcolite incorporates the iron oxides, and the presence of armalcolite after the conversion degree of "1" indicates revision of the assumptions used for conversion degree calculation. Also, the presence of reduced rutile species before the conversion degree of "1" indicates that phases in ilmenite reacts spontaneously throughout the reduction rather than separated steps.
- Future work considering the surface properties of ilmenite pellets and kinetic modeling can be done as additional work for supporting evidence of magnesium impact in ilmenite.

References

[1] "Titanium". Columbia Encyclopedia (6^{th} ed.). New York: Columbia University Press. 2000-2006. ISBM 0-7876-5015-3.

[2] "Titanium". Encyclopedia Britannica. 2006. Retrieved 2006-12-29.

[3] Barksdale, Jelks. "The Encyclopedia of the Chemical Elements: Titanium". In Clifford A. Hampel (editor). New York: Reinhold Book Corporation. 1986: 732-738.

[4] J. Matthew, J. Donachie. "Titanium: A Technical Guide". Metals Parks, OH: ASM International. ISBN 0-87170-309-2: 13-15.

[5] X. Wang, H. Zhao, X. Quan, Y. Zaho, S. Chen. "Visible Light Photoelectrocatalysis With Salicylic Acid-modified TiO_2 Nanotube Array Electrode For p-nitrophenol Degradation". Journal of Hazardous Materials 166 (2009): 547-552.

[6] A. Khataee, G. A. Mansoori. "Nanostructured Titanium Dioxide Materials: Properties, Preparation and Applications". World Scientific, Hackensack. 2012.

[7] J. Gambogi. "Mineral Commodity Summaries". USGS, Washington D. C. 2014: 170-171.

[8] S. Asadi, M. Hassan, A. Nadiri, H. Dylla. "Artificial Intelligence Modeling To Evaluate Field Performance of Photocatalytic Asphalt Pavement For Ambient Air Purification". Environ. Sci. Pollut. Res., 21 (14) (2014): 8847-8857.

[9] D. Nabi, I. Aslam, I. A. Qazi. "Evaluation of The Adsorption Potential of Titanium Dioxide Nanoparticles For Arsenic Removal". J. Environ. Sci., 21 (2009): 402-408.

[10] S. Seim. "Experimental Investigations & Phase Relations in The Liquid $FeTiO_3$-Ti_2O_3-TiO_2 Slag System". PhD thesis. Department of Material Science & Engineering (DMSE), Norwegian University of Science and Technology (NTNU). 2011.

[11] W. Zhang, Z. Zhu, C. Y. Cheng. “A Literature Review of Titanium Metallurgical Processes”. Hydrometallurgy 108 (2011): 177-188.

[12] H. Sibum, V. Günther, O. Roidl, F. Habashi, H. U. Wolf. “Titanium, Titanium Alloys, & Titanium Compounds” (Ullmann’s Encyclopedia of Industrial Chemistry 2005). Wiley-VCH, Weinheim. 2005.

[13] J. Välimaa. “Research on Ilmenite Concentrates”. M. Sc. Thesis. Department of Geology & Mineralogy, University of Turku. 1992.

[14] A. Mehdilo, M. Irannajad, B. Rezai. “Chemical & Mineralogical Composition of Ilmenite: Effects on Physical & Surface Properties”. Mineral Engineering 70 (2015): 64-76.

[15] K. Borowiec, T. Rosenqvist. “Phase Relations & Oxygen Potentials In The Fe-Ti-Mg-O System”. Scandinavian Journal of Metallurgy 14 (1985): 33-43.

[16] “Sierra Rutile Mine”. Titanium Resources Group. Retrieved 06-05-2009.

[17] P. C. Pistorius. “Ilmenite Smelting: The Basics”. The 6th International Heavy Minerals Conference ‘Back to Basics’, The Southern African Institute of Mining and Metallurgy, 2007.

[18] M. Tangstad. “Metal Production In Norway”. Akademika Publishing, 2013. ISBN 978-82-321-0241-9.

[19] R. G. Becher, R. G. Canning, B. A. Goodheart, S. Uusna. “A New Process For Upgrading Ilmenite Sands”. Proc. Aust. Inst. Miner. Metall. 21 (1965): 21-44.

[20] T. Rosenqvist. “Ilmenite smelting”. Transactions of The Technical University of Kosice, (2), 1992.

[21] S. Lobo, L. Kolbeinsen, S. Seim. “Reduction of Ilmenite With Synthesis Gas”. Heavy mineral conference 2013: 1-13.

[22] S. Lobo, L. Kolbeinsen, S. Seim. “Pre-reduction of Ilmenite With Natural Gas – Model Development & Use”. The 13th International Ferroalloys Congress: Efficient Technologies in Ferroalloy Industry, June 2013: 857-867.

[23] K. Sun, R. Takahashi, D. Sathiyamoorthy. “Pre-oxidation & Hydrogen Reduction of Ilmenite In A Fluidized Bed Reactor”. Metallurgical & Materials Transactions B, 27B(5): 731-738.

[24] N. Ashcroft, N. Mermin. “Solid State Physics 1st ed.”. Cengage Learning. ISBN 0-03-083993-9.

[25] http://www.mindat.org

[26] P. Hammond. “Allard Lake Ilmenite Deposits”. Society of Economic Geologist, Inc. v. 47. P. 645.

[27] D. Zhao. “Processing & Properties of Direct Reduced Iron Pellets Containing Material For Control of Steel Structure”. PhD thesis. Department of Material Science & Engineering (DMSE), Norwegian University of Science and Technology (NTNU). 2010

[28] A. Mehdilo, M. Irannajad, B. Rezai. “Effect of Chemical Composition & Crystal Chemistry on The Zeta Potential of Ilmenite”. Colloids & Surfaces A: Physicochem. Eng. Aspects 428 (2013): 111-119.

[29] A. Mehdilo, M. Irannajad, B. Rezai. “Chemical & Mineralogical Composition of Ilmenite: Effects on Physical & Surface properties”. Minerals Enineering 70 (2015): 64-76.

[30] L. Fletcher. “Geikielite & Baddeleyite, Two New Mineral Species”. Nature 46 (1200), 1892. P. 620.

[31] V. Canaguier. “Synthesis of Ilmenite”. Master’s thesis. Department of Material Science & Engineering (DMSE), Norwegian University of Science and Technology (NTNU). 2014.

[32] L. Taylor, R. Williams, R. McCallister. “Stability Relations of Ilmenite & Ulvöspinel In The Fe-Ti-O System & Application of These Data to Lunar Mineral Assemblages. Earth & Planetary Science Letters, 16,(2), 1972: 282-288.

[33] I. Grey, A. Reid, D. Jones. “Reaction Sequences In The Reduction of Ilmenite: 4 – Interpretation In Terms of The Fe-Ti-O & Fe-Mn-Ti-O Phase Diagrams”. Transactions of the Institution of Mining & Metallurgy, 83(811): C105-11.

[34] K. Borowiec, T. Rosenqvist. “Phase Relations & Oxidation Studies In The System Fe-Fe_2O_3-TiO_2 at 700-1100℃”. Scandinavian Journal of Metallurgy, 10: 217-224.

[35] http://webmineral.com

[36] L. Liborio. “Thermodynamics of Oxygen Defective Magnéli Phases In Rutile: A First Principles Study”. Physical Review B 77, 104104 (2008).

[37] I. Grey, A. Reid, D. Jones. “Reaction Sequences In The Reduction of Ilmenite: 4-Interpretation In Terms of The Fe-Ti-O & Fe-Mn-Ti-O Phase Diagrams”. Institution of Mining & Metallurgy 16th July, 1973: C105-C111.

[38] Y. Wang, Z. Yuan. “Reductive Kinetics of The Reaction Between A Natural Ilmenite & Carbon”. Int. J. Miner. Process 81 (2006): 133-140.

[39] M. Hussein, R. Kammel, H. Winterhager. “A Study on The Reduction Mechanism of Ilmenite Ores”. Indian Journal of Technology, 5 (Dem.) 1967: 369-377.

[40] D. Jones. “Kinetics of Gaseous Reduction of Ilmenite”. Journal of Applied Chemistry and Biotechnology (25) 1975: 561-582.

[41] P. Vijay, R. Venugopalan, D Sathiyamoorthy. “Pre-oxidation & Hydrogen Reduction of Ilmenite in a Fluidized Bed Reactor”. Metallurgical & Materials Transactions B, 27B (5), 1996: 731-738.

[42] S. Gupta, V. Rajakumar, P Grieveson. “Phase Transformations during Heating of Ilmenite Concentrats”. Metallurgical & Materials Transactions B, 22B (5), 1991: 711-716.

[43] W. Xiao, X. Lu, X. Zou, X. Wei, W. Ding. “Phase Transitions, Micro-morphology & its Oxidation Mechanism In Oxidation of Ilmenite ($FeTiO_3$) Powder”. Trans. Nonferrous Net. Soc. China 23 (2013): 2439-2445.

[44] D. Jones. “Reaction Sequences In The Reduction of Ilmenite: 2-Gaseous Reduction by Carbon Monoxide”. Transactions (Institution of Mining & Metallurgy), Section C, 82 (805), 1973: 186-192.

[45] K. Sun, L. Zhang. “Measurements of The Thermodynamic Properties of $Fe_2Ti_3O_9$ & Fe_2TiO_5”. Transactions of Nonferrous Metals Society of China, 1996, 6(1): 25-31.

[46] Y. Suzuki, Y. Shinoda. “Magnesium Dititanate ($MgTi_2O_5$) With Pseudobrookite Structure: A Review”. Sci. Technol. Adv. Mater. 12 (2011) 034301: 1-6.

[47] O. Boudouard, C. R. Acad. Sci, Paris Us, 824 and 1521 (1899).

[48] Jones, D. G. “Optical Microscopy & Electron-probe Microanalysis Study of Ilmenite Reduction. Transactions (Institution of Mining & Metallurgy), Section C, 83 (808), 1974: 1-9.

[49] S. Seetharaman, A. McLean, R. Guthrie, S. Sridhar. “Treatise on Process Metallurgy: Industrial Processes”. Elsevier, 2014. ISBN: 978-0-08-100000-7.

[50] J. Dang, G. Zhang, K. Chou. “Kinetics & Mechanism of Hydrogen Reduction of Ilmenite Powders”. Journal of Alloys & Compounds 619 (2015): 443-451.

[51] www.ntnu.no/wiki

[52] G. Leichtfried et al. “Properties of Diamond & Cubic Boron Nitride”. Berlin: Springer, 2002. ISBN: 973-3-540-42961-6.

[53] F. Fiorillo. “Measurement & Characterization of Magnetic Materials”. Elsevier Academic Press, 2004. ISBN: 0-12-257251-3.

[54] T. Zhang, C. Lei, Q. Zhu. “Reduction of Fine Iron Ore Via A Two-step Fluidized Bed Direct Reduction Process” Powder Technology 254 (2014): 1-11.

[55] P. Kim. “Impurities In Ilmenite – Magnesium” Master’s Project, Norwegian University of Science and Technology (NTNU), Department of Material Science and Engineering (DMSE) (2014).

[56] L. Kolbeinsen. “Modelling of DRI Processes with Two Simultaneously Active Reducing Gases” Steel Research Int. 81 (2010) No. 10: 819-828.

[57] R. Felice. “Pyrometry For Liquid Metals”. Advanced Materials & Processes, 166(7), 2008. – Appendix B

Appendices

Appendix A: Calculations of batches 1-5

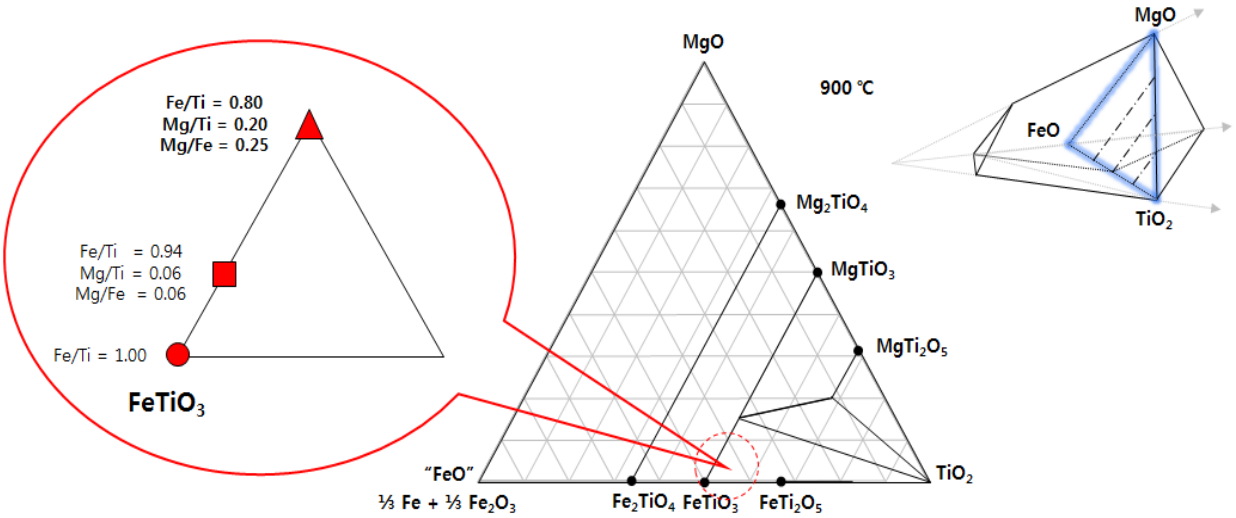

Material	g/mol
Fe	55.85
Fe_2O_3	159.70
TiO_2	79.88
MgO	40.31

Batch	Symbol
1	●
2	■
3	
4	▲
5	

Batch 1: Synthetic ilmenite (No Mg) ●

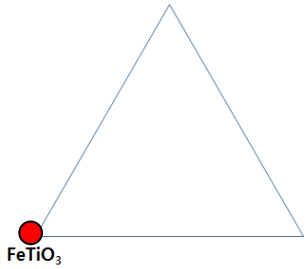

	FeO (= ⅓Fe2O3 + ⅓Fe)	TiO2	MgO
mol	1.98 (= 0.66 x 3)	1.98	-
mol %	FeO : TiO2 : MgO = 50 : 50 : 0		
Ratio	Fe / Ti = 1		

	Fe2O3	TiO2	Fe	MgO	Total
mol	0.66	1.98	0.66	-	
g	105.25	157.95	36.80	-	300.00

Batch 2: Synthetic Mg-rich ilmenite (Low Mg) ■

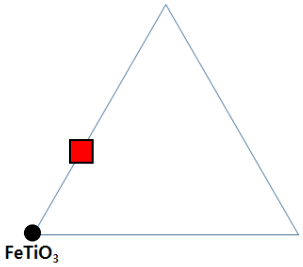

	FeO (= ⅓Fe2O3 + ⅓Fe)	TiO2	MgO
mol	1.88 (= 0.63 x 3)	2.00	0.12
mol %	FeO : TiO2 : MgO = 47 : 50 : 3		
Ratio	Fe / Ti = 0.94, Mg / Ti = 0.06, Mg / Fe = 0.06		

	Fe2O3	TiO2	Fe	MgO	Total
mol	0.63	2.00	0.63	0.12	
g	100.61	159.76	35.19	4.84	300.40

Batch 3-5: Synthetic Mg-rich ilmenite (High Mg) ▲

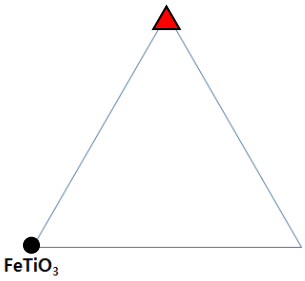

	FeO (= ⅓Fe2O3 + ⅓Fe)	TiO2	MgO
mol	1.68 (= 0.56 x 3)	2.10	0.42
mol %	FeO : TiO2 : MgO = 40 : 50 : 10		
Ratio	Fe / Ti = 0.80, Mg / Ti = 0.20, Mg / Fe = 0.25		

	Fe2O3	TiO2	Fe	MgO	Total
mol	0.56	2.10	0.56	0.42	
g	89.43	167.75	31.28	16.93	305.39

Appendix B: Procedure of CCIF.
Spectro-pyrometer.
Procedure of TGA vertical retort furnace.

B.1 Procedure of Cold Crucible Induction Furnace (CCIF)

The CCIF used for the synthesis in this study is the property of the Department of Material Science and Engineering (DMSE), NTNU.

1. Fill up the crucible. Make sure that the boron nitride (BN) coating is completely dried. Leftover moisture is likely to give splashing of the melt during the high temperature synthesis (Figure B.1). Also, check if the materials are completely moisture-free.

Figure B.1 Protection glass after splashing of the melt: rear view (left) and top view (right)

2. Push up the external glass tube through the induction coil and place the crucible on the platform. Cover the protection sheet around the crucible and cover the protection sheet with the external glass by lowering it. Make sure no obstacles are between the external glass and the platform.
3. Input the two internal protection glasses by inserting them from above the induction coil.
4. Cover the external glass with the protection sheet.
5. Plug the water tubes to the crucible. Then, use the crank until the external glass touches the top. The string press should be approximately 5mm. Be careful not to exceed this value, or otherwise the spring will be damaged.

6. Position the pyro-spectrometer. Use the LASER ON / OFF function on the software for aiming. You can see the aim of the laser through the mirror, which is placed on the top of the furnace. Aim the laser so that it is aimed at the center of the crucible top (center of the material mixture).
7. Close the furnace cage. Make sure to close the cage properly by using the two clips at each end. The right clip is also an emergency stop sensor, and the furnace will not work if the clips are not properly closed.
8. Open the ventilation. The ventilation can be found on the left-top of the furnace.

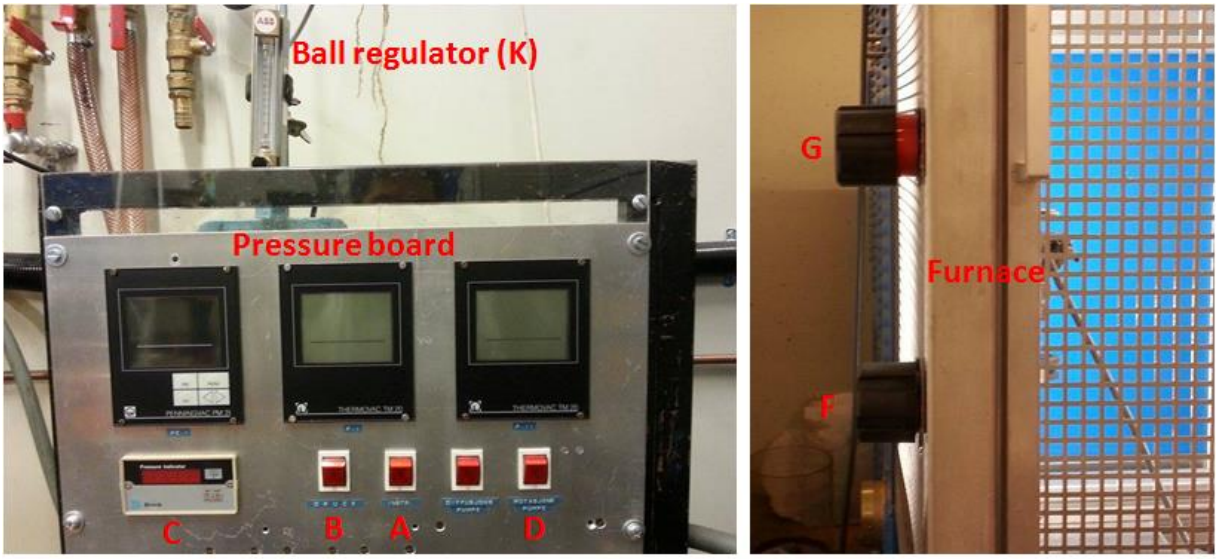

Figure B.2 Pressure board (left) and output/pump circuit (right)

9. Turn on the "INSTR" (A) and "DRUCK" (B) button on the pressure board. The "INSTR" button will turn on the pressure board, and the "DRUCK" button will enable the display of the pressure (C) inside the crucible. The pressure should be around 1000-1200 mbar.
10. Open the pump circuit (F), and close output circuit (G). The circuit is open if you see red.
11. Push "Rotasjon pump" (D) on and the pressure inside the crucible will start to decrease. When the pressure decreases to approximately 6-10 mbar, close the pump circuit (F) and stop the pump.

Figure B.3 Ar tank (left) and ball regulator (right)

12. Check the Ar gas in the tank. See if the white regulator (I) is closed.
13. Open the black regulator (H) on the top of the Ar tank to allow gas to enter the decompression chamber. Be careful not to stand in front of the white regulator (I).
14. Open the white regulator (I). Open the small output regulator (J).
15. Open the ball regulator (K), which is above on the pressure board. Adjust the flow to 70. The Ar gas is being inserted into the vacuumed crucible. The pressure on the display will increase. When the pressure is approximately 900 mbar, open the output circuit (G). Do not exceed 1000 mbar when the output circuit is closed because the protection glass will break from over pressure. After opening the output circuit, the pressure should be around 1000 mbar as before. Check again if the Ar flow is 70 on the ball regulator (K).

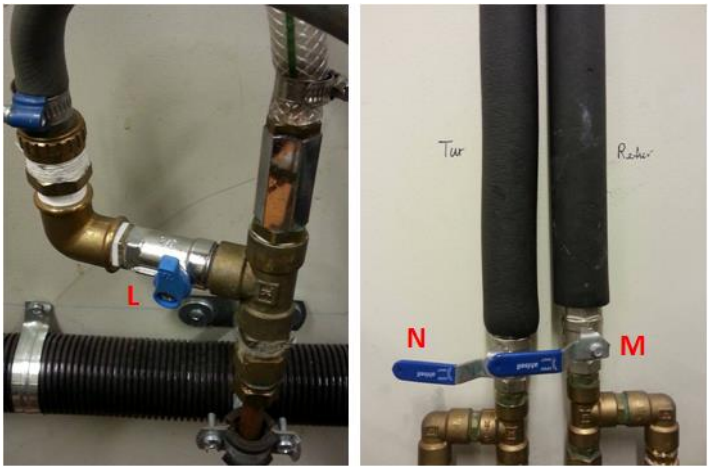

Figure B.4 Water supply switch (left) and cooling circuits (right)

16. Open the water circuit by turning the blue switch (L), which is on the left side of the Ar tank.
17. The cooling circuits can be found on the right side of the Ar tank. To open the cooling circuits, first turn “Retur” (M) and then turn “Tur” (N). Make sure to do follow this order or else there will be overpressures in the water circuits. Check the floor and see that water flows through the water tunnel. If confirmed, water is constantly going through the copper crucible.

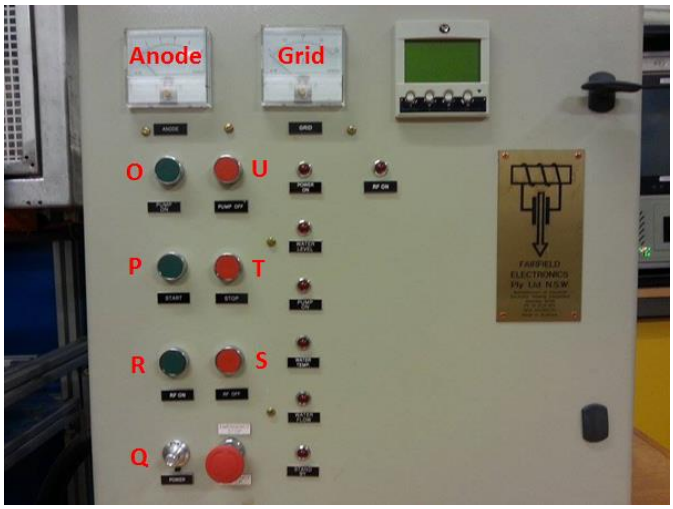

Figure B.5 CCIF controller

18. To supply power, turn the key to “2” on the electric desk. The electric disk is near the corner of the walls in front of the furnace.
19. Turn the switch to “1” on the furnace. The switch can be found on the right side of the furnace.
20. Press the “PUMP ON” (O) button on the control board and then press the “START” (P) button.
21. Check that the power knob (Q) is indicating 0.
22. Wait 5 minutes. The furnace is warming up.
23. Press the “RE ON” (R) button to apply power. Wait 1 minute.
24. Increase the power by turning the power knob (Q) to the desired level. Warning! Do not overreach 1.8 V on the GRID.
25. To shut down, press “RF OFF” (S) and “STOP” (T).
26. Wait until the crucible cools down. It takes approximately 30 minutes to cool down.
27. After 30 minutes, push the “PUMP OFF” (U).
28. Shut the furnace down by turning off the main button (right side of furnace). Then turn the electric disk to 0.
29. Close the Ar gas. First, turn off the black regulator (H). Wait until the barometer goes to 0.
30. Next, close the white regulator (I). Wait until the barometer stops decreasing.
31. Close the small output regulator (J).
32. Close the ball regulator (K).
33. Close the ventilation on the left-top of the furnace.
34. To close the water circuits, first turn “Tur” (N), then “Retur” (M) for avoiding overpressures in the water circuits. Turn off the blue switch (L) to shut off the water supply.
35. Open the cage. Lower the crucible by using a crank and unplug the water tubes. Use a plastic bottle to collect the leftover water in the crucible.
36. Remove the internal protection glasses. The glasses might still be hot: use gloves to remove them.
37. Remove the external glass and protection sheets. Retrieve the crucible.
38. Turn the crucible upside down and use a rubber hammer to apply force. Do not use a metal object to apply force to the crucible. It can damage the water pipes inside the crucible.

B.2 Spectro-pyrometer [10]

The equipment for measuring the temperature during the experiments in the cold crucible induction furnace is a FAR Associates spectropyrometer of the type FMP 2. This spectropyrometer measures on 500 wavelengths and thus calculates and corrects for the emissivity of the specimen. From the spectropyrometer the central temperature is logged along with the tolerance (standard deviation) of the measurement and the signal strength. The tolerance is the standard deviation calculated from the 500 measured temperatures. The signal strength is equal to the emissivity under ideal conditions, i.e. the area in focus must be filled, and there must be no attenuation and clean optics. The range of the pyrometer is from 800 to 2500 ℃ with an accuracy of ± 0.25 to 0.75 % on non grey targets. Automatic compensation for absorption or emission from the off-gas is also included. The log rate of the pyrometer can be set at given intervals or whenever the pyrometer has enough information for an accurate reading. It is this last log rate, which corresponds to a log interval of about 5 readings per second during the holding time. The log interval will decrease as the temperature is lowered due to less thermal radiation. It should also be noted that the temperature measurement is not coupled to the furnace power setting. For further information about the spectropyrometer the reader is referred to the FAR Associates website (www.pyrometry.com) or publications such as "Pyrometry for Liquid Metals" by Felice [57].

B.3 Procedure of TGA vertical retort furnace

The TGA vertical retort furnace used for the reduction of synthetic ilmenite pellets in this thesis is the property of the Department of Material Science and Engineering (DMSE), NTNU. Contact Edith Thomassen (SINTEF) for proper training and technical support.

1. Prepare the sample. It's usually good to use a container approximately the same diameter of the crucible (a 100ml beaker is a good example). Use a scale to measure the weight of the sample. Then, measure the height of your sample in the container. This is to set the thermocouple in the center of your sample (procedure 7).
2. If the crucible is clean enough, turn on the software and weigh the crucible on the mass balance before loading the sample. The crucible should be closed with its top (remember

how many bolts used for sealing the top). Tare the balance at the top of the furnace. The mass of the empty crucible is displayed on the computer screen. Record the mass on the log book.

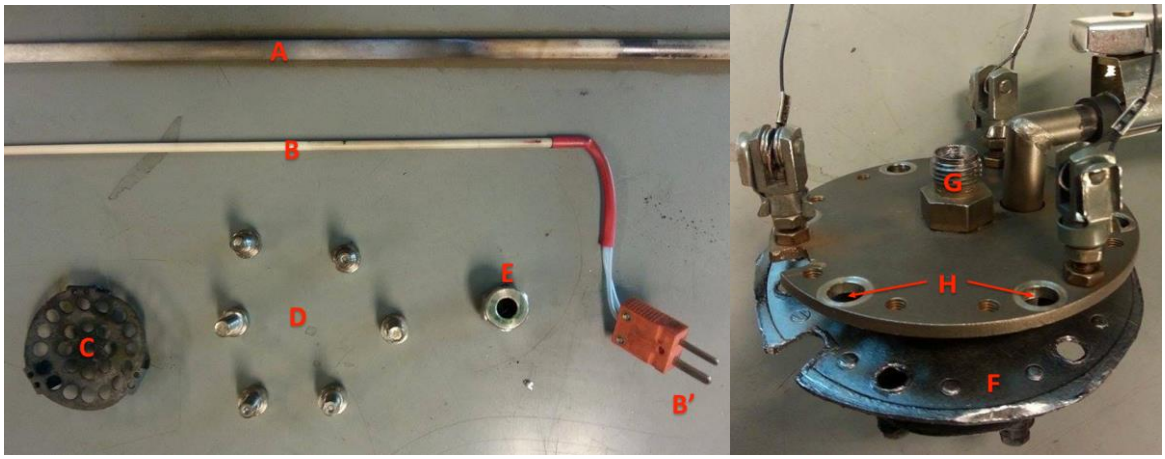

Figure B.6 TGA vertical retort furnace crucible components (left) & crucible top (right)

3. Take down the crucible and open the seal. Place the porous holder (C) inside the crucible (see that the holder is not upside down by using a flashlight).
4. Put the thermocouple sheath (A) into the crucible. Use a flashlight so that the thermocouple sheath is placed in the middle of the porous holder (C) (use the middle hole of the holder). Carefully pour your samples into the crucible (tilting the crucible as pour the sample usually helps breakage of the sample and prevention of dust).
5. Carefully seal the crucible top. Make sure the graphite gasket (F) has no cracks or dust particles (they can cause gas leakage). Also be careful not to damage the thermocouple sheath (A) when sealing the crucible top.
6. Use the 6 bolts (D) to tightly seal the crucible top. Apply pressure of bolt equally on the screws (H).
7. Place the thermocouple seal (E) carefully around the sheath (A) (the inner part of the thermocouple seal is made of graphite). Before tightening the seal (E), pull up the sheath (A) according to the half height of your sample, which was measured in procedure 1 (the end of the sheath is now placed at the middle of the sample).

8. Carefully insert the thermocouple (B) inside the sheath (A). Don't insert the thermocouple (B) by dropping it (the thermocouple can be fragile). Tightly seal the thermocouple seal (E).

Figure B.7 TGA vertical retort furnace gas tubes (left) and crucible (right)

9. Hang up the crucible on the furnace. Use the hook (I). Ensure that the crucible is hanging in such a way that when the tubes (,) are connected the clamps will have their adjustment screws on the top and there will be no tension in the tubes. Connect the gas input (J) and output tubes (K).
10. Connect the thermocouple plug (B' + L). Check the temperature display on software to see the thermocouple plug (L) is correctly connected (if not connected, the temperature displays 999999999).
11. Turn on the "HEAT" and "POWER" dial on the controller. Turn on the dials on the electrical box. Set the output control to 50% (this is approximately for 1000℃)
12. Make sure to run a leak test before the main experiment. During the leak test, use a portable CO / H_2 detector to see if any gas is leaking (check crucible top, tubes and other places possible of leak). If gas leak is detected stop the leak test, wait until the crucible is clean with Ar and start again from procedure 5. If gas leak is not detected, setup the program for the main experiment.

13. After the setup, start the experiment. During the experiment, it is important to regularly check for leaks and overpressures. Use the portable CO / H_2 detector to find any leaks, and check the lab's master alarm for gas leaks (the monitor can be found next to the door outside). The software on the computer screen displays the pressure of the output gas. This pressure should never exceed 5 bar otherwise there is risk of damaging the furnace or having leaks.
14. When the experiment is completed, make sure to turn off all the gas tanks. Turn off the "HEAT" dial, but leave the "POWER" dial on to allow for cooling. The dials on the electrical box can also be turned off. Allow the crucible to cool before dismantling.
15. Once cooled, carefully disconnect the thermocouple plug (L). Then disconnect the gas tubes (J, K) and unhook the crucible from the top of the balance. Put the crucible in a holder so that it doesn't falls down.
16. Carefully pull out the thermocouple (B), unseal the thermocouple seal (E), unseal the crucible top and empty the sample. weigh the sample and record the mass on the log book.

Appendix C: Informal know-how for successful pelletizing

Successful pelletizing of powder material requires long time with patient. An informal "Know-How" for successful pelletizing is described by using an analogy in this part.

In agriculture, a simple technique called "Pruning" is done to improve the quality of a crop. Pruning involves the selective removal of parts of a plant, such as branches, buds, or roots. Removing such parts of a plant is beneficial, because the nutrition can be focused to the desired product part of a plant. For instance, pruning the measly product on the lower part of a plant will make the nutrition to focus to the desired product on the upper part of a plant. An illustration of pruning is shown in **Figure C.1**. (a) is the growth of products after no changes, and (b) is the growth of products after pruning.

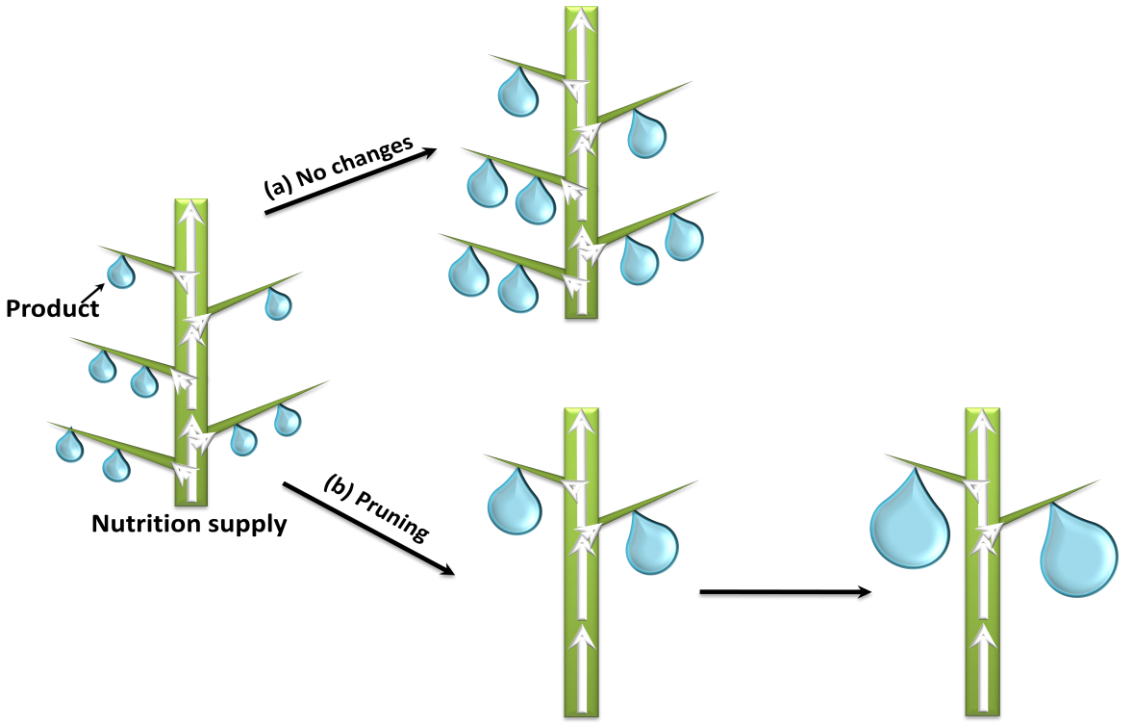

Figure C.1 A description of "Pruning"

Pelletizing can be similar to pruning. **Figure C.2** shows the powder particles being pelletized in a pelletizing drum. The measly products, which are described in **Figure C.1**, are the powder particles and the small pellets on the upper part of **Figure C.2**. The nutrition supply in **Figure C.1** can be water and input powder in **Figure C.2**. "Pruning" the powder particles (small pellets)

by crushing them with an appropriate tool, such as a spachler, will hinder their growth. Then the bigger pellets will have more chance to grow up into the desired size like in **Figure C.1** (b). "Un-pruning" the powder particles (small pellets) will likely to follow (a) in **Figure C.1**.

Therefore, the "Pruning" method can be used for successful pelletizing. This will allow the big pellets grow into the desired size.

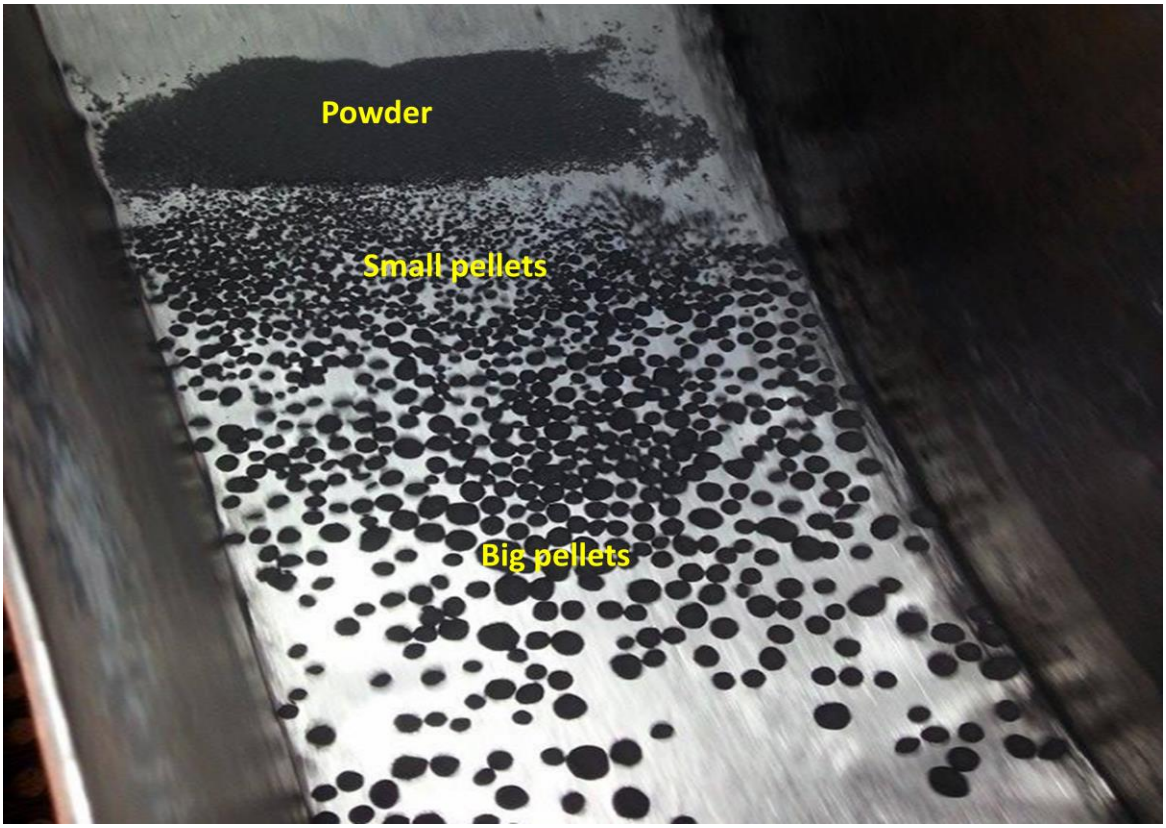

Figure C.2 Powder particles being pelletized

※ I would like to thank my late grandfather whom I have cherished many memories in his tomato garden. He taught me how to do "Pruning".

Appendix D: Temperature profiles for synthesis

The temperature profiles for batches 1-5 from the synthesis (Section 4.1.2) are shown in this part. The comparison between all batches is also shown.

Batch 1: Synthetic ilmenite (No Mg, instant cooling after complete melt)

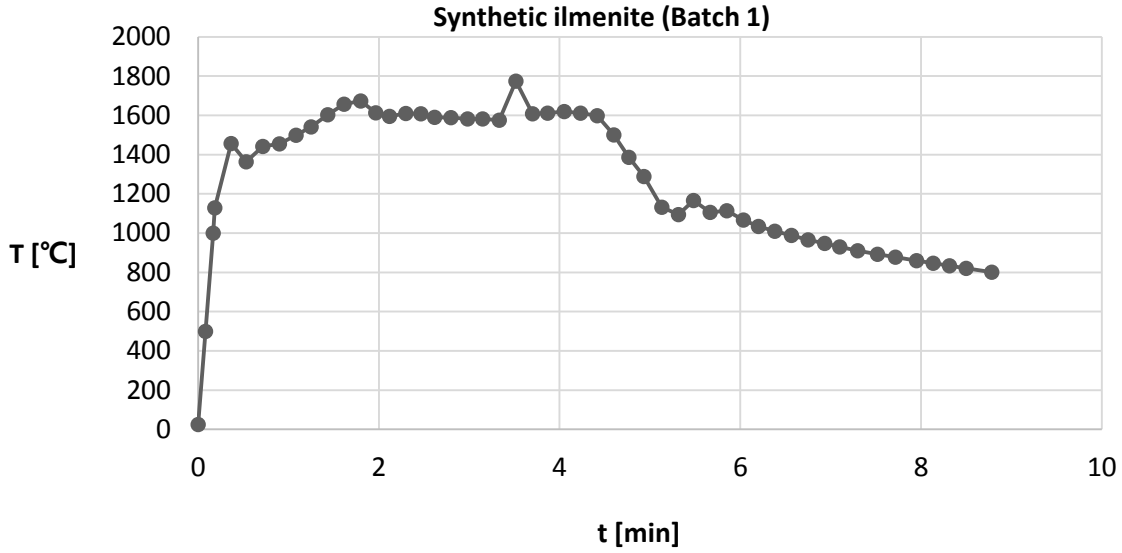

Figure D.1 Temperature profile for batch 1 synthesis

Batch 2: Synthetic Mg-rich ilmenite (Low Mg, slow cooling after complete melt)

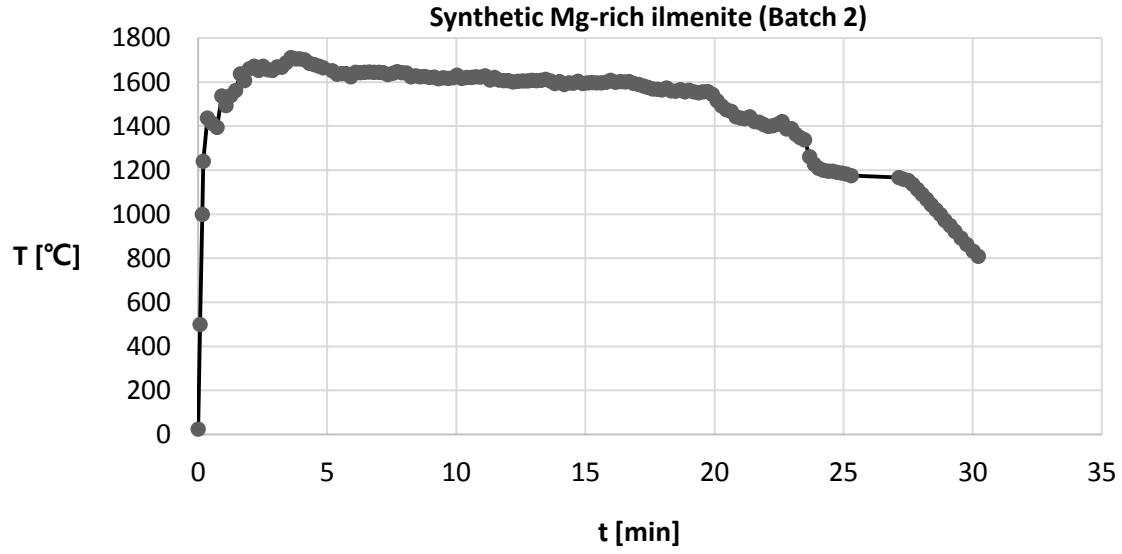

Figure D.2 Temperature profile for batch 2 synthesis

Batch 3: Synthetic Mg-rich ilmenite (High Mg, slow cooling after complete melt)

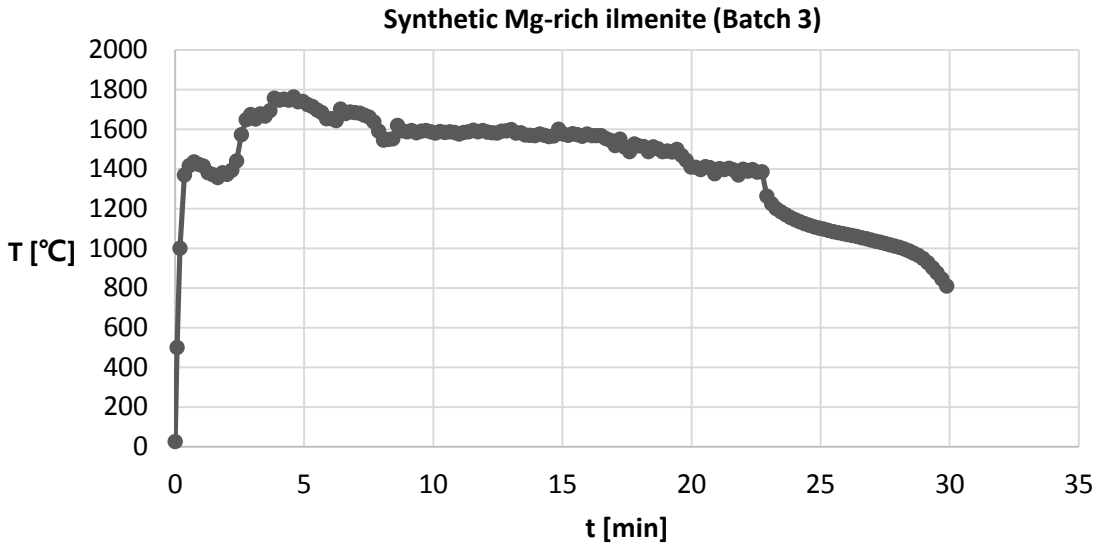

Figure D.3 Temperature profile for batch 3 synthesis

Batch 4: Synthetic Mg-rich ilmenite (High Mg, slow cooling after complete melt)

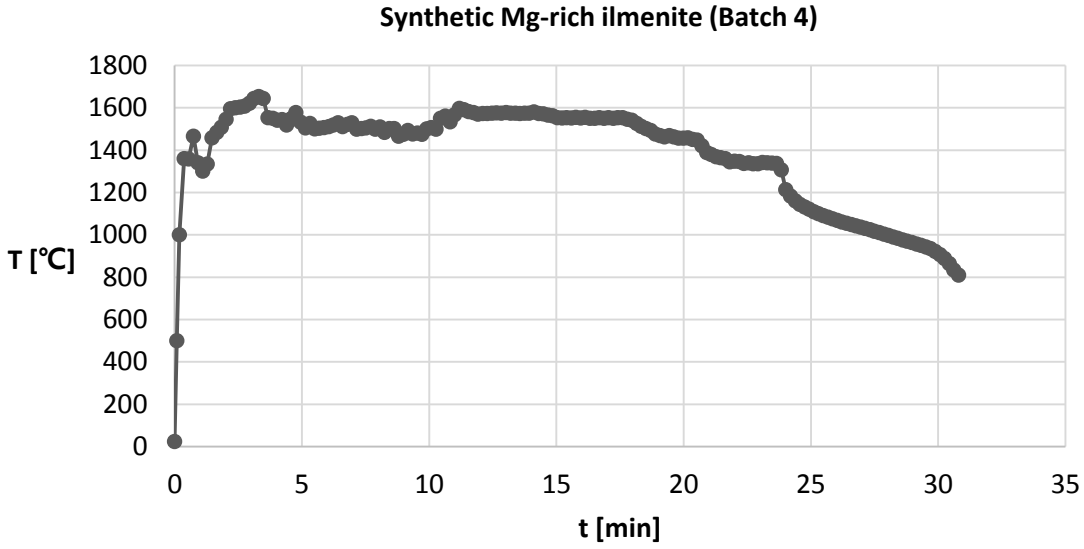

Figure D.4 Temperature profile for batch 4 synthesis

Batch 5: Synthetic Mg-rich ilmenite (High Mg, slow cooling after complete melt)

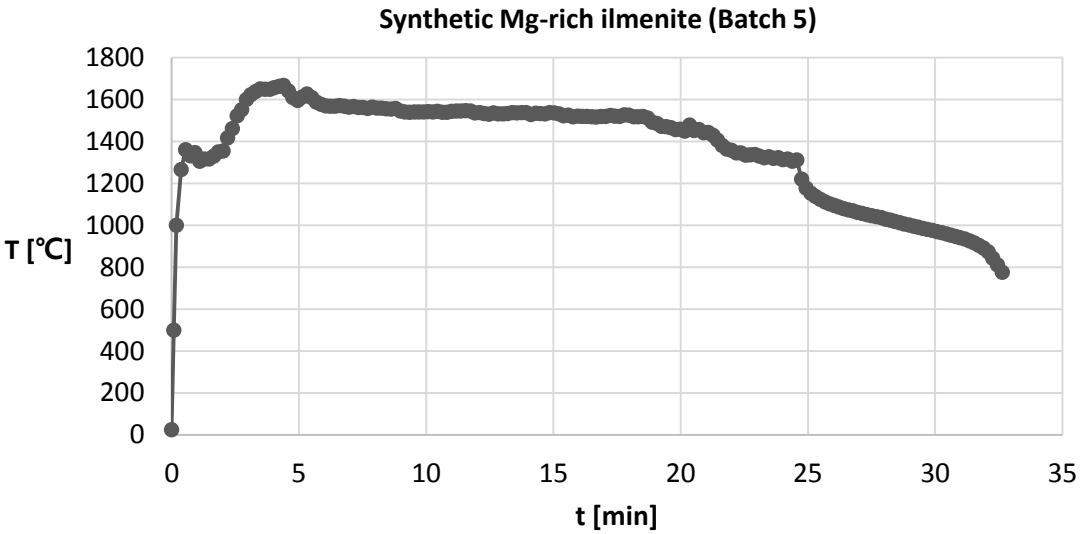

Figure D.5 Temperature profile for batch 5 synthesis

Comparison of all batches

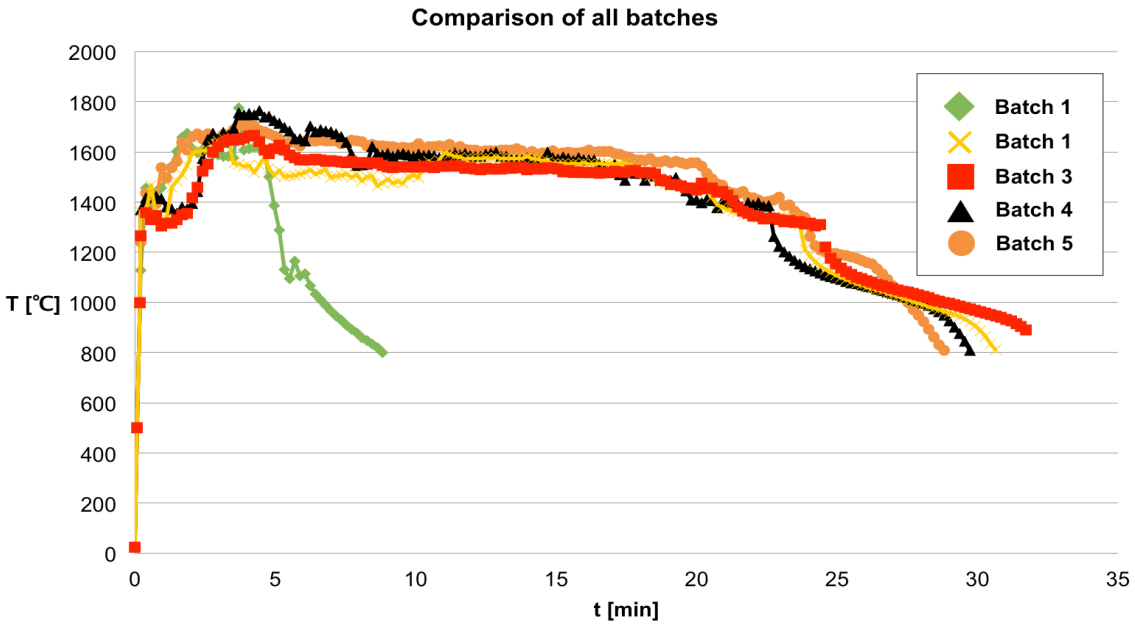

Figure D.6 Temperature profile for batches 1-5 synthesis

Appendix E: XRD analyses

The rest of the XRD results for Mg-rich ilmenites (batches 3-5) from Section 4.1.2 are shown in this part. In addition, an XRD comparison of batches 2-5 is also shown.

Batch 3 (After synthesis)

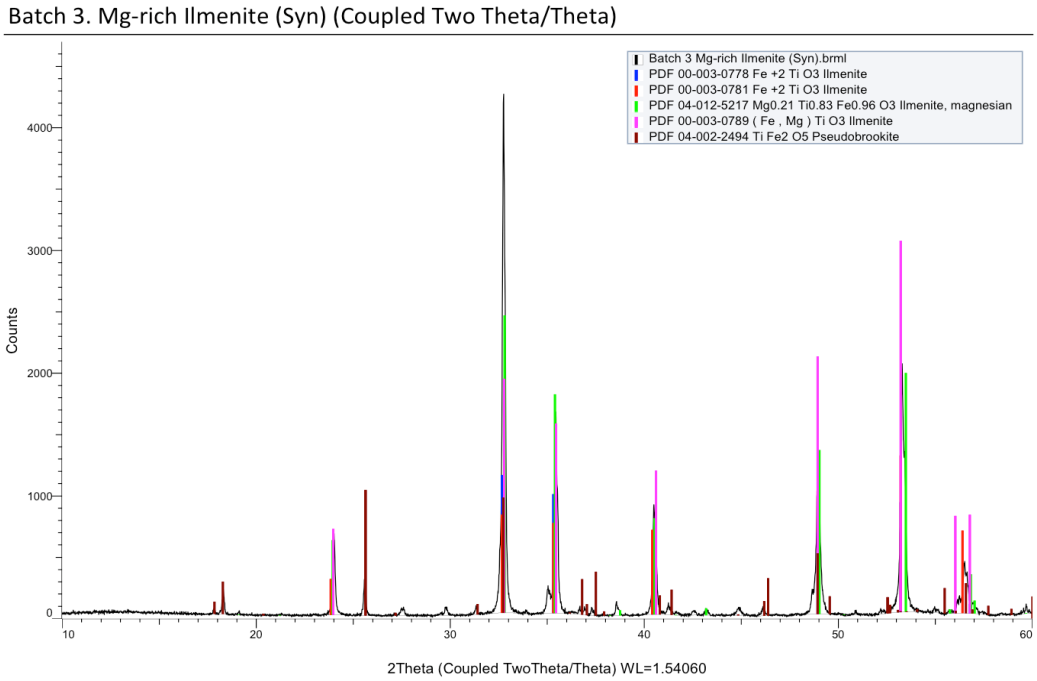

Figure E.1 XRD analysis for synthetic Mg-rich ilmenite (Batch 3)

Batch 4 (After synthesis)

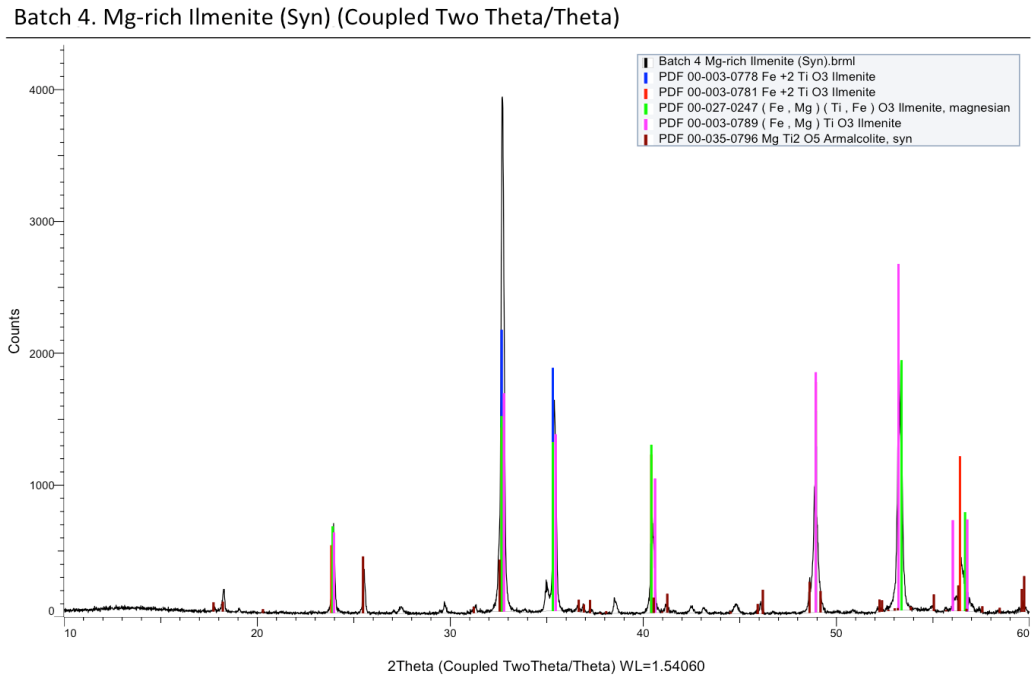

Figure E.2 XRD analysis for synthetic Mg-rich ilmenite (Batch 4)

Batch 5 (After synthesis)

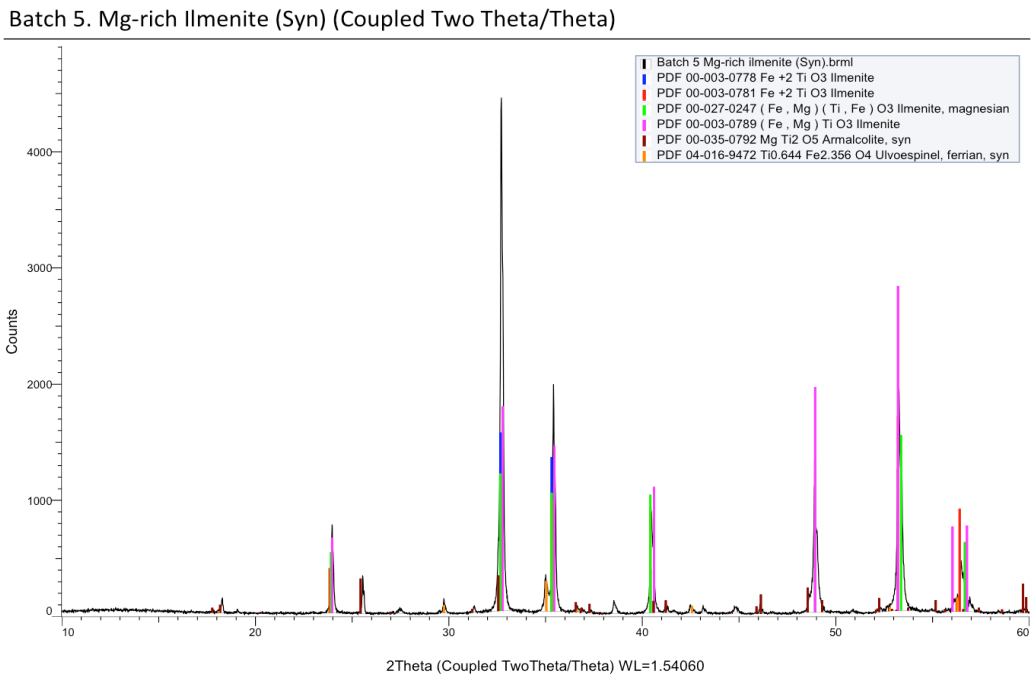

Figure E.3 XRD analysis for synthetic Mg-rich ilmenite (Batch 5)

Comparison of batches 2-5 (After synthesis)

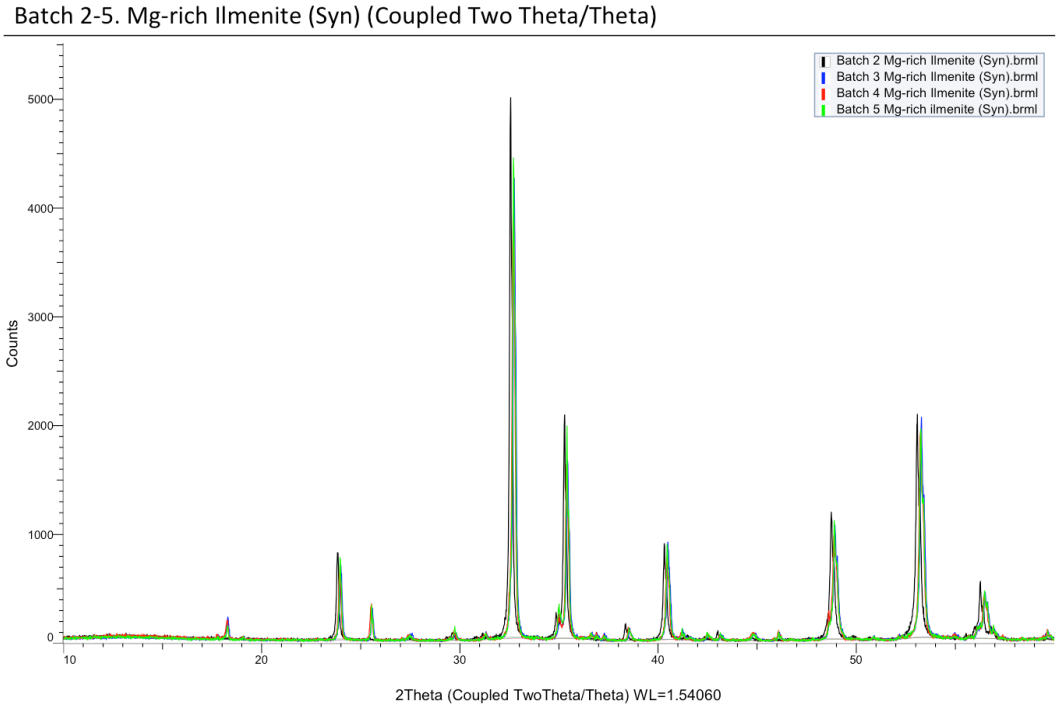

Figure E.4 XRD analysis for synthetic Mg-rich ilmenite (Batches 2-5)

Appendix F: Mass loss curves

The mass loss curves are shown in this part, and they are the raw data retrieved from the reduction (raw data before calculation into conversion degrees). Comparisons of batches 1-3, 3-5 and 1-5 are shown.

Batch 1-3: Difference in Mg amount / 50% CO + 50% H_2 for 4.0 hour

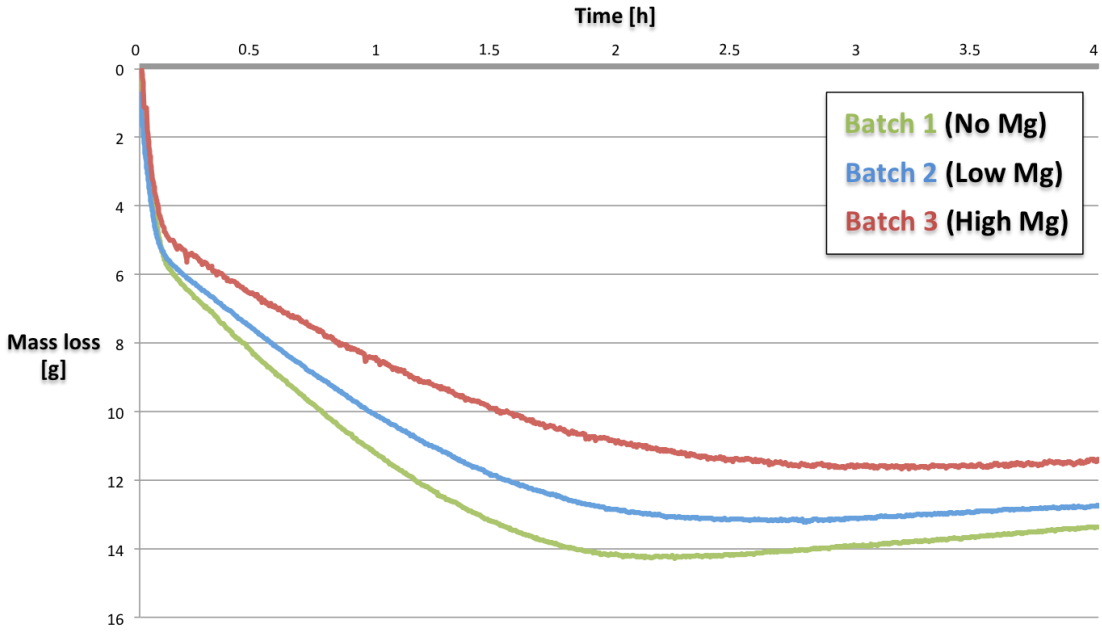

Figure F.1 Mass loss curves for batches 1-3

Batch 3-5: Difference in H_2 amount / 50-X% CO + 50+X% H_2, X = 0, 25, 50 for 4.0 hour

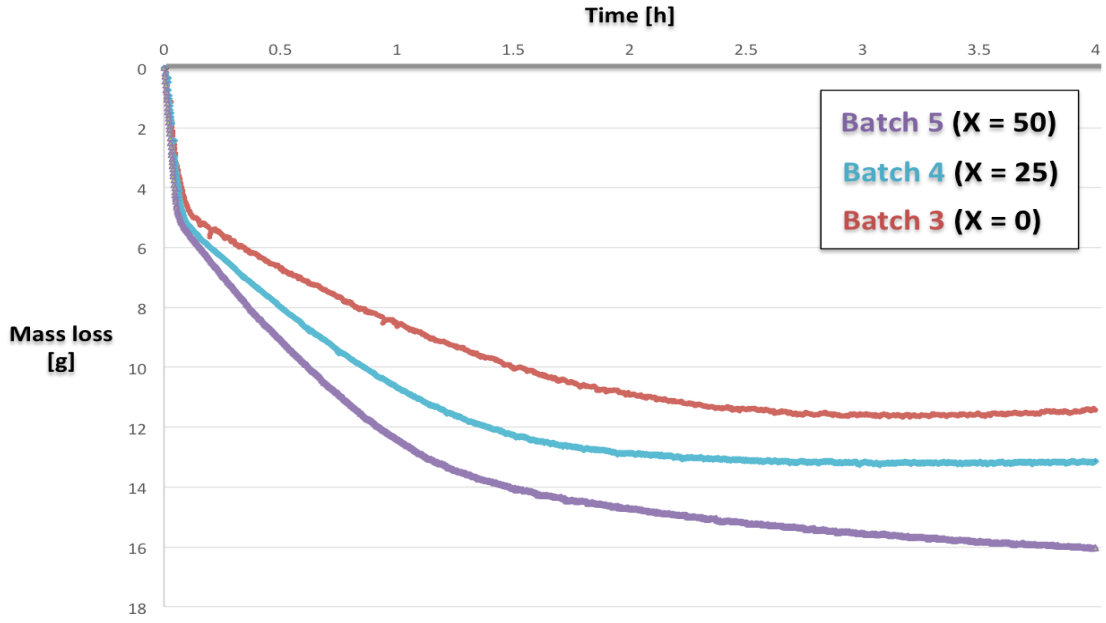

Figure F.1 Mass loss curves for batches 3-5

Batch 1-5: Batch 1-3 + 3-5

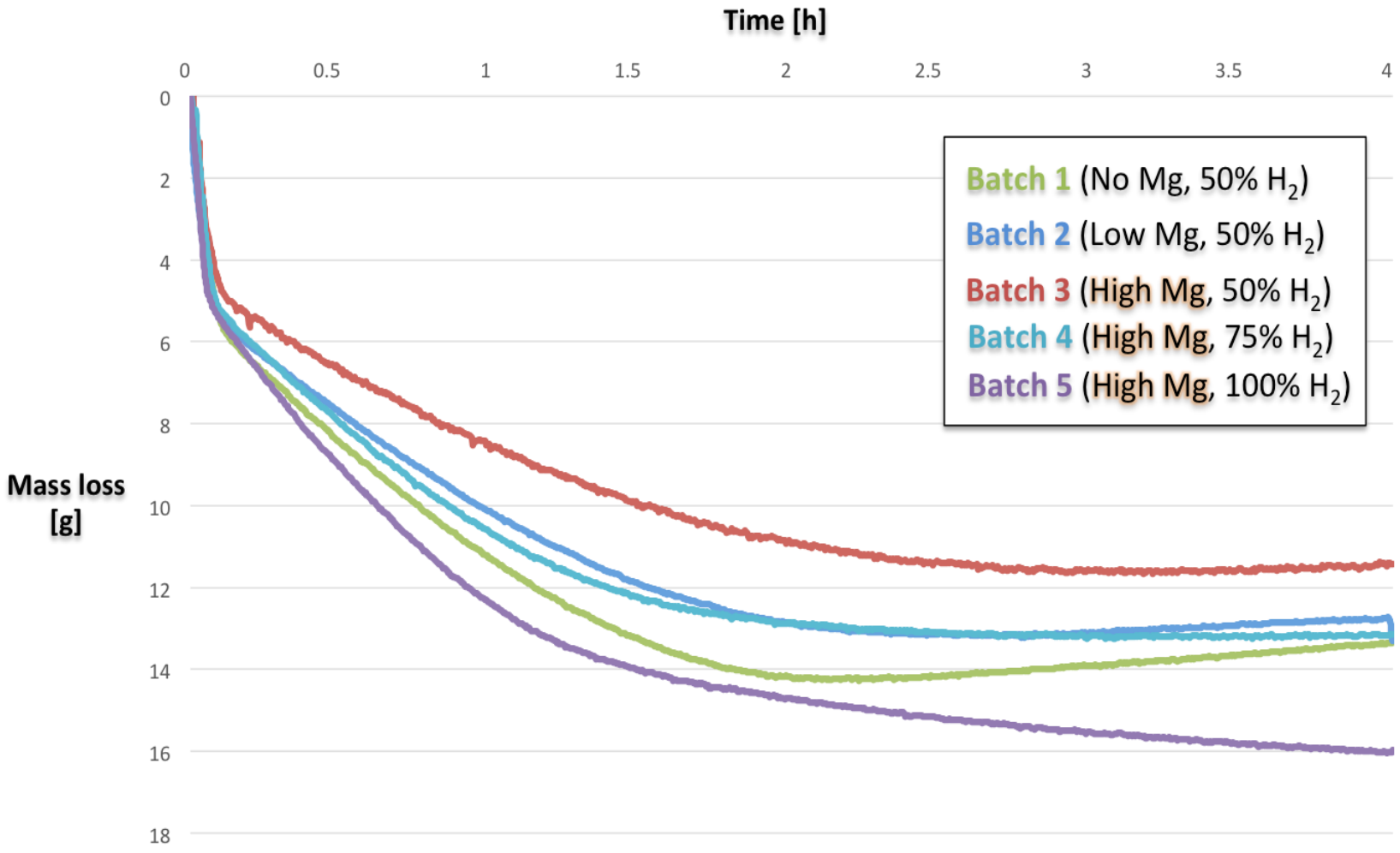

Figure F.3 Mass loss curves for batches 1-5

Appendix G: EPMA analyses

The rest of the EPMA results for batches 3 and 4 after reduction in Section 4.3.2 are shown in this part.

Batch 3 (After reduction): 50% CO + 50% H_2 / 4.0 hour

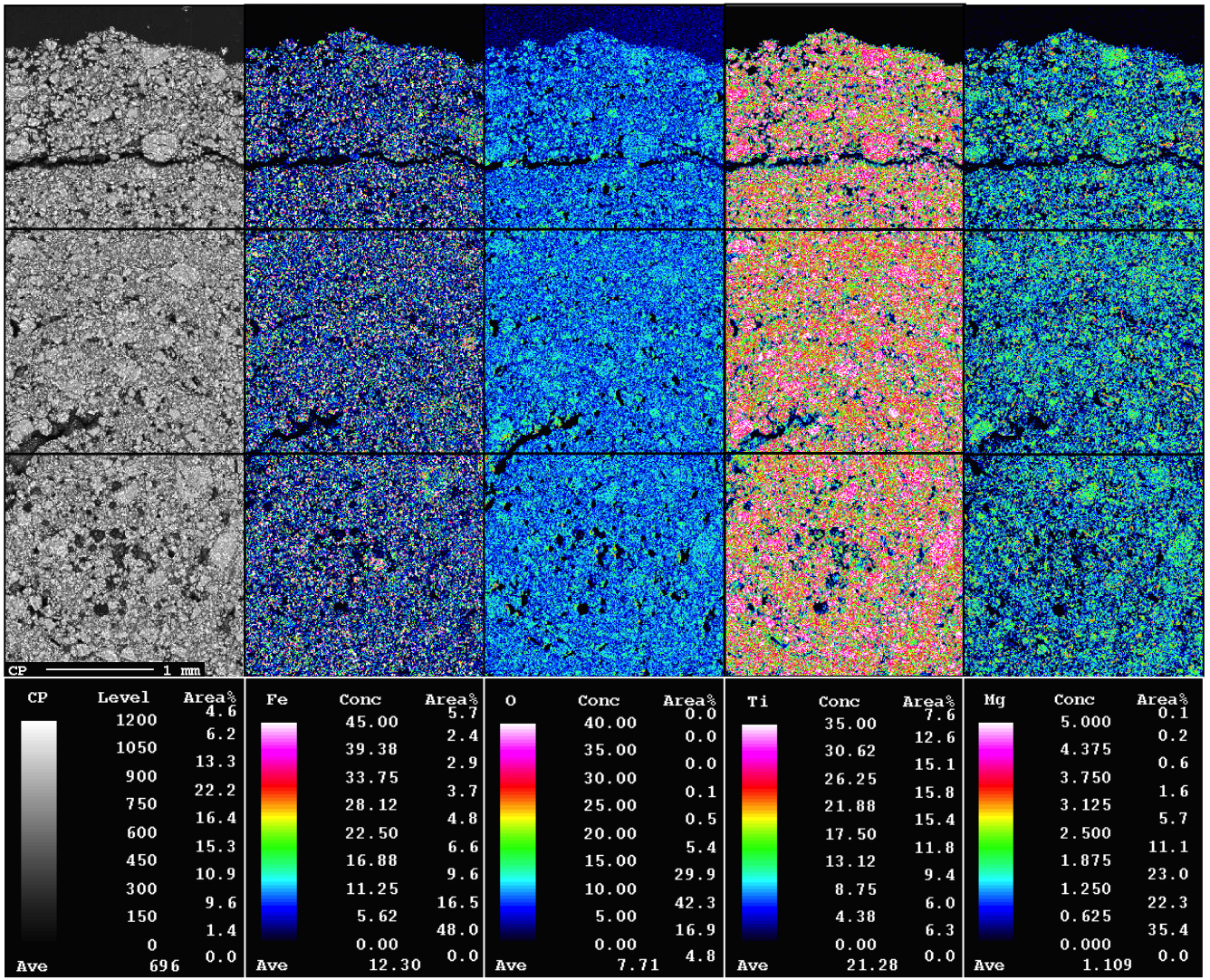

Figure G.1 SEM image & element mappings (Fe, O, Ti, Mg) of batch 3 after reduction

Batch 4 (After reduction): 25% CO + 75% H_2 / 4.0 hour

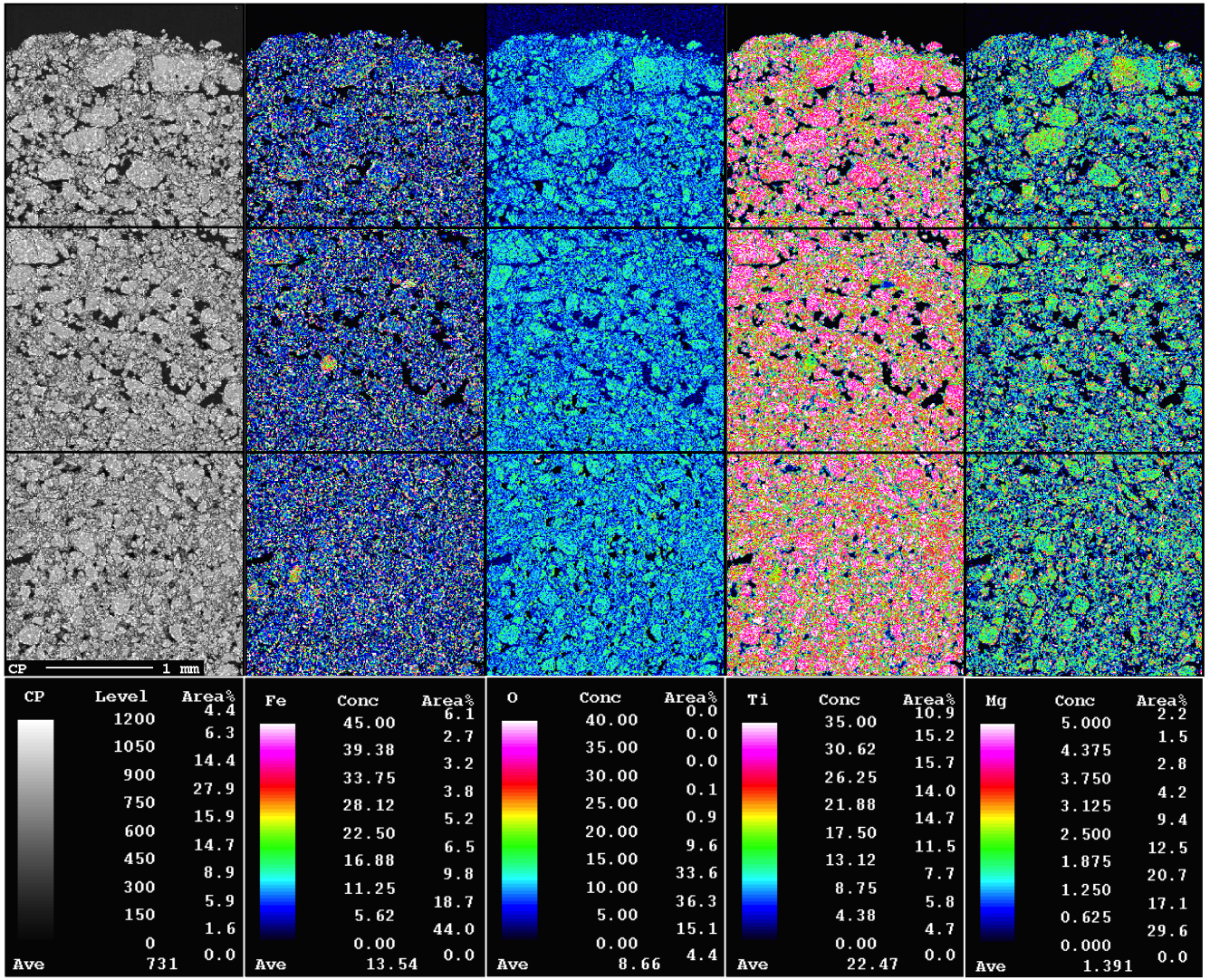

Figure G.2 SEM image & element mappings (Fe, O, Ti, Mg) of batch 4 after reduction